

HARVARD UNIVERSITY
Graduate School of Arts and Sciences



DISSERTATION ACCEPTANCE CERTIFICATE


The undersigned, appointed by the
Division of Medical Sciences
in the subject of Biological and Biomedical Sciences
have examined a dissertation entitled

*Targeting of proteins from the endoplasmic reticulum to
lipid droplets: a specific requirement for mitochondrial proteins*

presented by Christina Brandao Konami Jayson
candidate for the degree of Doctor of Philosophy and hereby
certify that it is worthy of acceptance.

Signature: 

Typed Name: Dr. Sichen Shao

Signature: 

Typed Name: Dr. Timothy Mitchison

Signature: 
Sudha Biddinger (Apr 30, 2021 09:11 EDT)

Typed Name: Dr. Sudha Biddinger

Signature: 
Michael A. Welte (Apr 30, 2021 10:58 EDT)

Typed Name: Dr. Michael Welte

Date: April 29, 2021

Targeting of proteins from the endoplasmic reticulum to lipid droplets: a specific requirement for mitochondrial proteins

A DISSERTATION PRESENTED

BY

CHRISTINA BRANDÃO KONAMI JAYSON

TO

THE DIVISION OF MEDICAL SCIENCES

IN PARTIAL FULFILLMENT OF THE REQUIREMENTS

FOR THE DEGREE OF

DOCTOR OF PHILOSOPHY

IN THE SUBJECT OF

BIOLOGICAL AND BIOMEDICAL SCIENCES

HARVARD UNIVERSITY

CAMBRIDGE, MASSACHUSETTS

APRIL 2021

©2021 CHRISTINA BRANDÃO KONAMI JAYSON
ALL RIGHTS RESERVED.

Targeting of proteins from the endoplasmic reticulum to lipid droplets: a specific requirement for mitochondrial proteins

ABSTRACT

Neutral lipid storage and metabolism in lipid droplets (LDs) is integral to energy homeostasis in eukaryotic cells. Dysregulation of LDs has been implicated in metabolic diseases including obesity and dyslipidemia. Proteins that localize to LDs play key roles in catalyzing and regulating energy storage and metabolism. Of particular interest, proteins involved in the rate-limiting steps of these processes target LDs from the endoplasmic reticulum (ER) via membrane bridges. Despite the fundamental importance of protein targeting to LDs from the ER, the mechanism by which the ER-LD bridges are formed and proteins gain access to LDs is incompletely understood.

To address this, I first tested the hypothesis that the LD Rab GTPase, Rab18, mediates ER-LD connections to facilitate protein targeting from the ER to LDs, and ultimately determined that Rab18 is not required for LD biogenesis or turnover, and does not play a key role in protein targeting from the ER to LDs. A recent genome wide screen in our lab identified numerous proteins that affect the targeting of a key triglyceride synthesis enzyme to the LD and confirmed that Rab18 is not necessary for ER to LD protein targeting. From this same genome-wide screen, I have investigated the uncharacterized protein, TMEM223, and determined that it is a mitochondrial protein that affects phospholipid homeostasis and ER function. Our results identify an important mitochondrial factor for maintenance of membrane lipid composition and further illustrate how LD phenotypes can be sensitive markers for ER membrane dysfunction.

Contents

1	INTRODUCTION	1
1.1	Lipid droplet homeostasis in physiology	1
1.2	Lipid droplet formation	3
1.3	LD catabolism	8
1.4	Interorganelle interactions	11
1.5	Protein targeting to LDs	14
2	RAB18 IS NOT NECESSARY FOR PROTEIN TARGETING	22
2.1	Introduction	22
2.2	Rab18 localizes to LDs and the ER	24
2.3	Deletion of Rab18 does not affect the structure of the ER	30
2.4	Rab18 is not required for LD biogenesis, but Rab18 deletion modestly reduces the size and numbers of LDs	30
2.5	Deletion of Rab18 does not affect the targeting of several key proteins to LDs . . .	32
2.6	Deletion of Rab18 has no effect on triglyceride turnover during cell starvation . .	36

2.7	Discussion	36
2.8	Materials and Methods	40
2.9	Author contributions	46
3	TMEM223 REVEALS A ROLE FOR MITOCHONDRIAL PROTEINS IN ERTOLD TARGETING	47
3.1	Preface	47
3.2	Introduction	48
3.3	RNAi screen for ERTOLD protein targeting identifies novel protein CG12935 as a strong determinant	49
3.4	CG12935 depletion impact on GPAT4 targeting is general for other late targeting ERTOLD proteins	51
3.5	TMEM223 is a highly conserved protein localizing to the mitochondria	55
3.6	Depletion of dTMEM223 results in ER abnormalities	57
3.7	dTMEM223 is required for cellular lipid homeostasis	60
3.8	Depletion of MICOS components QIL1 and CHCHD3 exhibit phenotypes similar to TMEM223 depletion	65
3.9	TMEM223 depletion in mammalian cells results in similar phenotypes	65
3.10	Discussion	71
3.11	Materials and Methods	74
3.12	Author contributions	88
4	CONCLUDING REMARKS	89
	APPENDIX A METHODS SUPPLEMENTARY TABLES	92

APPENDIX B GPAT_I IS SPECIFIC FOR ENDOGENOUS FATTY ACID INCORPORATION

INTO TRIACYLGLYCEROL	97
B.1 Introduction	97
B.2 GPAT _I localization	99
B.3 GPAT _I regulation	99
B.4 GPAT _I in physiology	101
B.5 GPAT _I can localize to mitochondria and LDs	101
B.6 GPAT _I is specific for the incorporation of de novo lipogenesis (DNL) derived FAs	106
B.7 GPAT _I N-terminus, and not the transmembrane domains, is necessary for mitochondria localization	106
B.8 Endogenous GPAT _I may localize to LDs only under specific metabolic conditions where GPAT _I expression is upregulated	108
B.9 Future directions	112
B.10 Materials and Methods	115
B.11 Author contributions	120
REFERENCES	144

Listing of figures

1.1	Triacylglycerol synthesis occurs at the ER from which LDs originate	4
1.2	Proteins target to LDs from the cytosol or the ER, though much remains unknown about the latter process	15
2.1	Rab18 localizes distinctly to LDs and the ER in SUM159 cells.	25
2.1	(continued)	26
2.2	Rab18 deletion does not affect ER morphology.	28
2.2	(continued)	29
2.3	Rab18 localizes distinctly to LDs and the ER in SUM159 cells.	31
2.4	LD biogenesis is not affected in Rab18 KO cells.	33
2.4	(continued)	34
2.5	Protein targeting to LDs is similar in Rab18KO and WT.	35
2.6	Rab18 deletion does not affect TG turnover.	37
2.6	(continued)	38
3.1	CG12935 is a determinant of late ERTOLD protein targeting.	52

3.1	(continued)	53
3.2	Seipin knockout bypasses the defects in ERTOLD protein targeting with CG12935 depletion.	54
3.3	TMEM223 is a highly conserved protein that localizes to mitochondria.	55
3.4	dTMEM223 localizes to mitochondria in <i>Drosophila</i> S2 R+ cells.	56
3.5	Endogenous tagging of TMEM223 in <i>Drosophila</i> S2 R+ cells.	57
3.6	dTMEM223 depletion affects ER organization and function.	59
3.7	dTMEM223 depletion alters the cellular lipidome, marked by a dramatic decrease in ceramide phosphoethanolamine.	62
3.7	(continued)	63
3.8	Depletion of MICOS components have similar effects on ERTOLD protein targeting, ER function and ceramide phosphoethanolamine levels as TMEM223 depletion.	66
3.8	(continued)	67
3.9	hTMEM223 localizes to mitochondria in a liver cell line.	68
3.10	TMEM223 is a bona fide integral membrane protein in the mitochondrial inner membrane whose depletion in mammalian cells results in similar phenotypes.	69
3.11	Depletion of CerPE synthesis enzymes, CPES and SMSr do not impair ERTOLD targeting despite altering glucosylceramide and/or CerPE levels.	73
B.1	Exogenously expressed GPAT _I localizes to mitochondria and around LDs.	102
B.1	(continued)	103
B.2	FIB-SEM studies reveal close proximity between mitochondria and LDs.	104
B.3	FIB-SEM studies reveal close proximity between mitochondria and LDs.	105
B.4	GPAT _I depletion specifically impairs incorporation of acetate derived fatty acids into triacylglycerol.	107

B.5	GPAT ₁ N-terminus prior to the predicted transmembrane domains is sufficient for mitochondrial localization.	109
B.6	GPAT ₁ transmembrane domains are not necessary for mitochondria localization and alpha helices are sufficient for LD localization.	110
B.7	GPAT ₁ localizes to mitochondria and LDs in various mammalian cell lines.	111
B.8	Endogenously tagged GPAT ₁ localizes to mitochondria and high expression promotes LD localization.	113
B.9	GPAT ₁ colocalizes with enzymes of de novo lipogenesis at the mitochondria and LDs.	114

I DEDICATE THIS THESIS TO MY PARENTS, ROBERT E. JAYSON AND DENISE M. JAYSON,
WITHOUT WHOM I WOULD NOT BE THE WOMAN, THE SCIENTIST, THE PERSON I AM TODAY.
THANK YOU FOR ALWAYS BELIEVING IN ME SINCE DAY 1.

Acknowledgments

There is a paper I cite with the title “It takes a village”³⁸ and this proverb rings true not only for fatty acid channeling, but for the completion of this thesis. It took a village to complete this dissertation. I have many people to thank, more than are acknowledged here, but who know the impact they have had on me.

To start, I'd like to thank my advisors, Dr. Bob Farese and Dr. Tobi Walther for the opportunity to work in their laboratory and for connecting me to many brilliant scientists and fruitful opportunities. I am grateful for the time they invested in me scientifically; with their guidance I became a critical thinker and better science communicator. I am also grateful for their support of my professional development, the freedom to participate in internships in industry and technology transfer, and for believing in me as I developed my career goals. I am also grateful for the mentors I had within the lab. Thank you to Dr. Michel Becuwe and Dr. Niklas Mejhert, who were my rotation mentors and good friends, and thank you to Dr. Henning Arlt and Dr. Jeeyun Chung for their collaboration and scientific advice. These incredible post-doctoral fellows were instrumental in my scientific training. I would also like to thank the entire Farese and Walther lab, both past and present members, for scientific feedback, support and fun memories. I particularly want to thank Dr. Laura

Bond and Dr. Pedro Carpio Malia for their friendship and for always being there to listen, to share a laugh, and to provide or help me consume delicious lab fuel/food.

I wish to thank the members of my dissertation advisory committee, Dr. Susan Shao, Dr. Vlad Denic and Dr. Wade Harper for their advice and perspective – I left every committee meeting feeling motivated and am grateful for the time they took to meet with me outside of our committee meetings.

I am grateful for the funding that I have received over the years from the National Science Foundation Graduate Research Fellowship for the first two years and from the National Defense Science and Engineering Graduate Fellowship for the final four years.

I am also grateful for the mentors I have had outside the lab. In particular I want to thank two incredible women: Dr. Bridget Wagner, who has been my mentor through the Harvard Graduate Women in Science and Engineering association and has helped me navigate challenging situations, develop and achieve my career goals, and has always been there to celebrate accomplishments; and Dr. Cindy Hong, who was my manager during my internship at Pfizer and who has helped me achieve fellowships, identify career goals and who has continued to remain a mentor and champion for me. Both of these women inspire and motivate me to dream big and believe in myself, and I am privileged to have their mentorship.

I also wish to express my gratitude for my BBS family – from potluck dinners and wine and whine nights, to ski trips and dance nights, to overcoming imposter syndrome, to celebrating engagements, marriages, new life and new PhDs, these people have kept me laughing and lifted me up when the going got tough. A special thank you to Rebeca Borges Monroy for being the best roommate, maid-of-honor and friend I could have ever asked for; our friendship means so much to me.

Most importantly, I want to thank the people who have been with me through it all and who have shaped me to be the person I am today. I would not be here today without the love and support of my parents, Rob and Denise Jayson and my little sister, Jessica Jayson. Thank you for the

sacrifices you have made to allow me to pursue my dreams and for supporting my endless nerdiness. A big thank you as well to my grandparents, Lloyd and Mae Nishimoto, and the entire Nishimoto clan, my aunts, uncles, and cousins, for the love, laughter and support at every stage in my life. My entire family has shaped me and inspired me throughout my life. I would also like to thank my in-laws André, Mariétte, Érica and the entire Brandão and Baggio families in Brazil for making me feel like family from the beginning.

Finally, I wish to thank my *outra metade da laranja*, my best friend, my source of endless love and laughter, who brings out the best in me, who literally and figuratively lifts me up, my husband, Hugo Brandão. I'm so grateful you found me in those first few months of my PhD as this adventure and the many others we have had would not have been nearly as fun without you. I'm looking forward to our next adventures together as Dr. Brandão and Dr. Jayson!

1

Introduction

1.1 LIPID DROPLET HOMEOSTASIS IN PHYSIOLOGY

LDs are dynamic organelles composed of neutral lipids (i.e. triacylglycerols [TG] and cholesterol esters) bound by a phospholipid monolayer in which enzymes involved in a myriad of functions, including TG synthesis and lipolysis, are embedded^{45,206,225}. Neutral lipids stored in LDs originate from exogenous lipoproteins or are synthesized via de novo lipogenesis^{20,232}. The biogenesis

and subsequent expansion of LDs occur at the ER where many neutral lipid synthesis enzymes are located^{20,225,234,232}.

The regulation of TG storage and metabolism from LDs is crucial to meet the cell's energy and proliferation demands. Under nutrient rich conditions, LDs expand to store excess lipids^{225,232}. Conversely, under conditions of nutrient deprivation free fatty acids (FFAs) are rapidly mobilized from LDs¹²¹. Similarly, FFAs are mobilized from LDs during conditions of cell growth to provide building blocks for phospholipids of expanding membranes²²⁵. The production and fate of FFAs is a tightly regulated process as excess FFAs are toxic to the cell. Moreover, dysregulation of fatty acid (FA) metabolism or FA trafficking can have severe consequences for cellular homeostasis, namely in the form of lipotoxicity. Lipotoxicity, the toxic accumulation of excess lipids in non-adipose tissues, is strongly associated with obesity-related diseases such as nonalcoholic fatty liver disease, cardiovascular disease, and diabetes^{43,52,140,255}. Lipotoxicity gives rise to insulin resistance and, if unaddressed, ultimately leads to cellular dysfunction and cell death^{2,5,43,255}.

LDs are also the main site for cholesterol storage and are thus implicated in cholesterol storage diseases²³⁹. Excessive accumulation of cholesterol ester containing LDs in macrophages that result in foam cell formation is a hallmark of atherosclerosis²⁴⁸. Many proteins associated with LDs, such as the cell death-inducing DNA fragmentation factor-like effector (CIDE) protein family and the perilipin, ADFP and Tip47 (PAT) family have been shown to play key roles in the formation and stabilization of atherosclerotic foam cell LDs^{7,243,248}. Furthermore, LDs have been implicated in viral infection, namely in Hepatitis C virus (HCV) infection and other RNA viruses^{24,135,143}. In HCV and Dengue Virus (DENV), viral proteins associate with LDs and hijack the LD as a site for assembly and replication of the virus that causes chronic liver disease^{24,27,135}. In DENV infections, LD binding of viral proteins is dependent on LD surface proteins, and these viral proteins recruit enzymes involved in fatty acid synthesis to sites of viral replication to provide a source of energy^{27,77}. Intriguingly, recent studies suggest that LDs may also be important for replication of

the novel SARS-Cov-2 (COVID19) virus⁶². Finally, imbalance in lipid storage is the underlying cause of neutral lipid storage disease (NSLD) – a disease of excessive lipid storage across tissues – and lipodystrophy – the inability to store lipids in adipose tissue^{114,239}. Both diseases are caused by mutations in genes involved in either lipid synthesis, catabolism or storage in LDs, highlighting the importance of LD homeostasis in physiology²³⁹.

1.2 LIPID DROPLET FORMATION

1.2.1 NEUTRAL LIPID SYNTHESIS

Triglycerides (TGs) are synthesized by cells to store FAs that can be later metabolized for energy or used as a building block for membrane phospholipid synthesis. When nutrients are in excess, TG synthesis increases and TGs are subsequently stored in LDs or secreted by the liver as very low-density lipoprotein (VLDL) particles²²⁵. As previously mentioned, dysregulation of TG synthesis and storage are associated with metabolic diseases such as diabetes and non-alcoholic fatty liver disease (NAFLD)^{26,60,72}. Therefore, understanding the molecular mechanisms of TG synthesis can provide insight into understanding the underlying pathology of these diseases.

TG synthesis can occur via two different pathways using exogenous FAs – FAs taken up by the cell from the extracellular environment – or endogenous FAs – FAs converted from excess carbohydrates. Studies have shown that numerous cell types prefer to use exogenous FAs for membrane or structural lipids^{132,244}. Exogenous FFAs are incorporated into the cell either via transport across the plasma membrane by CD36 or uptake of lipoproteins^{59,133,153}. In the cytosol, FFAs are esterified by long chain acyl-CoA synthetases (ACSLs) to generate fatty acyl-CoAs used in downstream TG synthesis steps at the endoplasmic reticulum (ER). Endogenous FAs are generated via the process of de novo lipogenesis (DNL)^{132,186}. Under conditions of excessive glucose or upregulation of DNL enzymes in cancer cells¹³², citrate produced by the Krebs' cycle in the mitochondria

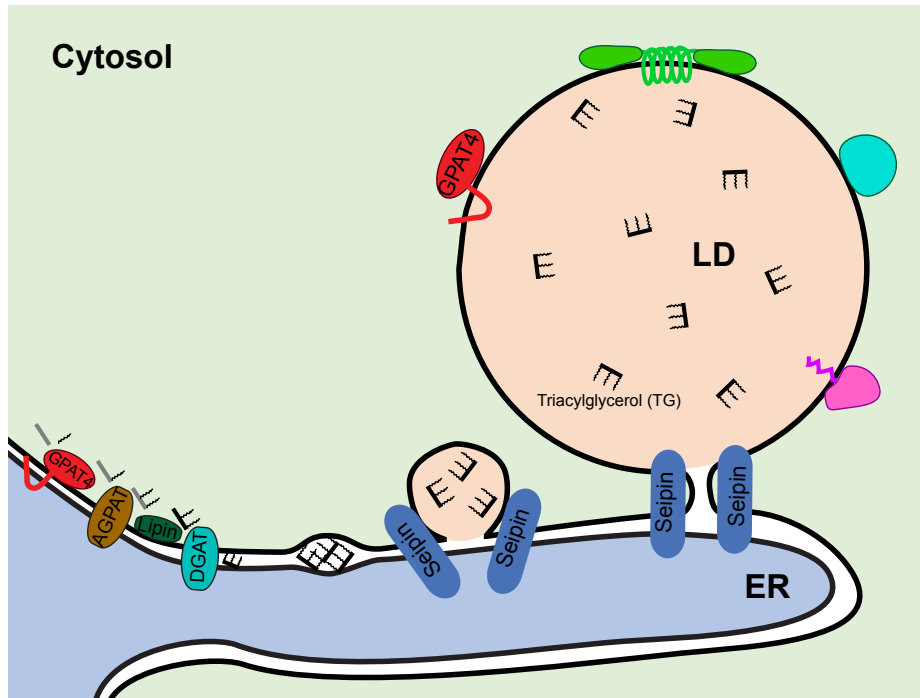


Figure 1.1: The enzymes of triacylglycerol synthesis localize to the ER bilayer where TG is synthesized and accumulates within the ER bilayer. With the help of proteins such as seipin, the TG lenses emerge as LDs that themselves become sites for protein localization and activity to maintain LD homeostasis.

is exported into the cytosol where it is converted by ATP-citrate lyase (ACLY) into acetyl-CoA. Acetyl-CoA is then converted to malonyl-CoA by acetyl-CoA carboxylase (ACC). Acetyl-CoA and malonyl-CoA are then combined by fatty acid synthase (FASN) and after a series of modifying steps, the FA palmitoyl-CoA is available for TG synthesis^{4,186}. TG synthesis begins with the enzyme glycerol-3-phosphate acyltransferase (GPAT) to generate lysophosphatidic acid (LPA) from a fatty acyl-CoA and a glycerol-3-phosphate molecule. LPA is handed off to sn-1-acylglycerol-3-phosphate O-acyltransferase (AGPAT) for the synthesis of phosphatidic acid (PA), which is converted to diacylglycerol (DG) by lipin, and the final step of TG synthesis is catalyzed by diacylglycerol acyltransferase (DGAT) (Figure 1.1). These enzymes mainly localize to the ER to coordinate TG synthesis at the ER bilayer for downstream storage in LDs or secretion²²⁵.

The rate-limiting step of TG synthesis is GPAT. There are four major isoforms of GPAT: GPAT₃ and GPAT₄ are mainly ER-localized isoforms, and GPAT₁ and GPAT₂ are mitochondrial isoforms^{231,242}. GPAT₁ is highly expressed in the liver and its regulation will be discussed in greater detail in Chapter 3. GPAT₃ and GPAT₄ are most prominently expressed in white and brown adipose tissue respectively^{202,236}. Their activity is upregulated by insulin stimulated phosphorylation²³⁶. Studies have shown that GPAT₄ relocates from the ER to expanding LDs to facilitate LD growth²³⁴. The microsomal localization of GPATs and the other members of TG synthesis is important for the accumulation of TG in the ER bilayer for LD biogenesis.

1.2.2 LD BIOGENESIS FROM THE ER

LD biogenesis originates at the ER with the accumulation of TG in between the ER bilayer leaflets^{154,209,224}. From a biophysical perspective, at equilibrium concentration of TG in the ER it is thermodynamically favorable for the TG in the ER bilayer leaflets to accumulate in lenses or oil blisters^{210,224,256}. Molecular dynamics studies reveal that the oil blister formation in ER bilayers can be described by a liquid-liquid phase separation (LLPS) process: TGs in lipid bilayers have

liquid-like behavior that, at equilibrium with concentrations above 4%, form lenses that are capable of coalescing, fusing and have exchange of TG molecules between the condensed TG lens and diluted TG phases^{106,256}. This suggests that TG lenses can form spontaneously, however, many other factors are involved to determine sites and directionality of LD.

Physical properties of the ER membrane play a key role in determining the sites of TG lens nucleation. Spontaneous lens formation occurs and remains stable at areas of high curvature in molecular dynamics simulations²⁵⁶, and in mammalian cells, nascent LD formation is enriched at ER tubules where there is higher membrane curvature¹⁷³. This may be because at sites of high curvature and membrane deformation due to phospholipid packing defects, TG accumulation may be energetically cheaper.

Phospholipid composition and density are also crucial for the directionality of LD emergence from the ER bilayer^{32,33,13}. Studies have shown that specific phospholipids – phosphatidylinositol (PI), and Lyso-phosphatidylcholine (Lyso-PC) or di-palmitoyl-phosphatidylcholine (DPPC) mixed with phosphatidic acid (PA) – decrease surface tension of the ER membrane, which favors LD budding^{33,13}. On the other hand, phospholipids with negative intrinsic curvature – phosphatidylethanolamine (PE) and diacylglycerol (DG) – do not favor LD budding, rather they favor the initial steps of TG lens formation in the ER^{33,256}. Furthermore, the directionality of LD budding depends on phospholipid excess; in that LDs bud toward the side of the ER bilayer that has excessive phospholipids³².

While studies have shown that phospholipid composition, physical properties of the membrane and the biophysical properties of TG permit spontaneous formation of TG lenses and LD budding from the ER, proteins influence the localization of these events by modifying all three of these aspects. Studies in yeast have shown that Pet10, the homologue of perilipin, can bind DAG in the ER and promote TG aggregation into LDs²⁵⁶. Perilipins are proteins containing amphipathic helix 11-mer repeats that bind to defects in phospholipid packing and therefore early TG lenses

and LDs^{200,199}. There are five perilipin genes expressing perilipin 1 through 5; these genes are differentially expressed across tissue types²⁰⁰. While perilipins function to protect LDs from lipolysis^{200,199,127}, they are also observed to bind TG lenses at the earliest stages of LD formation³⁵. Studies have shown that overexpression of perilipin 2 (PLIN2/ADRP) increases TG and sterol ester levels, and overexpression either PLIN1, PLIN2/ADRP or PLIN3/Tip47 induces LD formation⁹⁷ suggesting that perilipin localization to early TG lenses plays an important role mediating LD formation.

Similarly, the enzyme pah1, homologue to lipin that synthesizes DG from PA, is important for local DG concentrations in the ER that promoted LD formation^{3,256}. The enzyme FIT2, that is known to bind DG^{34,68} and was recently shown to acyl-CoA diphosphatase enzyme¹¹, is also important for LD formation and normal budding; perhaps due to its ability to bind DG and reduce levels near LD formation that would be inhibitory to LD budding¹¹.

Certain proteins may also play a role in marking sites of LD formation. Seipin is a widely studied protein shown to be involved in LD formation^{173,224,227,229} (Figure 1.1). Seipin localizes to sites of LD synthesis and is enriched at ER tubules where there is higher membrane curvature¹⁷³. Seipin forms a ring-shaped dodecamer at the ER, and each monomer has a hydrophobic helix at the ER luminal leaflet and two transmembrane domains that span the ER bilayer^{35,196}. It is this hydrophobic helix that allows seipin to target to LDs(Sui et al., 2018). As TG accumulates into lenses, it introduces packing defects of phospholipids in the ER membrane²⁰⁸. As hydrophobic helices and amphipathic helices (further discussed below) preferentially bind membranes with packing defects¹⁵⁶, this may contribute to seipin localizing to neutral lipid lenses. Recent studies show that the hydrophobic helix is also required for interaction with LDAF1, which forms a complex with seipin and is crucial for defining the site of initial LD formation³⁵. In the absence of LDAF1, cells accumulate similar levels of TG but LD formation is impaired, indicating that the LDAF1-seipin complex, and not seipin alone is important for LD formation³⁵. Interestingly, LDAF1 dissociates from

seipin and remains coating the LD monolayer as LDs emerge from the ER, and its depletion from the ER and onto LDs could be a regulatory mechanism for LD formation^{35,227}. As the phospholipid and protein composition of LDs is distinct from the ER, it is hypothesized that the LDAF1-seipin complex may act as a diffusion barrier for proteins and lipids⁶⁵.

1.2.3 LD EXPANSION

In the final steps of LD formation, LDs bud from the ER on the cytosolic side and this directionality is mediated by previously mentioned membrane asymmetry³², phospholipid^{32,33,13}, biophysical^{256,13} and protein factors^{32,229,208}. It remains unclear if LDs remained attached at LDAF1-seipin marked sites or if there is a fission event that separates the two organelles. There is evidence in yeast and *Drosophila* that LDs remain attached to the ER⁹⁶. After LD budding into the cytosol, LDs continue to expand, and the distinction between initial LDs and expanding LDs is most prominent in *Drosophila* cells, though is not limited to this model system^{224,234}. Initial LDs are observed anywhere from minutes to hours after nascent LDs depending on the model system, and they are typically greater than 250 nm¹⁹⁷. Expanding LDs can be upwards of 1 μ M in size²³⁴. In *Drosophila* cells, two sub-populations of LDs are observed^{227,234}, while in some mammalian cells (ie Cos-7) LD size is heterogenous within a cell^{224,160,197,207}. Other mammalian cells like adipocytes have a single unilocular LD that can grow to be up to 100 μ M in size¹⁹⁷. The expansion of LDs to larger sizes from their initial formation may be facilitated by the relocalization of a subset of TG synthesis enzymes from the ER to LDs²³⁴.

1.3 LD CATABOLISM

An important aspect of LD biology is the mobilization of TG and cholesterol esters stored in the LDs to be used as membrane building blocks or metabolized for energy. There are two main mecha-

nisms by which this process occurs: lipolysis, where enzymes located on the LD surface catalyze the hydrolysis of TG in a step-wise fashion, or lipophagy, a selective form of macroautophagy specific to LDs where LDs are trafficked to the lysosome for degradation of lipids and proteins^{145,209,250}. Different cell types rely more heavily on one pathway versus the other; for example lipophagy was first identified and since been shown to play a key role in lipid turnover in liver^{182,178}. Dysregulation of either pathway has been implicated in numerous lipid storage and lipid metabolism diseases¹⁰⁷.

1.3.1 LD LIPOLYSIS

The first and rate-limiting step of LD lipolysis is the hydrolysis of TG to diacylglycerol and FFA by adipose triglyceride lipase (ATGL) at the LD membrane^{58,254,66}. Downstream of ATGL, hormone sensitive lipase (HSL) and monoacylglycerol lipase (MAG) further hydrolyze DAG to FFAs and, ultimately, glycerol¹²¹.

The enzymatic activity of ATGL is controlled by a series of regulatory mechanisms^{251,249,184,254}. CGI-58/ABHD5 on LDs is the required coactivator protein whose association with ATGL is prevented by interaction with PLIN1 (in *Drosophila*, Lsd-1)^{195,251,14}. Studies have also identified fat specific protein - 27 (FSP27) as an interactor of ATGL, whose binding reduces lipolysis of LDs⁶⁴. In the signaling pathway, cAMP signaling activates protein kinase A (PKA), which phosphorylates PLIN1 and HSL^{251,121,249}. Phosphorylation of PLIN1 causes it to release CGI-58, which associates with ATGL, inducing its activity¹⁹⁵. Phosphorylation of HSL causes its association with phosphorylated PLIN1 on LDs. In cells that lack PLIN1, such as skeletal muscle, it is unclear what mechanisms mediate HSL access to LDs. HSL is also regulated by insulin levels, as insulin inhibits HSL enzyme activity strongly²⁵¹. Stimulation of lipolysis has been shown to alter the LD proteome¹⁹; for example, in adipocytes stimulated with isoproterenol to induce lipolysis, the Rab GTPase, Rab18, has increased localization to LDs¹³¹. Such lipolysis induced changes suggest that the lipid droplet proteome plays a key role in regulating LD homeostasis.

During nutrient deprivation, hydrolyzed FFAs are somehow trafficked to the mitochondria for FA oxidation (FAO). FAO in mitochondria generates acetyl CoA, NADH and FADH₂ for ATP production²²⁶. The FAO machinery resides in the mitochondrial matrix; consequently, FAs must be imported across the mitochondrial outer and inner membranes to be oxidized. This FA import is dependent on carnitine palmitoyl transferase 1 (CPT1)¹⁴⁶. There are multiple hypotheses for the mechanism by which FAs are trafficked to mitochondria for FAO, such as at membrane contact sites between mitochondria and LDs; simple diffusion in the cytosol; soluble lipid transport proteins that deliver FAs to mitochondria from LDs^{81,162,193,198}. Mitochondria-LD interactions are further discussed in the following section.

1.3.2 LD AUTOPHAGY - LIPOPHAGY

Studies in liver cells revealed that inhibition of autophagy led to increased levels of TG suggesting a role for autophagy in the mobilization of lipids stored in LDs¹⁸². Both macrolipophagy - involving the canonical autophagosome-mediated pathway for delivery of LDs to autolysosomes - and microlipophagy - the transient and directed interactions of lysosomes with LDs that function to degrade lipids from LDs - have been studied in LD biology¹⁷⁸. Studies have shown that autophagy coordinates with lipolysis under conditions of starvation to protect against a flux of free FAs released from lipophagy¹⁶². Namely, during starvation conditions, FAs released by lipophagy flux into LDs and are then trafficked to mitochondria for β -oxidation¹⁶². Intriguingly, studies have shown that the autophagosome marker LC₃ is able to interact with ATGL at the LD surface, suggesting that ATGL regulates LD turnover by autophagy¹⁷⁸. Other players, including Rab GTPases that localize to LDs, have been implicated in promoting LD autophagy. Rab7, for example, has been shown to localize to LDs under nutrient deprivation conditions and its depletion impairs LD colocalization with lysosomal markers as well as autophagic flux¹²⁹. Alternatively, Rab18 localizes to LDs and its depletion also impaired autophagic activity⁴⁶. This pathway for LD turnover is not unique to

hepatocyte; β -adrenergic signaling in adipocytes promoted Rab7 dependent lipophagy¹⁷⁸ and in enterocytes, lipophagy plays a key role in TG distribution and turnover¹⁰⁵. The balance between lipolysis and lipophagy is an important aspect of LD homeostasis, and is potentially regulated by LD size¹⁷⁵; the interplay is still under active investigation¹⁰⁷.

1.4 INTERORGANELLE INTERACTIONS

Inter-organelle associations are emerging as a major mechanism for transferring lipids between organelles, and have been implicated in the transfer of FAs from LDs to peroxisomes and between the endoplasmic reticulum (ER) and LDs^{15,225}. For the purpose of this thesis, interactions between mitochondria, ER and LDs will be the focus of this section.

1.4.1 ER-LD INTERACTIONS

Numerous studies have identified protein interaction pairs involved in tethering or connecting the ER and LDs and a few are highlighted here^{16,177,170,93}. As previously discussed, LDs originate from the ER and studies in yeast suggest they may form continuous contacts with the ER throughout their lifetime⁹⁶. The previously discussed protein seipin complexes with Fld1/Ldb16 in yeast to stabilize ER-LD connections during formation as well as to maintain ER-LD association at later points^{65,169,171}. Additional ER-LD interaction proteins have been identified in *Caenorhabditis elegans* (c. elegans) such as FATP1 at the ER and DGAT2 at the LDs, which is thought to mediate a TG synthesis complex for efficient LD growth²³⁸. Another ER resident protein, Snx14, is able to bind to LDs through its C-terminal amphipathic helix; overexpression of Snx14 enhances ER-LD contacts and loss of Snx14 decreases ER-LD contacts suggesting a role in mediate ER-LD contact⁴¹. Recently, VPS13A and VPS13C have been identified at ER-LD contact sites and are posited to help transfer lipids between these membranes¹¹⁹. One key complex thought to be involved in ER-LD

interactions is the ER localized NRZ (NAG, RINT1, ZW10) complex^{125,237,56}. The Rab GTPase, Rab18, that localizes to the ER and LDs was shown to interact with components of the NRZ complex^{237,56}, which may be important for LD homeostasis. Unpublished research from our lab has identified the Rab GTPase Rab1 as a component of ER-LD tethering that may also interact with the NRZ complex and be crucial for protein mobility from the ER to LDs; this process will be discussed in depth in the next section.

1.4.2 MITOCHONDRIA-LD INTERACTIONS

Extensive confocal and electron microscopy (EM) of cultured cells and isolated tissue have revealed that mitochondria and LDs become closely associated under conditions of lipolysis or nutrient deprivation^{5,37,81,162,246,252}. Additionally, studies using Förster resonance energy transfer (FRET) have indicated that mitochondria and LDs in association are within 10 nm¹⁹⁴. Proteins functioning as tethers may mediate this close association; such tethers play a key role in forming established membrane contact sites (i.e. between the ER and mitochondria)¹⁵⁷. Currently, only a few proteins are known to localize to both mitochondria and LDs that could be potential candidates. One protein of interest to this proposal is vacuolar protein sorting-associated protein 13C (VPS13C), which has been identified in separate studies as an LD protein and is associated with the mitochondria outer membrane¹²³. Its association to both mitochondria and LDs suggests a role in mitochondria-LD associations.

Proteomic studies also strongly support mitochondria and LD interaction during nutrient deprivation. Studies in 3T3L1 adipocytes identified mitochondrial proteins in the LD proteome only under conditions of lipolysis stimulation¹⁹. Furthermore, in proteomic studies of skeletal muscle, a highly oxidative tissue, mitochondrial proteins were selectively enriched in the LD fraction, and this finding was supported by observation of mitochondria in close association with LDs by transmission electron microscopy (TEM)²⁵². These observations point to mitochondria-LD associations

having a specific role during nutrient deprivation. However, how these associations are mediated and their physiological function remains unclear.

1.4.3 ER-MITOCHONDRIA INTERACTIONS

Of similar importance are the interactions between the ER and the mitochondria. This interaction has been characterized by an intermediate sub-domain of the ER and mitochondria membranes termed the mitochondria-associated membranes (MAM)²¹⁸. The MAM is a region of the ER that is enriched in specific proteins and is the proposed location for numerous processes that occur between the ER and mitochondria, namely calcium transport and lipid metabolism^{218,164,167}. One key exchange that occurs between the mitochondria and the ER is that of phospholipids, specifically phosphatidylserine (PS) and phosphatidylethanolamine (PE)²²⁰. It has been reported that the enzyme phosphatidylserine synthase, which catalyzes the formation of PS from CDP-DAG, is enriched at the MAM¹⁹². This provides a convenient substrate for the mitochondrial localized enzyme phosphatidylserine decarboxylase proenzyme (PISD), which converts PS to PE at the mitochondria^{189,29}. The exchange of phospholipids between the mitochondria and the ER is crucial for both of their functions; disruption in mitochondrial PE synthesis results in impaired mitochondrial fusion, oxidative phosphorylation and embryonic lethality in mice^{220,203,29,189,79}.

The efficient exchange of phospholipids between these two organelles is also mediated by the mitochondrial contact site and cristae organizing system (MICOS)¹⁰⁹. MICOS is composed of two subcomplexes, Mic27/Mic10/Mic12/QILI and Mic60/CHCHD3/Mic25, that make up a machinery localizing in the mitochondrial inner membrane to cristae junctions^{50,163,235}. Each subunit is crucial for the overall function of MICOS in maintaining cristae architecture, organization of the electron transport chain, mitochondrial DNA segregation and therefore biogenesis and inheritance of mitochondria^{228,50,163,69,214}. Importantly, MICOS has strong genetic interactions with the ER mitochondria encounter structure (ERMES) in yeast, which are similar to MAMs in mammalian

cells⁸⁹. Further studies in yeast have shown that the transfer of PS by the Ups2-Mdm35 complex requires MICOS^{1,136}. These studies also revealed that MICOS facilitated the synthesis of mitochondrial PE which was important for the conversion of PE to PC at the ER, strongly suggesting a key role for MICOS in phospholipid exchange between the mitochondria and the ER¹. However, it is unclear how MICOS mediates this phospholipid transfer; some hypothesis include that MICOS may mediate the exchange of phospholipids between the inner and outer mitochondrial membranes for transport between the mitochondria and ER¹.

1.5 PROTEIN TARGETING TO LDs

Lipid droplets have a unique proteome that differs based on cell type. While some LD proteins are consistent across cells, making up a core proteome of around 50 proteins^{85,207}, the overall LD proteome across cell types differs, and even within the same cell type protein composition may differ between LDs²⁰⁷. A fascinating aspect of the LD proteome is how these proteins localize to the LDs.

1.5.1 CYTOSOL TO LD (CYTOLD) PROTEIN TARGETING

The current model for protein targeting to LDs divides LD proteins into two classes (Figure 1.2)¹¹⁰. Proteins that target LDs from the cytosol proteins are termed here Cytosol TO LD (CYTOLD) targeting proteins. These proteins localize to the LD monolayer based on secondary structure motifs: amphipathic helices, or multiple amphipathic and hydrophobic helices. The LD monolayer is subject to phospholipid packing defects and it is to these defects that the large, hydrophobic residues of amphipathic helices bind to¹⁵⁶. However, the binding of these proteins to LDs is also subject to protein crowding. As LDs are dynamic organelles central to neutral lipid storage, their size is determined by the metabolic conditions of the cell. Mobilization of neutral lipids in the hydrophobic core – TG and cholesterol ester molecules – during lipolysis decreases the surface area of the LD¹¹¹.

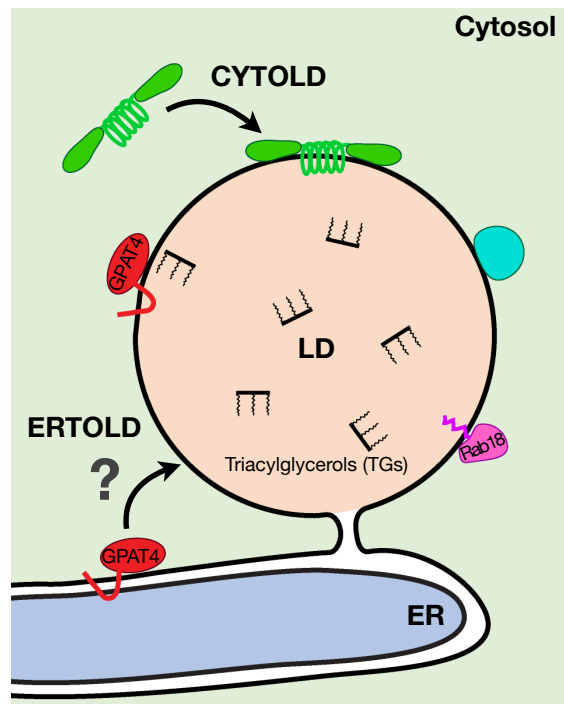


Figure 1.2: Protein targeting from the cytosol to LDs (CYTOLD) relies in many cases on secondary structure, while protein targeting from the ER to LDs (ERTOLD) is incompletely understood and the focus of this thesis.

The consequence of this is fewer packing defects and a displacement of CYTOLD proteins¹¹¹. This can also be observed with overexpression of some LD proteins; their increased binding to LDs leaves no room for CYTOLD proteins to bind¹¹⁰. Studies have also shown that the ratio of PE to PC (PE:PC) is critical for protein targeting to LDs, and that the targeting of CTP:phospho-choline cytidyltransferase (CCT) to LDs from the cytosol is important to maintain LD localized PC homeostasis¹¹³. Alternative mechanisms by which CYTOLD proteins target LDs is via lipid anchors (such as Rab GTPase proteins) or via binding to other LD associated proteins¹¹⁰.

1.5.2 ER TO LD (ERTOLD) PROTEIN TARGETING

The second class of proteins originate from the ER (ERTOLD) and are thought to localize to LDs upon LD formation from the ER or to localize to LDs at later time points via reconnection of LDs to the ER through ER-LD bridges^{110,234,233}. Examples of these proteins include GPAT₄, involved in TG synthesis and LD expansion²³³, and ATGL, the rate-limiting step for lipolysis¹²¹. ERTOLD proteins lack an ER luminal domain, allowing them to embed in either the ER membrane or LD monolayer by hydrophobic sequences that often form a hairpin structure¹⁴⁴. Molecular dynamics simulation studies of the hairpin motif have shown that the amino acid tryptophan and positively charged residues are required for LD accumulation of the protein¹⁴⁴. Within ERTOLD proteins, there are some that translocate from the ER to the LD monolayer at the initial stages of LD formation. An example of this is the previously mentioned LDAF₁ who remains on the LD monolayer, dissociating from seipin, as the LD begins to bud³⁵. Alternatively, some ERTOLD proteins relocalize from the ER to LDs at later stages in the LD life-cycle via membrane bridges between the two organelles^{110,234} (discussed below). GPAT₄ is characteristic of the latter group of proteins, and has been studied extensively as a read out for later ERTOLD protein targeting^{233,234,144,227}. Particularly in *Drosophila* S2 cells, GPAT₄ has been shown to localize to the ER in the absence of LDs, and then translocate to LDs about 3 hours after their induction with FA incubation²³⁴. This

is in contrast to proteins like LDAF1 that localize to LDs within a few minutes of incubation with FAs³⁵. Intriguingly, GPAT4 targeting to LDs in *Drosophila* S2 cells also reveals that there are distinct sub-populations of LDs, as GPAT4 only targets some, not all LDs²³⁴. Studies have also tested if this is due to two independent lineages of LDs or if LDs can acquire GPAT4 after initial formation, and shown that GPAT4 can translocate rapidly to LDs that were initially formed without GPAT4²³⁴. Targeting to a subset of LDs is also observed for other later ERTOLD proteins such as Ldsdh1 in *Drosophila* cells²¹². On average, both GPAT4 and Ldsdh1 localize to a subset of larger LDs, suggesting that the size or metabolic status of the LD influences protein targeting^{212,234,175}. Interestingly, CCT also targets the same subset of LDs as GPAT4, suggesting that these droplets are indeed expanding as CCT specifically localizes to expanding LDs by detecting deficiencies in monolayer PC^{113,234}.

Live imaging studies with GFP tagged GPAT4 have revealed that, upon photo-bleaching of fluorescently tagged GPAT4 localized to LDs in a fluorescence recovery after photobleaching (FRAP) assay, GPAT4 from the ER migrates back to the photo-bleached LD via what look like membrane connections, or bridges²³⁴. These and other studies detailed below support a model in which proteins like GPAT4 translocate to the LD from the ER via membrane bridges²³⁴.

1.5.3 ER-LD MEMBRANE BRIDGE FORMATION

The current model for late ERTOLD protein targeting is via membrane bridges that form between the ER and LDs. This bridge is thought to be different than the ER-LD formation bridge mediated by Seipin. These are best visualized by thin-section electron microscopy (EM) analysis of *Drosophila* cells, where membranous continuities, termed ER-LD bridges due to their architecture, are observed between the ER and LDs²³⁴. Elegant cell fusion assays have also revealed that Arf1/COPI facilitate bridge formation²³³. Arf1/COPI had been previously identified in a genome wide screen for factors involved in LD formation⁷¹. Depletion of either Arf1 or COPI subunits in

Drosophila S2 cells led to LDs of a uniform size, impaired targeting of ATGL and GPAT₄ to LDs, and impaired lipolysis^{12,71,187,233}. ATGL is thought to translocate to LDs via similar mechanisms as GPAT₄. Both of their targeting is inhibited by Brefeldin A treatment, which stabilizes the inactive form of Arf1 and causes dissociation of COPI from membranes, further supporting Arf1/COPI involvement in ERTOLD protein targeting^{187,233}. As COPI is typically involved in retrograde Golgi-ER trafficking, this group also investigated the relationship between ER exit sites (ERES) and ER-Golgi intermediate compartments with LDs, observing close apposition between the two¹⁸⁷. ERES are specialized membrane regions of the ER where membrane trafficking between the ER and Golgi occurs, and in some species goes through the ERGIC, which is an intermediate compartment between the ER and Golgi¹²⁰. While it has been suggested that ATGL protein targeting occurs via ATGL-containing vesicles budding from the ERES or ERGIC and fusing with pre-existing LDs, another interpretation is that the machinery used for membrane tethering and fusion of vesicles at the ERES and ERGIC are repurposed for ER-LD membrane fusion.

Further supporting the role of Arf1/COPI in ERTOLD protein targeting, Arf1/COPI machinery have been localized to LDs, and in vitro are capable of budding nano-LDs from an oil-water interface covered by phospholipids²⁰⁶. These studies suggest that Arf1/COPI may act directly on LDs to bud off nano-LDs, thereby modifying the phospholipid composition of LDs, increasing the surface tension and making reconnection with the ER favorable^{206,233}. This function would be consistent with the vesicular trafficking function of Arf1/COPI, in which Arf1 recruits the COPI coatamer to the Golgi apparatus for the budding of coated transport vesicles for retrograde Golgi to ER protein and membrane trafficking^{247,6}.

Another more recent genome wide RNAi screen in *Drosophila* S2 cells for modulators of ERTOLD protein targeting revealed that protein factors involved in membrane fusion are required in addition or Arf1/COPI (J. Song, unpublished). These studies also support the notion that seipin may act as a protein diffusion barrier during LD biogenesis, as deletion of seipin on top of deple-

tion of these required protein factors is able to rescue ERTOLD targeting that is thought to occur via bridges (J. Song, unpublished). Separate studies are also supportive of this model, as deletion of seipin alone leads to earlier targeting of GPAT₄ to LDs, in the timescale of minutes similar to proteins like LDAF₁²²⁷. This could be achieved either by increased connections between the ER and LDs in the absence of seipin or via access of ER proteins to the LD via seipin connections²²⁷. Based on hits from this unpublished screen and others' work, our current model of ER-LD membrane bridge formation is as follows step-wise:

1) Rab₁ is recruited to the LD monolayer by the TRAPP complex^{102,211}. The TRAPP complex has been shown to bind to COPI coated vesicles, suggesting that Arf₁/COPI may also have a role in triggering the membrane fusion steps^{241,245}.

2) Membrane tethering between the ER and LDs occurs, mediated by Rint₁ of the Dsl₁ complex. The Dsl₁ complex, which in mammals is known as NRZ composed of NAG, RINT₁ and ZW₁₀, that has been shown to protrude from the ER membrane to tether COPI coated vesicles in retrograde Golgi-ER trafficking^{201,102,211}.

3) SNAREs (Soluble N-ethyl-maleimide-sensitive fusion protein Attachment protein REceptor) mediate ATP dependent membrane fusion of the LD monolayer with the cytosol leaflet of the ER bilayer. SNAREs are demonstrated to bestow intracellular membrane trafficking specificity by the specific combination of SNAREs involved³⁰. For a successful SNARE mediated fusion reaction, a SNARE from each subfamily of SNAREs (Qa, Qb, Qc and R) is required to form a productive complex for membrane fusion^{87,17}. In the screen, one SNARE from each subfamily was identified as necessary from ERTOLD protein targeting (Bet₁, Syntaxin₅, membrin/Gos27, and Ykt6). Moreover, the combination of SNAREs was unique, suggesting that this particular SNARE complex imparts specificity on ER-LD membrane fusion. Importantly, while SNAREs typically promote complete fusion of bilayer membranes, studies have shown that they can also successfully promote hemi-fusion of membranes, which is the equivalent of the LD monolayer fusing with one

leaflet of the ER bilayer^{57,240}.

4) After fusion, ERTOLD proteins accumulate on the LD monolayer. For this step to occur, ERTOLD targeting proteins would need to preferentially accumulate on a monolayer when given the option between a monolayer and bilayer. Recent studies support this event, as the hairpin motif common to ERTOLD proteins has been shown by molecular dynamics simulations to favor a monolayer environment with a hydrophobic core as opposed to a bilayer, as the monolayer environment provides a lower free energy¹⁴⁴. Furthermore, *in vitro* studies of GFP tagged GPAT₄ embedded in microsomes and exposed to buffer-in-oil micro-reactors to promote a monolayer bordering the TG phase reveal that GPAT₄ will naturally accumulate on the monolayer correlative to the monolayer's surface tension based on phospholipid composition²³³.

Both CYTOLD and ERTOLD protein targeting are important for LD biogenesis and homeostasis. While we have a basic understanding of the mechanisms by which CYTOLD proteins target¹⁵⁶, the mechanism of ERTOLD protein targeting to LDs remains to be fully elucidated. ERTOLD proteins GPAT₄ and ATGL, key enzymes in TG synthesis and TG mobilization respectively, highlight the the importance of this mechanism of protein targeting for both LD expansion and catabolism. While it is now clear that specific protein factors that mediate membrane fusion for ER-LD bridge formation are involved, it remains unclear what other cellular requirements there are for ERTOLD protein targeting.

To address this, I systematically tested the function of two proteins for their role in ERTOLD protein targeting. The first, Rab18, had been proposed in the literature to affect LD size and turnover by an unknown mechanism^{158,147}. I hypothesized that Rab18's role in LD biology and effect on these two contrasting pathways was attributed to a function in mediating LD-ER tethering for bridge formation. As previously discussed, both GPAT₄ and ATGL, enzymes responsible for LD growth and turnover respectively, localize to LDs by ERTOLD protein targeting^{187,234}. Although we found that Rab18 localizes to LDs, we surprisingly found no evidence of a direct role for

Rab18 in LD homeostasis with respect to LD formation, the targeting of selected LD proteins, or TG turnover. This suggests that Rab18 is not required for the basic machinery of these processes. This was supported by a genome wide RNAi screen in *Drosophila* S2 cells for genes who affected ERTOLD protein targeting; Rab18 was not a hit. However from this screen emerged a strong hit whose depletion impaired ERTOLD protein targeting: TMEM223. Previously uncharacterized and having a dramatic effect on ERTOLD protein targeting, I sought to determine the mechanism by which TMEM223 affected ERTOLD protein targeting and its general cellular function. My studies support a hypothesis that TMEM223 at the mitochondria is crucial for ER morphology and function, particularly in protein trafficking between the ER and Golgi, and that disruption of this process leads to alterations in lipid metabolism and ERTOLD protein targeting. These studies suggest that ERTOLD protein targeting and ER-Golgi protein trafficking rely on similar processes, such as membrane fusion mediated by ATP dependent SNAREs, and that both depend on the mitochondrial protein TMEM223. Furthermore, I explored additional mitochondrial proteins identified by the screen whose depletion give rise to the same phenotypes observed with TMEM223 depletion. Ultimately, I propose a novel role for mitochondrial proteins in ERTOLD protein targeting.

Hoping for the best, prepared for the worst, and unsurprised by anything in between.

Maya Angelou

2

RAB18 is not necessary for protein targeting

2.1 INTRODUCTION

How organelles achieve their specific identity is a central question for cell biology. Key for determining the identity of many membrane-bound organelles are small GTPases of the Rab fam-

ily^{94,185,190}. These proteins are switch-like molecules that regulate recruitment of specific proteins to membranes. In the inactive, GDP-bound state, Rab proteins bind to GDP-dissociation inhibitor (GDI) chaperones in the cytosol. Membrane-bound guanine nucleotide exchange factors (GEFs) on specific organelles activate Rabs by removing the bound nucleotide, allowing the binding of GTP and switching the protein to an active conformation^{9,152}. Once activated, they provide binding surfaces to recruit effector proteins with functions specific to the organelle. Through such a mechanism, each organelle of the endomembrane system contains specific Rab proteins that act to determine its identity⁹.

Lipid droplets (LDs) are cellular organelles found in most cells that store neutral lipids, such as triacylglycerols (TG) and sterol esters, as precursors for cellular membrane lipids and as reservoirs for metabolic energy^{67,154,225}. Among cellular organelles, LDs are unique inasmuch as they are bounded by a monolayer of phospholipids rather than a bilayer membrane²⁰⁴. LDs bind specific proteins, and the principles of protein targeting to LDs are just beginning to be understood^{40,110,156,165,234}. How the identity of LDs is determined molecularly is poorly understood: neither specific lipid species nor Rab proteins that define droplet identity have been identified.

Among Rab proteins, evidence suggests Rab18 may be important for LD identity. Rab18 localizes to the ER⁵⁵ and to LDs^{131,147} in several different human and mouse cell lines. Depletion of Rab18 causes defects in ER tubule integrity and affects LD morphology and protein localization to LDs^{25,55,131,147}. The overexpression of Rab18 increases apposition of ER and LD membranes, possibly indicating a role for the protein at ER-LD contact sites¹⁴⁷. Consistent with these findings, Rab18 has been implicated in LD biogenesis at the ER by recruiting the NAG-RINT1-ZW10 (NRZ) tethering complex and SNARE proteins^{56,237}. These findings suggest that Rab18 is a determinant of LD organelle identity. However, this hypothesis has not been extensively tested, and the function of Rab18 at LDs is unclear.

Here we tested whether Rab18 has a direct role in LD homeostasis by studying the protein in

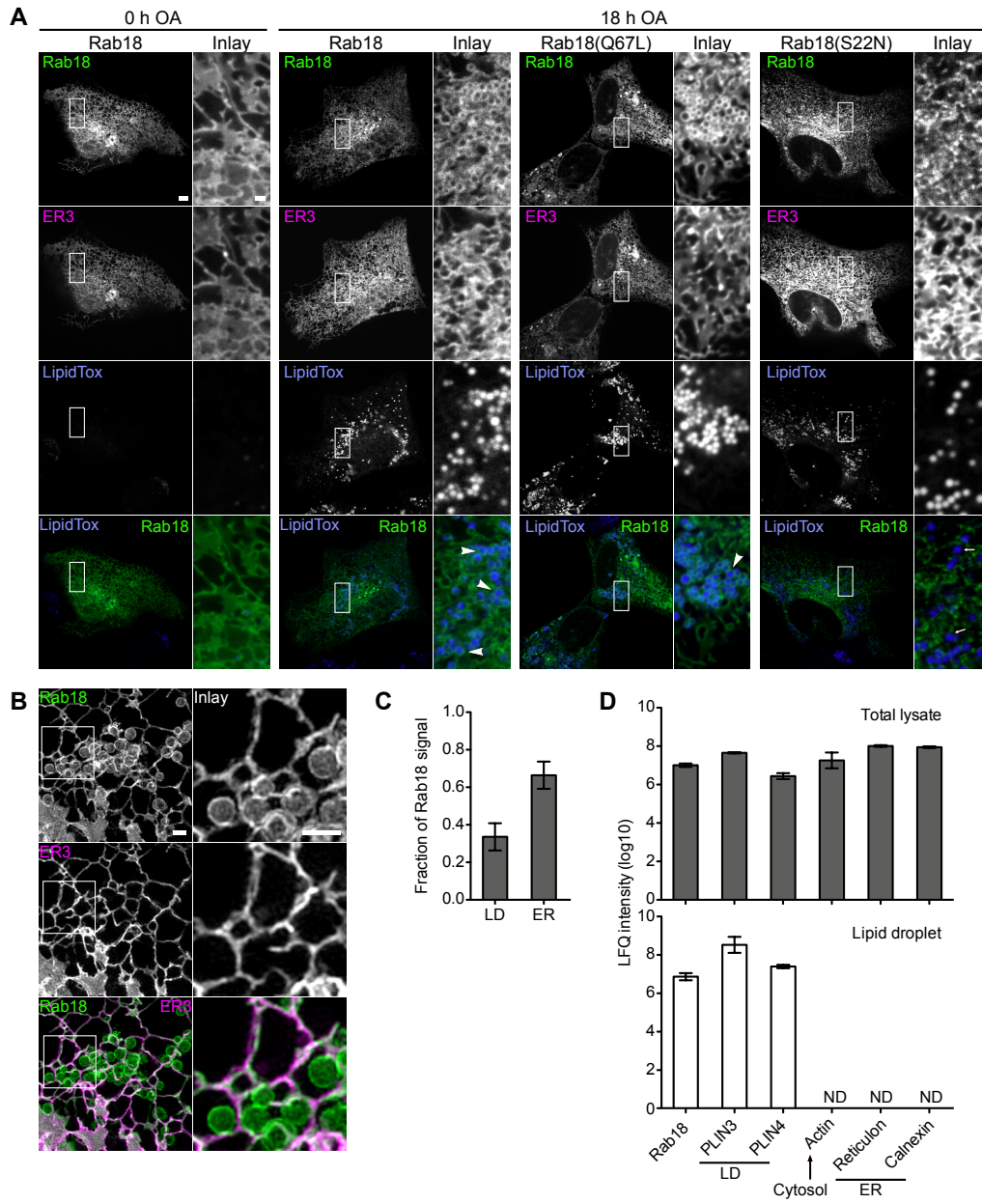
mammalian cells. Although we found that Rab18 localizes to LDs, we surprisingly found no evidence of a direct role for Rab18 in LD homeostasis with respect to LD formation, the targeting of selected LD proteins, or TG turnover. This suggests that Rab18 is not required for the basic machinery of these processes.

2.2 RAB18 LOCALIZES TO LDs AND THE ER

To investigate the role of Rab18 in LD biology, we first analyzed its subcellular localization. We chose to study Rab18 in SUM159 cells⁴⁷, a human mammary carcinoma cell line that we use extensively to study LD biology. These cells 1) express both TG synthesis enzymes, DGAT1 and DGAT2, 2) generate LDs readily on incubation with fatty acid-containing medium, 3) express factors involved in LD biogenesis (including seipin, FIT2, and perilipins 3 and 4^{22,68,232,34,227}), and 4) are diploid and amenable to clustered regularly interspaced short palindromic repeats (CRISPR)-based genome engineering and microscopy imaging^{227,60}. Additionally, SUM159 cells express Rab18 (see below).

Figure 2.1 (following page): Rab18 localizes distinctly to LDs and the ER in SUM159 cells. (A) Overexpressed GFP-Rab18 localizes to LDs (LipidTox) (white arrowheads) and the ER (mCherry-ER3), and localization depends on GTP state (white arrows). SUM159 cells coexpressing mCherry-ER3 and GFP-tagged WT Rab18, GDP-bound Rab18(S22N) mutant, or GTP-bound Rab18(Q67L) mutant were incubated with OA for 0 or 18 h and imaged with spinning disk confocal. Scale bar 5 μm and for inlay 1 μm . (B) Rab18 localizes to the ER and LD structures. SUM159 cells co-expressing mCherry-ER3 and GFP-Rab18 were incubated with oleic acid for 18 h and imaged by SIM. Max projections of 1.25- μm stacks are shown. Scale bars, 1 μm . (C) Quantification of Rab18 signal distribution in SIM images. $n = 5$ fields. (D) Rab18 was detected in LD fractions and total cell lysates of SUM159 cells. LD fractions and cell lysates isolated from SUM159 cells after 18 h oleic acid were analyzed by mass spectrometry to detect proteins on LDs compared with total lysate. ND = not detected.

Figure 2.1: (continued)



We expressed green fluorescent protein (GFP)-Rab18 in these cells, and imaging by spinning-disk confocal microscopy showed that Rab18 colocalized with the calreticulon-KDEL ER marker mCherry-ER3 (Figure 2.1A). When cells were treated with oleate for 18 h to induce LD formation, we found that Rab18 localized to LDs (stained with LipidTox) (Figure 2.1A), as reported^{131,147,126}.

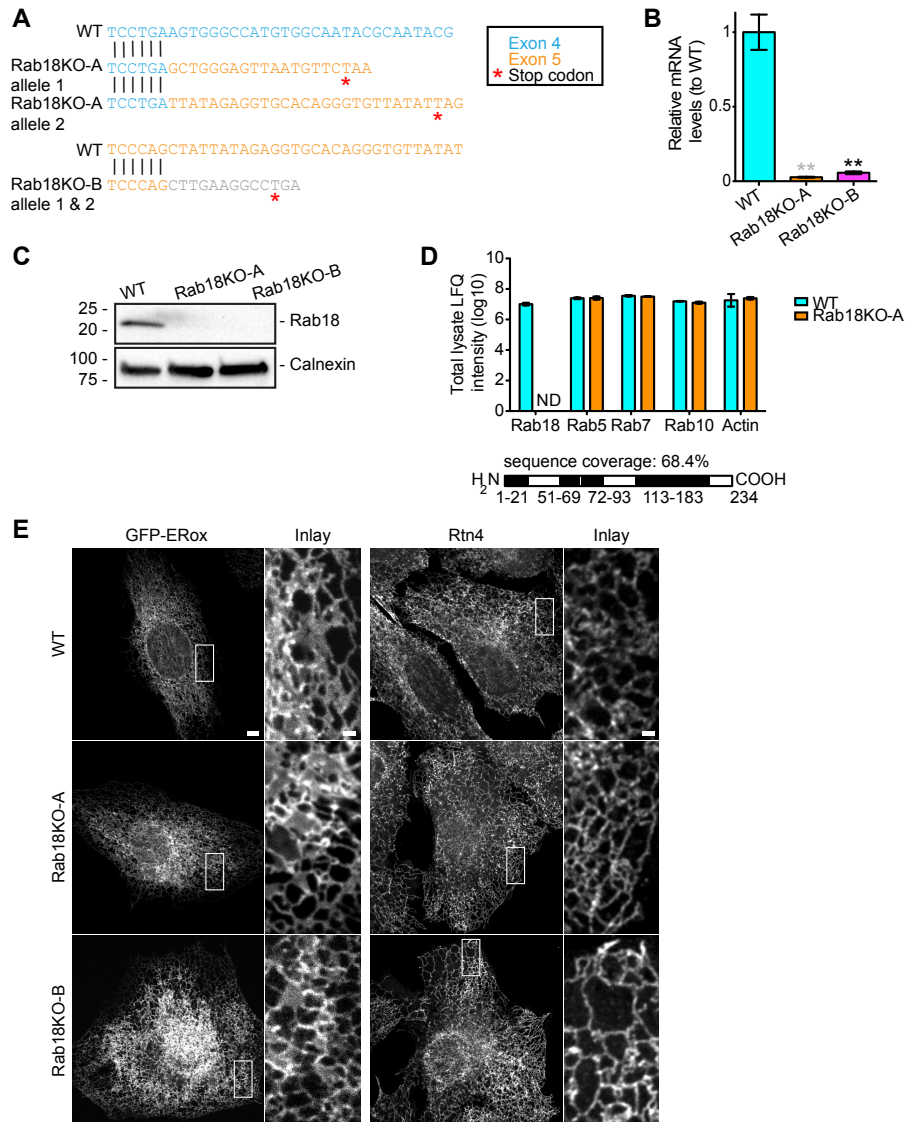
We determined whether the localization of Rab18 to LDs depends on the activation state of Rab18. We found that the hydrolysis-deficient mutant Rab18Q67L, which is locked in the active, GTP-bound form, localized to LDs with fatty acid loading, whereas the nucleotide-binding deficient, inactive Rab18S22N mutant was absent from LDs and instead localized to discrete puncta on the ER (Figure 2.1A).

Overexpression of Rab18 induces close apposition of ER and LD membranes¹⁴⁷, which might confound localization interpretations. To distinguish between direct localization of Rab18 to LDs versus ER localization close to LDs, we used structured illumination microscopy (SIM), which provides greater imaging resolution than confocal microscopy. We analyzed colocalization of GFP-Rab18 with the luminal ER marker mCherry-ER3. We found that Rab18 localizes to both ER and LDs, with a portion of the signal clearly localizing to LDs and distinct from the ER marker (Figure 2.1, B and C).

To complement the microscopy studies, we also determined the localization of endogenous Rab18 by examining its biochemical fractionation behavior. In oleate-loaded cells, we detected Rab18 in total lysate and LD fractions, which were enriched for the LD marker proteins PLIN3 and PLIN4 (Figure 2.1D). Other ER proteins, such as reticulon and calnexin, were absent from the LD fraction, but readily detected in the total lysate (Figure 2.1D). Our results indicate that Rab18 is an ER-localized protein in SUM159 cells that becomes activated and localizes in part around LDs on their formation.

Figure 2.2 (following page): Rab18 deletion does not affect ER morphology. (A) Sequence analysis of Rab18 KO clones A and B. CRISPR/Cas9-mediated genome editing of the Rab18 locus introduces early stop codons at exons 4 (clone A) and 5 (clone B). (B) qPCR data reveal decreased Rab18 mRNA levels by 98 and 96% in Rab18KO-A and -B, respectively, compared with WT control. WT vs. Rab18KO-A* in gray, WT vs. Rab18KO-B* in black. (C) No Rab18 protein is detected in knockout clones by Western blot. Expression levels of Rab18 protein in WT and Rab18 KO cells were analyzed by Western blot with an antibody against endogenous Rab18. No detectable Rab18 protein was found in the Rab18KO-A or Rab18KO-B. (D) Rab18 peptide fragments were not detected by mass spectrometry in Rab18KO-A. WT SUM159 cell lysates and Rab18KO-A cell lysates were analyzed by mass spectrometry with sequence coverage of 68.4% for Rab18. (E) ER morphology in Rab18 KO clones is similar to WT cells. Cells were transfected with GFP-ERox to analyze general ER morphology. Separately, cells were fixed and probed with Reticulon 4 (Rtn4) antibody to visualize ER tubules. Scale bar 5 μ m and for inset 1 μ m.

Figure 2.2: (continued)



2.3 DELETION OF RAB18 DOES NOT AFFECT THE STRUCTURE OF THE ER

Rab18 has been implicated in LD and ER function by overexpression and depletion experiments, but it is unclear whether Rab18 is required for LD biogenesis or turnover. This may be due to the difficulties in interpreting overexpression experiments or residual Rab18 activity in cells with RNAi-mediated depletion of the protein^{131,147,55}. To overcome the latter problem, we generated a knockout cell line by CRISPR/Cas9-mediated genome editing. Using this technology, we isolated a SUM159 cell clone with two alleles of Rab18 that were mutated to generate a premature stop codon at the beginning of exon 5, which results in depletion of Rab18 mRNA levels and a complete absence of the protein by Western blot and mass spectrometry analyses (Figure 2.2, A–D). To rule out clone-specific effects, we also generated a second clone with a 172-bp deletion in exon 5 of both alleles, which results in a premature stop codon. We then evaluated both knockout clones in each of the following experiments.

Since Rab18 is an ER-localized protein in standard culture conditions, we first investigated ER morphology in wild-type (WT) and Rab18 knockout cells. Compared with control cells, Rab18 knockout cells appeared to have normal ER when analyzed by immunofluorescence with antibodies directed against the tubular ER protein Rtn4 or by in vivo fluorescence microscopy using GFP-ERox (Figure 2.2E). Reintroduction of GFP-Rab18 into Rab18 knockout cells revealed no differences in its localization compared with that found in wild-type cells (Figure 2.3).

2.4 RAB18 IS NOT REQUIRED FOR LD BIOGENESIS, BUT RAB18 DELETION MODESTLY REDUCES THE SIZE AND NUMBERS OF LDs

The dual localization of Rab18 to ER and LD membranes on LD induction prompted us to test whether Rab18 is involved in LD biogenesis. We monitored LD size and number on induction of LD biogenesis by addition of oleate to the culture medium of control and Rab18 knockout

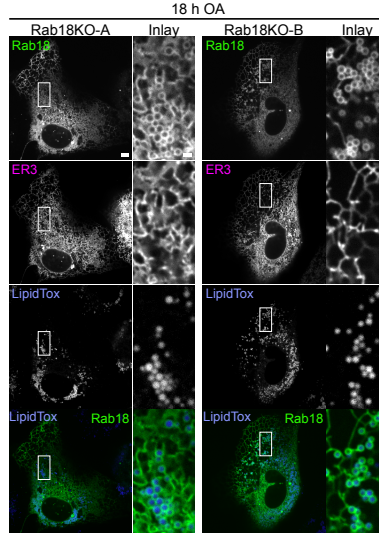


Figure 2.3: GFP-Rab18 expressed in Rab18 knockout cells has a similar localization pattern as in WT cells. SUM159 WT or Rab18KO cells co-expressing mCherry-ER3 and GFP-tagged WT Rab18 were incubated with OA for 18 h and imaged with spinning disk confocal. LDs stained with LipidTox. Scale bar 5 μm , for inlay 1 μm .

SUM159 cells. Whereas LDs appeared similar in both cell types at 2 h after oleate addition, there was a modest reduction in the numbers and areas of LDs in Rab18 knockout clones after 24 h (Figure 2.4, A–C). By using radioactive oleate as a tracer, we found no differences in TG accumulation between Rab18 knockout and wild-type cells (Figure 2.4, D and E), suggesting that any changes in LD accumulation were not due to changes in TG synthesis rates.

2.5 DELETION OF RAB18 DOES NOT AFFECT THE TARGETING OF SEVERAL KEY PROTEINS TO LDS

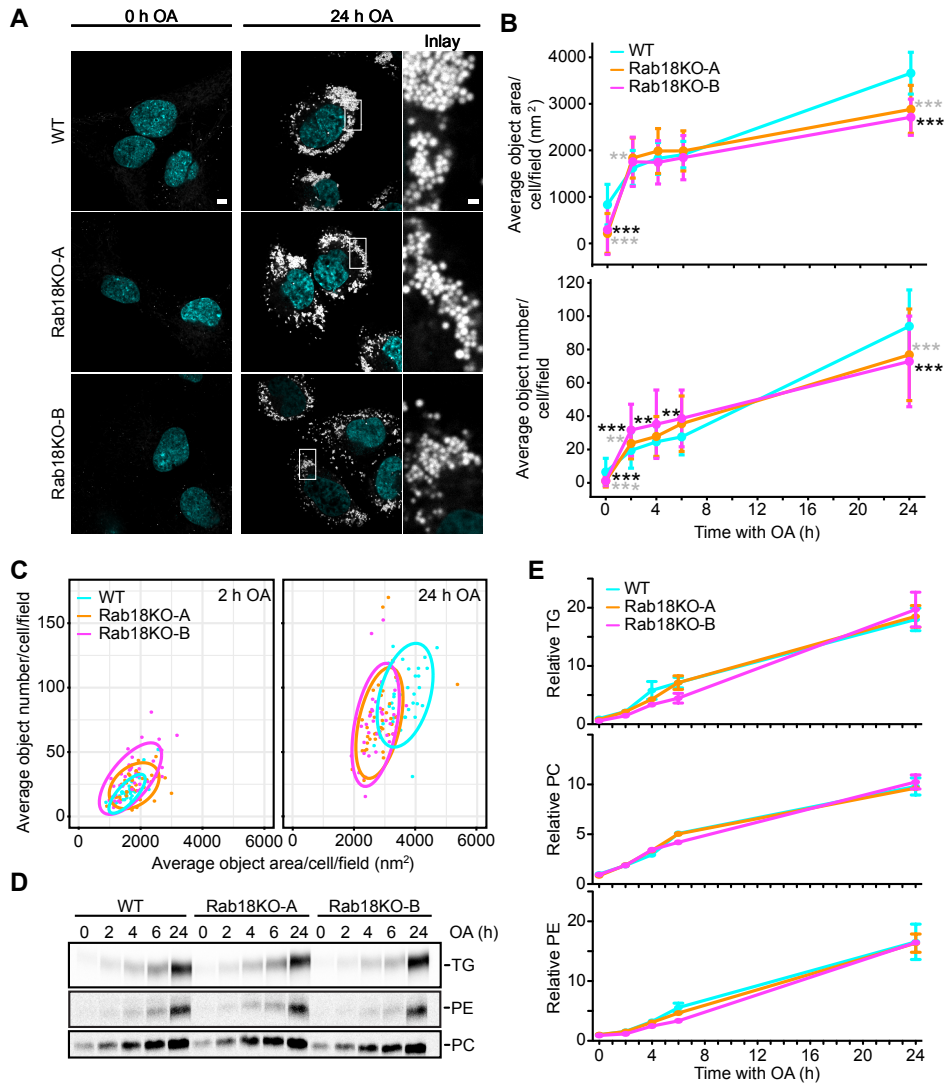
During LD biogenesis, several enzymes of the TG synthesis pathway localize to LDs, including ACSL₃, GPAT₄, and DGAT₂^{191,104,234}. These proteins, known as ERTOLD targeting proteins (previously Class I), are anchored to the membrane by hydrophobic sequences that are embedded in the bilayer membrane and the LD surface. Thus, moving them from the ER to LDs for targeting to LDs requires a membrane continuity or membrane bridge^{234,233}. Since Rab proteins regulate membrane tethering and fusion reactions, as well as membrane contacts^{94,88}, we hypothesized that Rab18 may be involved in establishing ER–LD bridges for ERTOLD membrane protein targeting to LDs. We first tested targeting of GPAT₄-GFP to LDs after treatment of cells with oleate for 24 h. As found in control cells, deletion of Rab18 did not affect the dual localization of GPAT₄ to ER and LD membranes (Figure 2.5A).

To further test localization of proteins involved in key aspects of LD biology, we examined adipose triglyceride lipase (ATGL), a TG hydrolase that localizes to LDs via membrane-embedded targeting sequences^{179,187}. Like GPAT₄, ATGL localization depends on Arf1/COPI proteins¹⁸⁷ and may occur via ER–LD bridges. We expressed a fluorescently tagged catalytically inactive mutant of ATGL that localizes to LDs¹⁸⁴. Similarly to the findings for GPAT₄, targeting of ATGL to LDs was unaffected by the absence of Rab18 (Figure 2.5B).

CYTOLD targeting proteins (previously Class II) localize to the LD monolayer directly from the cytosol by inserting one or several amphipathic helices into the monolayer of the LD surface^{23,156}. We examined the localization of PLIN₃, a CYTOLD targeting protein, and also did not detect differences in targeting for Rab18 knockout and wild-type cells (Figure 2.5C). Thus, Rab18 is not required for targeting of two ER proteins (GPAT₄ and ATGL) or one cytosolic protein (PLIN₃) that localize to LDs.

Figure 2.4 (following page): LD biogenesis is not affected in Rab18 KO cells. (A) LD morphology is similar in Rab18KO clones and WT cells with oleic acid incubation. Representative images of WT and Rab18 KO cells pre-starved for 5 h before addition of oleic acid and after 24 h of oleic acid incubation. Scale bar 5 μm and for inlay 1 μm . (B) Rab18 KO average BODIPY object area and number are slightly smaller than WT after 24 h oleic acid incubation. WT and Rab18 KO cells were incubated with oleic acid for indicated time points, fixed, and imaged by high-throughput microscopy. Average BODIPY object area and number per cell per field (>five cells per field to obtain representative measurements) were quantified per condition. $n > 27$ fields/point. WT vs. Rab18KO-A* in gray; WT vs. Rab18KO-B* in black. (C) Rab18KO and WT average object area vs. number 90% confidence intervals overlap at 2 and 24 h oleic acid incubation. Average object number plotted against average object area per cell per field with 2 and 24 h oleic acid. Ellipses represent 90% confidence intervals. (D, E) Rab18KO clones have similar synthesis of TG, PE, and PC as WT cells with oleic acid incubation. Incorporation of [^{14}C] oleate into triglycerides (TGs), phosphatidylethanolamine (PE), and phosphatidylcholine (PC) were measured over time. Lipids were extracted from cells and separated by TLC. Representative autoradiographs of three replicates per genotype are shown (D). (E) Quantified TG, PC, and PE levels are similar between Rab18KO clones and WT cells over time. TLC plates were developed and incorporation of [^{14}C] oleate into TGs, PE, and PC was quantified using Fiji. Data presented are normalized CPM to mg/ml protein and relative to WT at $t = 0$ h. $n = 3$.

Figure 2.4: (continued)



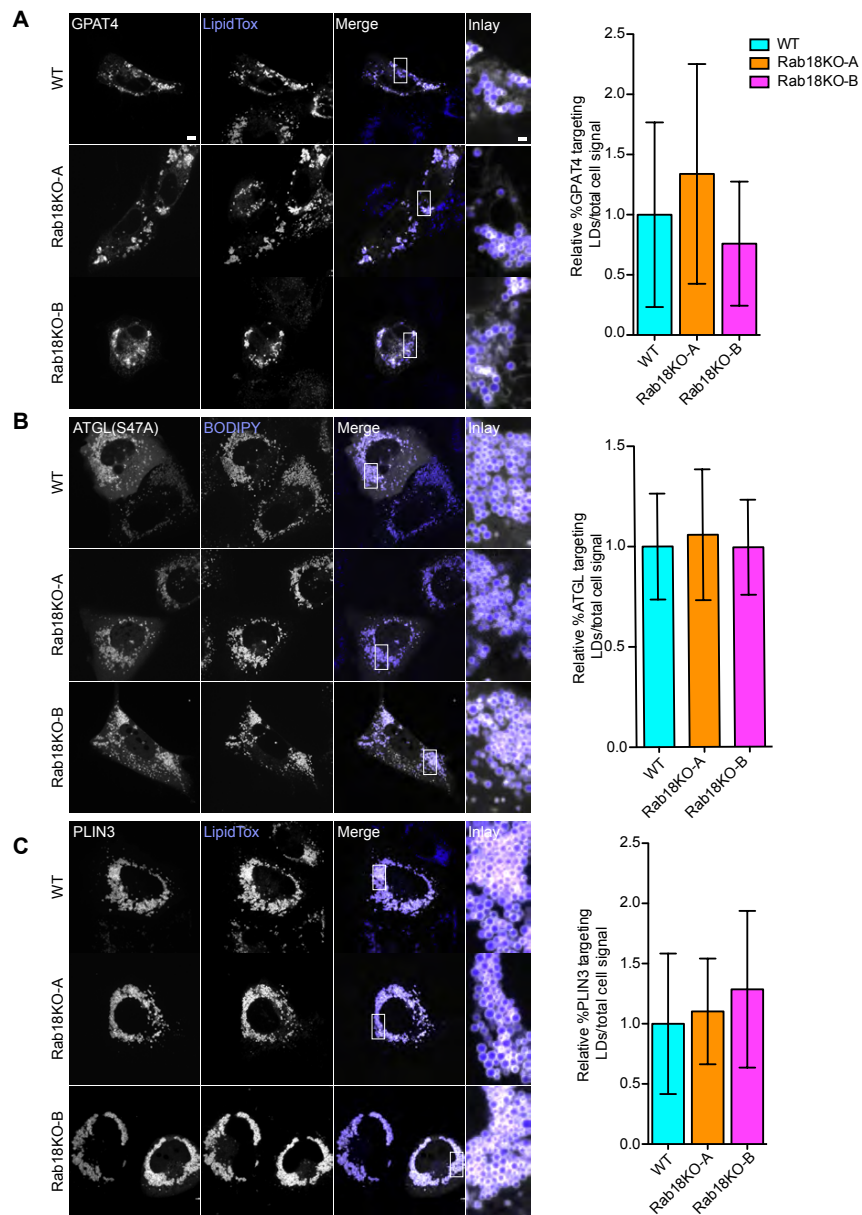


Figure 2.5: Protein targeting to LDs is similar in Rab18KO and WT. (A–C) Representative confocal images of WT, Rab18KO-A, and Rab18KO-B cells transfected with GPAT4-GFP (A), catalytically inactive mCherry-ATGL(S47A) (B), and GFP-PLIN3 (C) were incubated with oleic acid for 24 h. Targeting to LDs stained with LipidTox (A, C) or BODIPY (B) compared with total cell signal quantified in (A) $n \geq 39$ cells, (B) $n \geq 36$ cells, and (C) $n \geq 43$ cells. Scale bar 5 μm and for inlay 1 μm .

2.6 DELETION OF RAB18 HAS NO EFFECT ON TRIGLYCERIDE TURNOVER DURING CELL STARVATION

Induction of lipolysis in cultured adipocytes increases Rab18 targeting to LDs^{131,158}. We thus tested the hypothesis that Rab18 may be involved in turnover of LD-stored TGs. We generated cells with abundant LDs (incubating them in oleate containing medium for 12 h) and induced starvation and TG turnover by removing fetal bovine serum (FBS), insulin, and oleate from the culture medium. We found that, by 48 h of starvation, most LDs were degraded (Figure 2.6A). When we analyzed LD size and numbers (by boron-dipyrromethene [BODIPY] staining using high-throughput microscopy and automated image analysis) during a time course of LD catabolism, Rab18 knockout cells (and in particular one clone) showed evidence of increased turnover of LDs, but after 48 h, we did not detect differences in Rab18 knockout and wild-type cells (Figure 2.6, A and B).

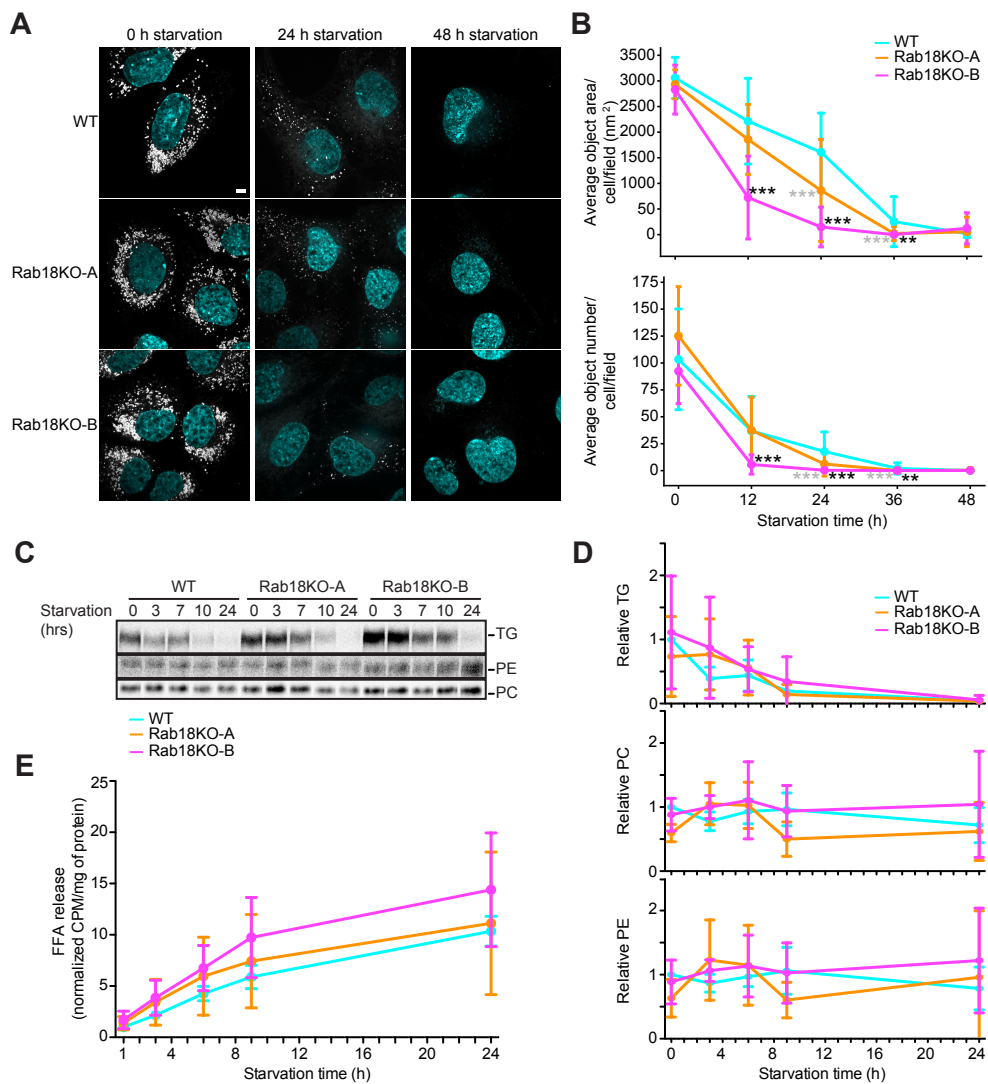
We also analyzed the amounts of free fatty acids released into the culture medium (using radioactive oleate as tracer material) and, consistent with the microscopy studies, detected no major differences between Rab18 and wild-type cells with respect to TG consumption or fatty acid release (Figure 2.6, C–E).

2.7 DISCUSSION

In the current study, we found little effects of deleting Rab18 on LD biogenesis or turnover in a mammary carcinoma cell line. The most significant phenotype we found was a modest reduction in LD size and numbers with oleate induction of LDs. We also did not find effects of Rab18 deletion on the targeting of several key LD proteins, although we cannot exclude that Rab18 activation at LDs is involved in recruiting other proteins. Considering these data, we conclude that Rab18 is not a necessary component of the basic cell machinery required for LD formation, expansion, or

Figure 2.6 (following page): Rab18 deletion does not affect TG turnover. (A) LDs are degraded similarly in Rab18KO clones and WT cells with starvation. Representative images of WT, Rab18KO-A, and Rab18KO-B cells after 12 h OA loading ($t = 0$) and 24 or 48 h of starvation. LDs stained with BODIPY 493/503 and nuclei with Hoechst. Scale bar 5 μm and inlay 1 μm . (B) Rab18KO average BODIPY object area and number are similar to WT after 48 h starvation. WT and Rab18KO cells were incubated with oleic acid for indicated time points as in A. Cells were fixed and imaged by high-throughput microscopy. Average BODIPY object area and number per cell per field (>5 cells per field) was quantified per condition. $n > 7$ fields. WT vs. Rab18KO-A * in gray; WT vs. Rab18KO-B * in black. (C) Rab18KO clones have similar synthesis of TG and PE and less PC than WT cells with starvation. WT and Rab18KO cells were incubated with [^{14}C] oleic acid for 18 h, followed by starvation for increasing time. Total lipids were extracted at each time point and separated by TLC to detect radiolabeled TG, PE, and PC levels. Representative autoradiographs of three replicates per genotype. (D) Quantified TG and PE levels are similar, and PC levels are less between Rab18KO clones and WT cells over time with starvation. TG, PC, and PE signals were quantified from TLC plates using Fiji. Data presented are normalized CPM to mg/ml protein and relative to WT at $t = 0$ h. $n = 3$ biological replicates. (E) Rab18KO clones have decreased free fatty acid release over time with starvation. The [^{14}C]-labeled free fatty acid release measured over time with starvation after WT; Rab18KO-A, and Rab18KO-B cells were incubated with [^{14}C] oleic acid for 18 h. $n = 3$ biological replicates.

Figure 2.6: (continued)



consumption. In comparison, other key components of this machinery, such as seipin, FIT2, or perilipins for LD biogenesis^{22,68,232,34,227}, or Arf1/COPI proteins for ER-LD targeting²³³, have prominent effects on cells and tissues that store neutral lipids. Homozygous Rab18 knockout mice show an eye and neuronal phenotypes, and embryonic fibroblasts derived from this line have a mildly affected LD morphology, but neutral lipid storage in liver or adipose tissue is not affected²⁵, further arguing against a strong requirement for Rab18 in fundamental LD processes.

In contrast to our findings in SUM159 cells, defects in LD formation were found when Rab18 was knocked out in murine adipocytes, suggesting that Rab18 is an important component of LD growth and maturation in this cell type²³⁷. However, consistent with our findings, deficiency of Rab18 in several other mammalian cell lines (AML12, HeLa, Cos7, and 293T) did not show an effect on LDs²³⁷.

It is unclear why Rab18 depletion might affect LD formation and maturation in murine adipocytes, but not other cell types, and why it has no dramatic effect on murine adipose tissue. One possibility is that Rab18, while not a component of the basic LD formation machinery in cells, is involved in specific processes of LD growth in specialized cells such as adipocytes, which generate much larger, unilocular LDs (tens of microns diameter) than most cell types (0.5- to 2- μ diameter) using specific machinery, such as CIDE-C/Fsp27^{142,159}. Thus, Rab18 may be similarly involved in adipocyte-specific processes. An alternative explanation may be that Rab18 has functional redundancy with other Rab proteins in some cells (SUM159, AML12, HeLa, Cos7, and 293T) but not in murine adipocytes. Further studies are needed to clarify the physiological function of Rab18 and to determine the specific downstream molecular consequences of Rab18 recruitment to LD surfaces.

2.8 MATERIALS AND METHODS

2.8.1 ANTIBODIES

We used rabbit polyclonal antibodies against Rab18 (Proteintech; 11304-1-AP), ATGL (CST; 2138S), Calnexin (Enzo: ADI-SPA-860), reticulon 4 (Santa Cruz; Nogo N18 SC11027) and GAPDH (Santa Cruz Biotechnology; sc-25778). Tip47 antibody from guinea pig was from Fitzgerald (20RTP001). Mouse (monoclonal) anti- α tubulin was from Sigma (T5168). We used HRP-conjugated secondary antibodies against mouse (Santa Cruz Biotechnology; sc-2004), rabbit (Santa Cruz Biotechnology; sc-516102) and guinea pig (Santa Cruz Biotechnology; sc-2438) for immunoblotting, and anti-rabbit Alexa Fluor 488 (Abcam; ab150077) for immunofluorescence.

2.8.2 PLASMIDS

Human expression vectors were generated by cloning Rab18, Rab18(S22N), Rab18(Q67L) into pEGFP-C1 vector (Clontech) using BamHI and SalI and PLIN3 into pEGFP-C1 vector with pTK promoter using KpnI and BamHI. C-terminal mCherry-tagged ATGL(S47A) was expressed from pcDNA3.1 (Thermo Fisher), C-terminal GFP-tagged human GPAT4 from pcDNA-DEST47 vector (Thermo Fisher), C-terminal GFP-tagged KDEL from oxGFP vector (Addgene #68069), and mCherry-ER3 Addgene (#55041).

2.8.3 CELL CULTURE AND TRANSFECTION

SUM159 cells (RRID:CVCL_5423) were obtained from the laboratory of Professor Tomas Kirchhausen (Harvard Medical School) and were maintained in DMEM/F-12 GlutaMAX (Life Technologies) with 5 μ g/ml insulin (Cell Applications), 1 μ g/ml hydrocortisone (Sigma), 5% FBS (Gibco 10082147; Thermo Fisher), 50 μ g/mL streptomycin and 50 units/mL penicillin. Where noted,

cells were incubated with media containing 500 μ M oleic acid complexed with 0.5% essentially fatty acid free BSA (Sigma Aldrich). Transfection of plasmids into SUM159 cells was performed with FuGENE HD transfection reagent (Promega) 18-24 h before imaging.

2.8.4 GENERATING RAB18 KNOCKOUTS IN SUM159 CELLS

Three independent targeting sequences to direct Cas9 to exons 4, 5 and 7 of the Rab18 locus were used simultaneously as gRNA in the Cas9 and gRNA expression plasmid px459 (Addgene) (primer sequences: exon 4, CACCGGAAATAGTCCAAT CCTGAAG, AAACCTTCAGGATTGGAC-TATTTCC; exon 5, CACCGCTGTGCAC CTCTATAATAGC, AAACGCTATTATAGAG-GTGCACAGC; exon 7, CACCGCG TGAAGTCGATAGAAATGA, AAACTCATTTCTAT CGACTTCACGC). 600 μ g of each gRNA px459 plasmid or 1 μ g of empty px459 plasmid were transfected into 80,000 cells. Transfected cells were isolated by treatment with puromycin for 4 days, followed by single-cell sorting using flow-cell cytometry (FACS Aria II; BD Biosciences) as described (Ran et al, 2013). Knockout clones were verified by western blot analysis of cell lysates using Rab18 antibodies and sequencing of PCR amplified gRNA target regions subcloned into pCR Blunt II TOPO vector (Thermo Fisher Scientific). Positive clones were verified by qPCR (sense primer: CCATGTTATTTATAGAGGCAAGTG, and anti-sense primer: CAAGTTCTTCAAAGGCACATT) using power SYBR green (Life Technologies). For all experiments with Rab18 knockout cells, wild-type cells transfected with an empty px459 plasmid were used as control wild-type cells.

2.8.5 IMAGING AND IMAGE ANALYSIS

Live cell imaging was performed on a Nikon Eclipse Ti inverted microscope equipped with CSU-X1 spinning disk confocal head (Yokogawa), 405-, 488-, 561-, or 639- nm laser lines, 100x ApoTIRF 1.4 NA objective (Nikon, Melville, NY), and iXon Ultra 897 EMCCD or Zyla 4.2 Plus sCMOS

cameras (Andor, Belfast, UK). Cells were annually tested for mycoplasma contamination by Universal Mycoplasma Detection Kit (ATCC). For quantification of ER morphology, 3 μm Z stacks with 0.25 μm steps were acquired.

Imaging experiments of SUM159 cells were carried out in Gibco Fluorobrite DMEM (Life Technologies) supplemented with SUM159 maintenance media components. LDs were stained with 0.5 $\mu\text{g}/\text{mL}$ BODIPY 493/503 (Life Technologies) or HCS LipidTOX™ Deep Red Neutral Lipid Stain (Thermo Fisher Scientific) 20 minutes prior to imaging. Nuclei were stained with 1 $\mu\text{g}/\text{mL}$ of Hoechst 33342 (Thermo Fisher).

For immunofluorescence experiments cells were fixed in 4% formaldehyde (Polysciences.) for 20 min at RT, followed by permeabilization and staining as described previously²³⁴. Slides were mounted with ProLong Gold Antifade mounting medium with DAPI (Thermo Fisher Scientific) and stored at 4 °C.

High-throughput imaging was performed on a IN CELL Analyzer 6000 microscope (GE Healthcare Life Sciences) using 60x 0.95 NA objective. Cells were fixed in 4% formaldehyde (Polysciences) at RT for 20 min, washed 3x with PBS and stained for LDs and nuclei as described above. 24 to 64 images were acquired per well.

Structured-illumination microscopy of living cells was performed on an OMX V4 Blaze (GE Healthcare Life Sciences) equipped with three PCO.edge sCMOS cameras, 488- and 568-nm laser lines, 60x 1.42 Plan APOCHROMAT objective (Olympus). Usually 2.5 μm stacks with 0.125 μm step size with 15 raw images (three rotations with five phases each) per z-section were acquired. Spherical aberration was minimized by immersion oil matching⁸⁴. Super-resolution images were reconstructed from raw data sets with channel specific, measured optical transfer function and Wiener filter constant of 0.001 using CUDA-accelerated 3D-SIM reconstruction code based on Gustafsson et al.⁷³. TetraSpeck beads (Thermo fisher) or a nano-grid control slide (GE) were used to measure axial and lateral chromatic misregistration. Experimental data sets were registered using imwarp

function in MATLAB (MathWorks).

For image analysis, LD area and number from high-throughput microscopy images were quantified using CellProfiler software (Carpenter et al., 2006). Two workflows were developed for analysis of images from OA loading conditions and from starvation conditions.

Protein targeting was quantified using FIJI software¹⁷⁴. As developed by Prévost et al. (2018)¹⁵⁶ to identify the region of LDs, a threshold was applied to the BODIPY or LipidTox channels. The mean intensity of mCherry or GFP protein signal within the LD region was measured and divided by the mean intensity of the total signal in the cell.

2.8.6 METABOLIC LABELING AND ANALYSIS OF LIPIDS

Incorporation of TG during fatty acid loading was measured by addition of 500 μM [¹⁴C] oleic acid (25 $\mu\text{Ci}/\mu\text{mol}$), followed by lipid and protein extraction in hexane/isopropanol (3:2) or RIPA buffer, respectively. Lipid loading to TLC plates (Merck) was normalized to total protein. Phospholipids were separated in $\text{CHCl}_3/\text{CH}_3\text{OH}/\text{H}_2\text{O}$ (65:35:4) and neutral lipids in hexane/diethyl ether/acetic acid (80:20:1). TLC plates were exposed to imaging screens and scanned in a Typhoon FLA 7000 (GE Healthcare) to visualize radioactive compounds. For starvation experiments, cells were incubated with 500 μM [¹⁴C] oleic acid (25 $\mu\text{Ci}/\mu\text{mol}$) for 16 h, followed by washing 3x with PBS and addition of starvation medium (DMEM low glucose, 10 mM HEPES, pH 7.0, 1% penicillin and streptomycin, 1% essentially fatty acid-free BSA). At each time point, lipids and proteins were extracted as described above. To measure free fatty acid release, 10% of medium was collected, and radioactivity was measured in a Hidex 300SL liquid scintillation counter (Hidex). Radioactivity was measured and counts per minute (CPM) measurements were normalized to mg/mL of protein.

2.8.7 SUBCELLULAR FRACTIONATION

Cells were harvested, washed once with ice cold PBS followed by a wash in homogenization buffer (20 mM Tris-HCl pH 7.4, 250 mM sucrose, 1 mM EDTA pH 8, Roche complete protease inhibitor tablet), followed by resuspension in 1 mL of homogenization buffer (HB), and lysis through a 23G needle 30x. NaCl was added to final concentration of 100 mM and lysates were cleared for 10 min, 1,000 x g and 8,000 x g to remove unlysed cells, nuclei and mitochondria. Cleared lysate was subjected to ultracentrifugation for 1 h at 100,000 x g at 4 °C. The pellet was resuspended in homogenization buffer, followed by SDS-PAGE and western-blot analysis. To purify LDs, the 100,000 x g supernatant was mixed 1:1 with 50% OptiPrep in HB, and layered with 500 µL 16% OptiPrep, 1.5 mL 8% OptiPrep, 500 µL 2% OptiPrep and 500 µL HB. Gradients were subjected to ultracentrifugation in a swinging bucket rotor (TLS55, Beckman-Coulter) for 16 h at 150,000 x g at 4 °C. LDs were collected from the top layer. Protein was precipitated from this layer and the remaining layers collectively to analyze the cytosol (Wessel and Flügge, 1984). Protein concentration was determined by Bradford or absorption at 280 nm (nanodrop, Thermo Fisher Scientific).

2.8.8 MASS SPECTROMETRY ANALYSES OF TOTAL CELL LYSATES AND LDs

Precipitated proteins from total cell lysates and purified LD fractions were resolubilized in 100 mM NaOH aided by sonication at 4°C, and the solution was brought to pH 7.5 with 200 mM HEPES (4-(2-hydroxyethyl)-1-piperazineethanesulfonic acid). Proteins were reduced using 5 mM dithiothreitol (Sigma-Aldrich) at 37°C for 1 h, followed by alkylation of cysteine residues using 15 mM iodoacetamide (Sigma-Aldrich) in the dark at RT for 1 h. Excessive iodoacetamide was quenched using 10 mM dithiothreitol. Protein mixtures were diluted in 1:6 ratio (v/v) using ultrapure water prior to digestion using sequencing grade trypsin (Promega) at 37°C for 16 h. Digested peptides were subsequently desalted using self-packed C18 STAGE tips (3M Empore™) for LC-MS/MS

analysis (Rappsilber et al., 2003). Desalted peptides were resuspended in 0.1% (v/v) formic acid and loaded onto HPLC-MS/MS system for analysis on an Orbitrap Q-Exactive HF (Thermo Fisher Scientific) mass spectrometer coupled to an Easy nanoLC 1000 (Thermo Fisher Scientific) with a flow rate of 300 nl/min. The stationary phase buffer was 0.5 % formic acid, and mobile phase buffer was 0.5 % (v/v) formic acid in acetonitrile. Chromatography for peptide separation was performed using increasing organic proportion of acetonitrile (5–40 % (v/v)) over a 265-min gradient) on a self-packed analytical column using PicoTip™ emitter (New Objective, Woburn, MA) using Reprosil Gold 120 C-18, 1.9- μ m particle size resin (Dr. Maisch, Ammerbuch-Entringen, Germany). The mass spectrometry analyzer operated in data dependent acquisition mode with a top 10 method at a mass range of 300–2000 Da.

Mass spectrometry data were processed by MaxQuant software version 1.5.2.8 (Cox and Mann, 2008) with the following setting: oxidized methionine residues and protein N-terminal acetylation as variable modification, cysteine carbamidomethylation as fixed modification, first search peptide tolerance 20 ppm, main search peptide tolerance 4.5 ppm. Protease specificity was set to trypsin with up to 2 missed cleavages were allowed. Only peptides longer than five amino acids were analyzed, and the minimal ratio count to quantify a protein is 2 (proteome only). The false discovery rate (FDR) was set to 1% for peptide and protein identifications. Database searches were performed using the Andromeda search engine integrated into the MaxQuant environment (Cox et al., 2011) against the UniProt-human database containing 71,579 entries (October 2017). “Matching between runs” algorithm with a time window of 0.7 min was employed to transfer identifications between samples processed using the same nanospray conditions. Protein tables were filtered to eliminate identifications from the reverse database and also common contaminants. Mass spectrometry source files generated were deposited to the ProteomeXchange Consortium via the PRIDE partner repository²²² with the dataset identifier PXD009683.

2.8.9 STATISTICAL ANALYSIS

Data are presented as mean \pm standard deviation. Statistical significance of qPCR data was analyzed by unpaired two-tailed Student's t test. For high throughput imaging data that was not normally distributed, the non-parametric Wilcoxon rank-sum test for single comparisons was used. Following analyses for normally distributed data were performed using GraphPad Prism 5.0. For free fatty acid release from the same samples over time, statistical significance was evaluated by repeated measures two-way ANOVA; for quantification of protein targeting, one-way ANOVA followed by the Tukey post-hoc test. For all other data involving multiple comparisons, statistical significance was evaluated by two-way ANOVA followed by the Bonferroni post-hoc test. For all analyses, values of $P < 0.01$ were considered statistically significant, **, $P < 0.01$; ***, $P < 0.001$. All experiments were repeated at least two independent times.

2.9 AUTHOR CONTRIBUTIONS

Experiments designed by CBKJ, HA, AWF, RVF, and TCW. Experiments were carried out by CBKJ, HA, AWF. Manuscript was written by CBKJ, HA, RVF, and TCW. Proteomics was carried out by ZWL.

Over the long term, symbiosis is more useful than parasitism. More fun, too. Ask any mitochondria.

Larry Wall

3

TMEM223 reveals a role for mitochondrial proteins in ERTOLD targeting

3.1 PREFACE

The work presented in this chapter was written before the final manuscript was assembled. For final data and conclusions we request that the reader consult the published manuscript once available.

3.2 INTRODUCTION

Because LDs are derived from the ER membrane, screens of LD biology can reveal genes that are important for maintenance of ER homeostasis. A recent genome-wide RNAi screen in *Drosophila* for proteins whose depletion affects targeting of the ERTOLD targeting protein GPAT₄ from the ER to LDs revealed a breadth of candidates previously unknown to be involved in LD protein targeting. Here, we investigate one of these previously unidentified candidates, TMEM₂₂₃ (CG12935 in *Drosophila*), whose depletion dramatically impairs GPAT₄ localization from the ER to LDs. Little is known about the role of TMEM₂₂₃ in cells; TMEM₂₂₃ was identified in a screen for genes that impair *Drosophila* embryonic nervous system development¹⁰⁸. Recently, TMEM₂₂₃ was proposed to be a part of the TMEM_{70/186/223} family and localized to the mitochondria like the other family members TMEM₇₀ and TMEM₁₈₆¹⁷². Intriguingly, beyond these studies the role of TMEM₂₂₃ at the mitochondria remains elusive.

Maintenance of cellular phospholipid homeostasis is important for proper function of the membrane trafficking system. Sphingolipids in particular are important components of cellular membranes, particularly in the secretory pathway. Sphingolipids form gradients along the secretory pathway and disruption of this can lead to impaired protein sorting^{86,149,181}. Accumulation of lactosylceramide and other glycosphingolipids in Nieman Pick C Disease disrupt endosomal trafficking by potentially affecting the localization of membrane microdomains²⁰⁵. Inhibition of the *Drosophila* ceramide synthase gene *schlank*, whose depletion also impairs GPAT₄ targeting, leads to alterations in sphingolipid levels and defects in intracellular protein trafficking. There are two key differences in *Drosophila* and mammalian lipidomes: 1. *Drosophila* have PE-centric lipidome and a reversal in the ratio of PE to PC²⁸; 2. *Drosophila* synthesize ceramide phosphoethanolamine (CerPE) instead of sphingomyelin. CerPEs are unique molecules synthesized in *Drosophila* by CPES at the Golgi or minimally by dSMSr at the ER²¹⁷. Interestingly, studies have shown that a block in dSMSr

leads to ER ceramide and glucosylceramide accumulation that dramatically disrupts transitional ER (tER)-Golgi structures²¹⁶.

We validated the effect of TMEM223 on protein targeting using quantitative cell microscopy, and with biochemical methods define TMEM223 as an integral membrane protein resident to the mitochondrial inner membrane. Further analysis identified that TMEM223 depletion results in ER dysfunction, including defective ER trafficking of secreted proteins and ER stress. We also identify that these changes were strongly correlated with altered lipid metabolism, in particular the depletion of cellular CerPE levels and accumulation of glucosylceramides. As sphingolipid synthesis depends on ER to Golgi trafficking, and on ATP for transport of ceramide from the ER to the Golgi, disruption of the ER or cellular ATP levels could result in the protein secretion and lipid phenotypes we are seeing. We propose that the phenotypes revealed by TMEM223 depletion support our model of ERTOLD protein targeting via ATP dependent SNARE mediated membrane fusion of the ER and LDs as following similar principles to those in ER-Golgi vesicular trafficking.

3.3 RNAI SCREEN FOR ERTOLD PROTEIN TARGETING IDENTIFIES NOVEL PROTEIN CG12935 AS A STRONG DETERMINANT

A genome-wide screen was conducted in a *Drosophila* S2 R+ cell line in which GPAT4 fluorescently tagged with EGFP was stably overexpressed. This screen will be reported in its entirety elsewhere. GPAT4 is known to target to LDs via ERTOLD protein targeting pathways at late time points after incubation with oleate²³⁴. However, the mechanism by which ERTOLD protein targeting occurs for GPAT4 and other proteins is unknown; this prompted unbiased approaches to identify genes involved in ERTOLD protein targeting. For the screen, cells were treated with a library of dsRNAs to knock down a single gene per well by RNAi. After four days of knock down, cells were treated with 1 mM oleate to induce LD formation. 20 hours after oleate addition, and five

days after knock down, cells were fixed and stained for LDs and nuclei. Automated imaging using a confocal microscope captured 8 fields per well. Images were analyzed using a machine learning based image analysis pipeline that segmented individual cells and the nuclei, LDs, and GPAT₄ signal within each cell. The per cell ratio of the average intensity of GPAT₄ signal on LDs divided by the average intensity of GPAT₄ signal not on LDs was calculated and will henceforth be referred to as the LD targeting ratio. The median LD targeting ratio was taken per well, which represents a dsRNA. The screen was repeated in duplicate and one to two dsRNAs were used per gene. dsRNA against LacZ was used as a negative control as it does not exist in the genome. As controls for genes whose depletion impairs ERTOLD protein targeting, Arf79f and β -COP were used as they've previously been shown to impair GPAT₄ targeting upon their depletion²³³. dsRNA against seipin was used as a control for genes whose depletion enhances ERTOLD protein targeting. The robust Z-score was calculated for each LD targeting ratio, and a cut off was set at robust Z-score < -2.5 (LD targeting ratio of < 1.9950) to determine hits whose depletion impaired GPAT₄ targeting. A cut off was also set at a robust Z-score of > 2.5 (LD targeting ratio of > 2.8398). Of the close to 14,000 genes tested, 896 were hits whose depletion impaired GPAT₄ targeting and are thus required for GPAT₄ targeting to LDs. 214 genes were hits whose depletion enhanced GPAT₄ targeting. Among the hits whose depletion impaired GPAT₄ targeting, CG12935 was of high interest because its depletion had one of the most dramatic effects on GPAT₄ targeting along with the Arf79f and β -COP controls with a robust Z-score of -6.36, yet it has been poorly characterized (Figure 3.1A).

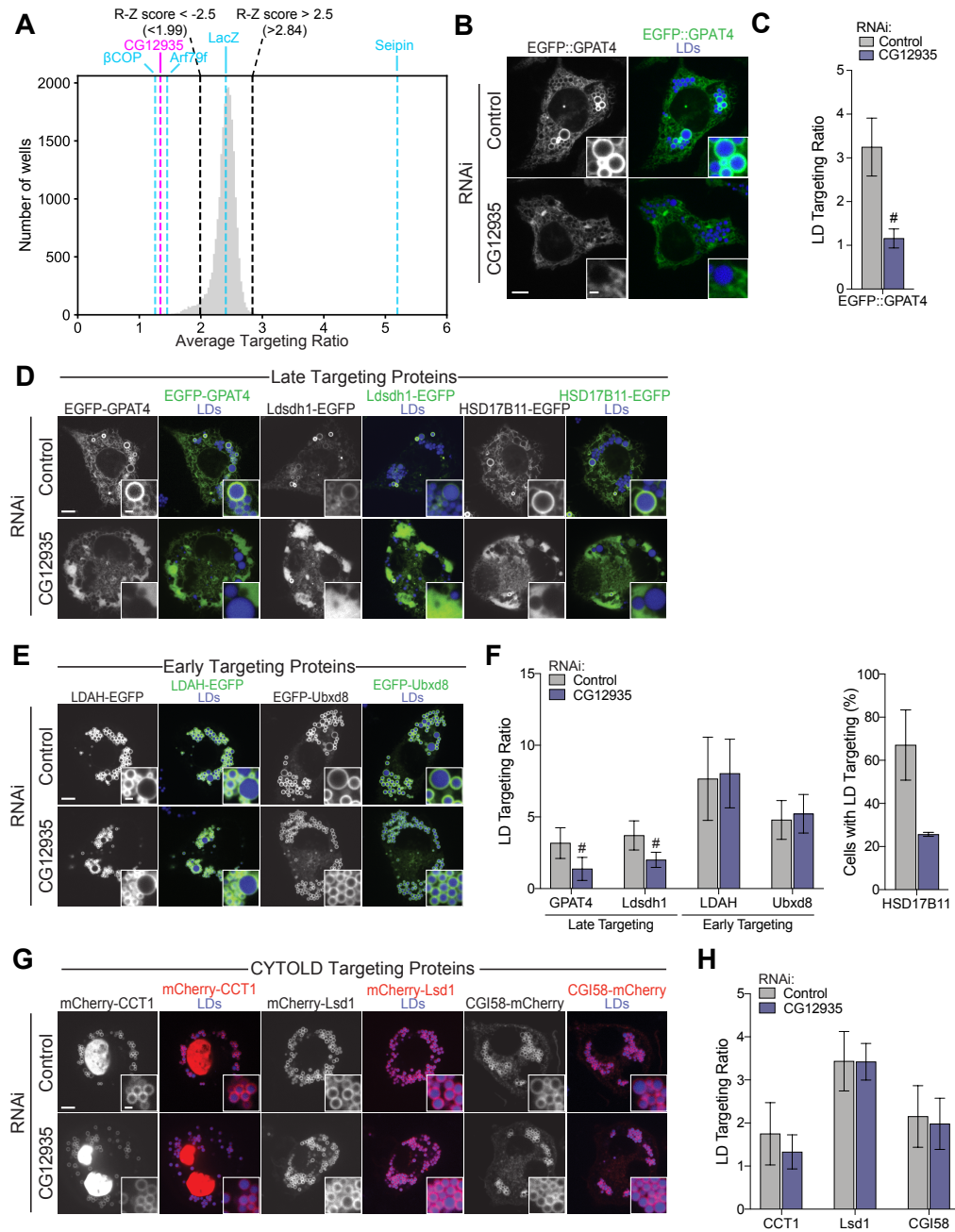
We first sought to independently verify the screen results, using an additional dsRNA designed against CG12935. Using an *Drosophila* S2 R+ cell in which GPAT₄ has been fluorescently tagged with GFP at its endogenous locus to avoid artifacts of overexpression, I tested the effects of CG12935 knockdown on GPAT₄ targeting to LDs on a spinning disk confocal for higher resolution images and quantification (Figure 3.1B). As a control I used dsRNA against pBlueScript KS II+ which, similarly to LacZ used in the screen, is not a part of the genome and therefore controls for the knock-down process. CG12935 depletion by dsRNA drastically impaired cell viability (data not shown), therefore a knockout cell line was not attempted. By confocal microscopy, TMEM223 depletion dramatically decreased endogenous GPAT₄ localization to LDs (Figure 3.1, B-C). Furthermore, patches of GPAT₄ appeared to accumulate in contrast to the robust enrichment of GPAT₄ to LDs in control knock down cells (Figure 3.1B).

3.4 CG12935 DEPLETION IMPACT ON GPAT₄ TARGETING IS GENERAL FOR OTHER LATE TARGETING ERTOLD PROTEINS

While CG12935 depletion dramatically affects GPAT₄ targeting, we wanted to test if this effect was unique to GPAT₄ or a general effect on the fundamental process of ERTOLD protein targeting. To test this, we looked at the localization of other ERTOLD targeting proteins, Ldsdh-1 and HSD17B11, that target at later time points after oleate addition like GPAT₄. Similar to GPAT₄ these two proteins have been shown to target from the ER to LDs after 3 to 6 hours of incubation with oleate, compared to earlier ERTOLD targeting proteins that localize to LDs as early as tens of minutes after oleate incubation. CG12935 depletion impairs targeting of both of these proteins with the addition of oleate, indicating that CG12935 has a general effect on late protein targeting (Figure 3.1, D & F). Interestingly, CG12935 depletion did not affect LDAH and Ubx8 targeting from ER to LDs; these proteins are early targeting, arriving at the LDs within 30 minutes of incuba-

Figure 3.1 (following page): (A) Distribution of targeting ratios from all genes in the screen (n = 50,688). Median LD targeting ratios for controls (β -COP, Arf79f, LacZ and seipin) are denoted by blue lines. Cut offs to identify screen hits are denoted by black lines. Median LD targeting ratio of CG12935 is marked by a magenta line. (B) Representative images of *Drosophila* S2 R+ cells with endogenously tagged GPAT4 (EGFP::GPAT4) by CRISPR knock in were treated with dsRNA against CG12935 or control for 5 days, incubated in oleic acid for 21 hours, then stained with MDH and imaged by confocal microscopy. Scale bar 5 μ m and for inset 1 μ m. (C) Quantification of LD targeting ratio from images represented by (B). n=17 for Control, n=19 for CG12935. Two-tailed unpaired t test, #p<0.0001 compared to control. (D) Representative images of wildtype *Drosophila* S2 R+ cells treated with dsRNA against CG12935 or control for 5 days, transfected with EGFP constructs of late ERTOLD targeting proteins, incubated in oleic acid for 21 hours, then stained with MDH and imaged by confocal microscopy. CG12935 is also required for targeting of other late ERTOLD targeting proteins. Scale bar 5 μ m and for inset 1 μ m. (E) Representative images of wildtype *Drosophila* S2 R+ cells treated with dsRNA against CG12935 or control for 5 days, transfected with EGFP constructs of early ERTOLD targeting proteins, incubated in oleic acid for 21 hours, then stained with MDH and imaged by confocal microscopy. CG12935 requirement for ERTOLD targeting proteins is specific to late, not early targeting proteins. Scale bar 5 μ m and for inset 1 μ m. (F) Quantification of transfected proteins LD targeting ratio with control or CG12935 depletion in (D) and (E) reveal specificity of CG12935 for ERTOLD targeting of late targeting proteins n=13-21 cells. Multiple t test with Bonferroni-Dunn multiple comparisons test, *p<0.05, **p<0.01 compared to control. Cells transfected with HSD17B11-G were quantified as percentage of cells with >2 LDs with LD targeting. Data represented as mean +/- SD of 2 independent experiments n>50 for control, n>34 for CG12935 for each experiment. Two-tailed unpaired t test. (G) Representative images of wildtype *Drosophila* S2 R+ cells treated with dsRNA against CG12935 or control for 5 days, transfected with mCherry constructs of CYTOLD targeting proteins, incubated in oleic acid for 21 hours, then stained with MDH and imaged by confocal microscopy. CG12935 is not required for CYTOLD targeting proteins. Nuclear signal was removed in quantification of mC-CCT1 transfected cells. Scale bar 5 μ m and for inset 1 μ m. (H) Quantification of transfected proteins LD targeting ratio with control or CG12935 depletion in (G) reveal CYTOLD targeting does not require CG12935 n=15-21 cells.

Figure 3.1: (continued)



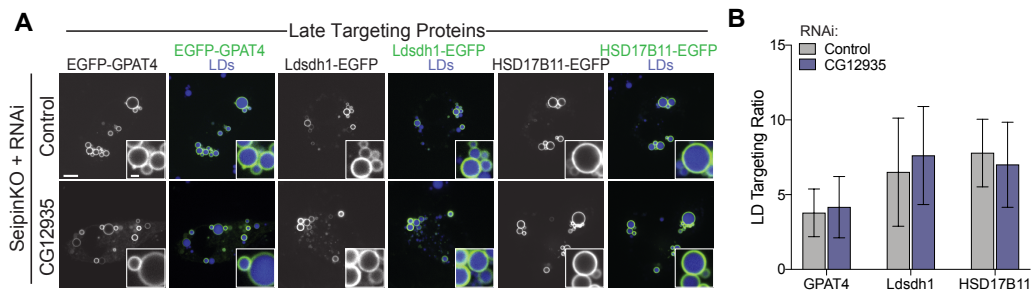


Figure 3.2: (A) Representative images of Seipin knock out *Drosophila* S2 R+ cells were treated with dsRNA against CG12935 or control for 5 days, transfected with EGFP constructs of late ERTOLD targeting proteins, incubated in oleic acid for 21 hours, then stained with MDH and imaged by confocal microscopy. Scale bar 5 μ m and for inlay 1 μ m. (B) Quantification of LD targeting ratio from images represented by (A). n=19-23 for Control, n=22-25 for CG12935. Two-tailed unpaired t test.

tion with OA (Figure 3.1, E-F). These observations suggest that TMEM223 is uniquely required for targeting of late ERTOLD proteins

To test if CG12935 depletion effect on protein targeting was specific to ERTOLD targeting proteins, we looked at the localization of CYTOLD targeting proteins with CG12935 knockdown. Indeed, we see that CCT1 and Lsd1 targeting to LDs from the cytosol is not impaired with CG12935 knockdown (Figure 3.1, G-H). Finally, we asked if, similar to components identified in the screen involved in forming ER-LD membrane bridges, knockout of Seipin would bypass the impaired targeting of late targeting proteins with CG12935 knockdown. Seipin is thought to be a protein barrier, and this model is supported by the screen as depletion of seipin in the screen leads to enhanced targeting of proteins from the ER to LDs. CG12935 knockdown in Seipin knockout cells did not impair the targeting of GPAT4, Ldsdh1 or HSD17B11, indicating that there is a bypass to the normal targeting pathway that CG12935 affects in the absence of Seipin (Figure 3.2).

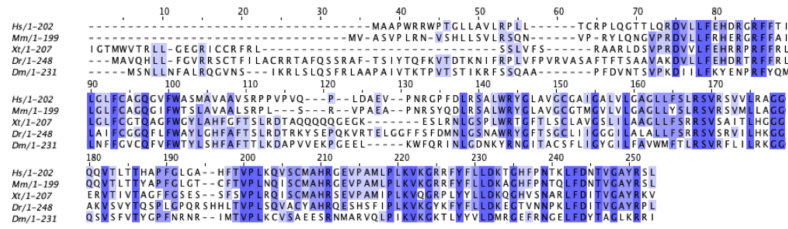


Figure 3.3: TMEM223 is highly conserved across species¹⁸⁰. Hs = *Homo sapiens*, Mm = *Mus musculus*, Xt = *Xenopus tropicalis*, Dr = *Danio rerio*, Dm = *Drosophila melanogaster*.

3.5 TMEM223 IS A HIGHLY CONSERVED PROTEIN LOCALIZING TO THE MITOCHONDRIA

CG12935 encodes a 27 kDa protein that is highly conserved across species, including in mammalian cells where the homologue is TMEM223 (Figure 3.3). The highest levels of conservation across species are within the transmembrane domains and the C-terminus of TMEM223 (Figure 3.3). TMEM223 is predicted to have two transmembrane domains^{53,253}, and both human and fly TMEM223 are predicted by MitoFates to have a mitochondria targeting sequence⁵¹. While little is known about this protein, CG12935, henceforth TMEM223, has been identified in an inner mitochondrial membrane proteome¹²² as well as a potential substrate of the Sec61-auxiliary translocon-associated protein (TRAP) complex¹⁴¹, posing an intriguing localization dichotomy. One yeast two-hybrid study identified TMEM223 as an interactor of the Cav2.2 Ca²⁺ channel and localized the protein to mitochondria in mouse embryo fibroblasts, however no follow up studies were performed¹³⁰. Intriguingly, recent studies suggest that TMEM223 is part of the TMEM70/TMEM186/TMEM223 family^{80,172}. TMEM70 and TMEM186 are implicated in the assembly of Complex V and Complex I, respectively, and both are predicted to localize to the mitochondrial inner membrane by two transmembrane domains that are similar to the two transmembranes predicted for TMEM223, with termini facing the matrix^{49,70,112,116,172,223}.

As the function of TMEM223 is largely unknown and its depletion profoundly decreased GPAT₄

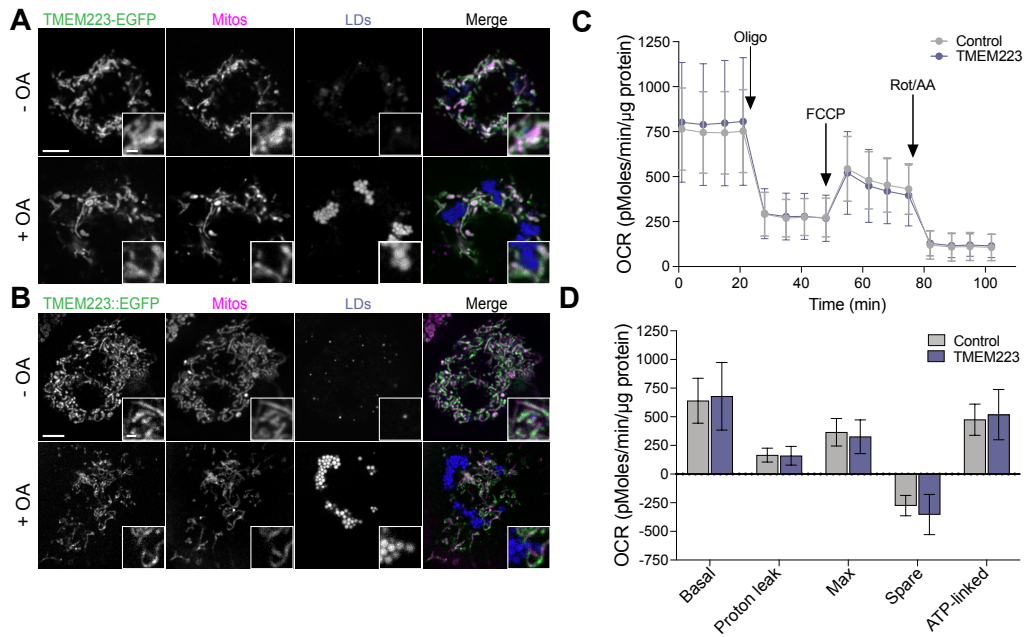


Figure 3.4: (A) Overexpressed TMEM223-GFP localizes to mitochondria (MitoTracker Red CMXRos) in the presence or absence of oleic acid (OA). LDs marked by MDH. Scale bar 5 μm and for inlay 1 μm . (B) TMEM223 tagged endogenously with EGFP at the C-terminus by CRISPR Cas-9 knock in (TMEM223::EGFP) localizes to the mitochondria (MitoTracker Deep Red FM) in the presence or absence of oleic acid (OA). LDs marked by MDH. Scale bar 5 μm and for inlay 1 μm . (C) Oxygen consumption rate (OCR) was measured in pMoles per minute at baseline, normalized to protein concentration in *Drosophila* S2 R+ cells subjected to dsRNA against control or TMEM223. 2.5 μM oligomycin (Oligo), 1 μM carbonyl cyanide p-trifluoromethoxyphenylhydrazone (FCCP), and 5 μM each of rotenone and antimycin A (Rot/AA) were injected sequentially at respective arrows and OCR was measured after each injection. (D) Respiratory parameters calculated from oxygen consumption rates measured in (C).

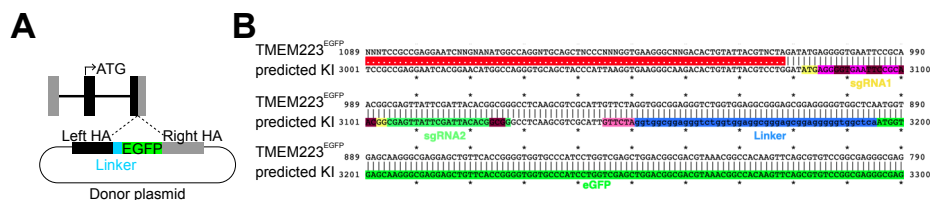


Figure 3.5: (A) Schematic of endogenous tagging dTMEM223 with EGFP by CRISPR/Cas9 knock in. (B) Sequencing of genomic DNA isolated from endogenously tagged TMEM223::EGFP cells confirms that EGFP is in frame and inserted into the genome as expected.

targeting ratio in the screen, we sought to characterize TMEM₂₂₃ in the context of ERTOLD protein targeting by first determining its cellular localization. In *Drosophila* S2 R+ cells exogenously expressed TMEM₂₂₃ conjugated to EGFP at the C-terminus localized to the mitochondria in the absence or presence of oleate, colocalizing with MitoTracker which labels the mitochondria (Figure 3.4A). In some cells highly overexpressing TMEM₂₂₃-EGFP, signal was observed at the ER or near LDs (data not shown), this was exacerbated when TMEM₂₂₃ was tagged at the N-terminus. To determine the localization of endogenous TMEM₂₂₃, CRISPR/Cas9 was used to generate a knock-in cell line where TMEM₂₂₃ is endogenously tagged at the C-terminal locus with EGFP (TMEM₂₂₃EGFP) in S2 R+ cells. This was confirmed by gDNA sequencing (Figure 3.5, A-B). In these cells TMEM₂₂₃ clearly localizes to mitochondria in the presence or absence of oleate (Figure 3.4B). As TMEM₂₂₃ is a mitochondrial protein it suggests that aspects of the mitochondria and its relationship with the ER or LDs may influence ERTOLD protein targeting.

3.6 DEPLETION OF dTMEM₂₂₃ RESULTS IN ER ABNORMALITIES

We first sought to determine if depletion of TMEM₂₂₃ affected mitochondrial function by looking at mitochondria respiration. We reasoned that changes in cellular energy production with impaired mitochondrial respiration could impair ERTOLD protein targeting phospholipid transport

between membranes and membrane fusion require ATP^{87,219}. We measured oxygen consumption between S2 R+ cells treated with either control or TMEM223 dsRNA and observed no significant changes in mitochondrial respiration with TMEM223 depletion (Figure 3.4, C-D).

We next hypothesized that TMEM223 at the mitochondria could be affecting ERTOLD protein targeting by affecting the communication between mitochondria and the ER. Numerous studies have characterized the intricate relationship between the ER and the mitochondria for the exchange of calcium and phospholipids among other molecules. We therefore investigated any changes to the ER with TMEM223 depletion, particularly as GPAT4 accumulation in patches had been observed with TMEM223 depletion. Using a *Drosophila* S2 R+ cell line in which the ER-resident protein Calnexin99A (CNX99A) has been endogenously tagged with the fluorophore EGFP¹⁰³, we observed dramatic changes in ER morphology with TMEM223 depletion that matched the GPAT4 patches: patches of CNX99A ER were consistently observed in cells treated with TMEM223 dsRNA compared to control dsRNA (Figure 3.6A).

As TMEM223 depletion induces strong aberrations to normal ER morphology, we wondered if common processes dependent on ER organization were also disrupted, such as protein trafficking from ER exit sites (ERES) for secretion¹²⁰. To test this, we expressed a construct that is composed of ssHRP conjugated to an ER targeting signal (BiP) under a *Drosophila* metallothionein promoter⁸. The expression of this ssHRP construct once transfected into cells is induced by the addition of copper sulfate to the medium. As this construct is packaged into vesicles at the ERES, trafficked through the ER and Golgi, and ultimately secreted, the level of HRP detected in the medium reflects the function of ER-Golgi trafficking originating from the ERES and protein secretion⁸. As positive controls we used knockdown of Syntaxin5 (Syx5), which is a t-SNARE involved in the secretion pathway, and Tango1, which was identified through a screen using this readout as an organizer of protein transport and the Golgi apparatus⁸. Interestingly, both Syx5 and Tango1 were identified in the genome wide RNAi screen (J. Song unpublished) and are known to localize to the

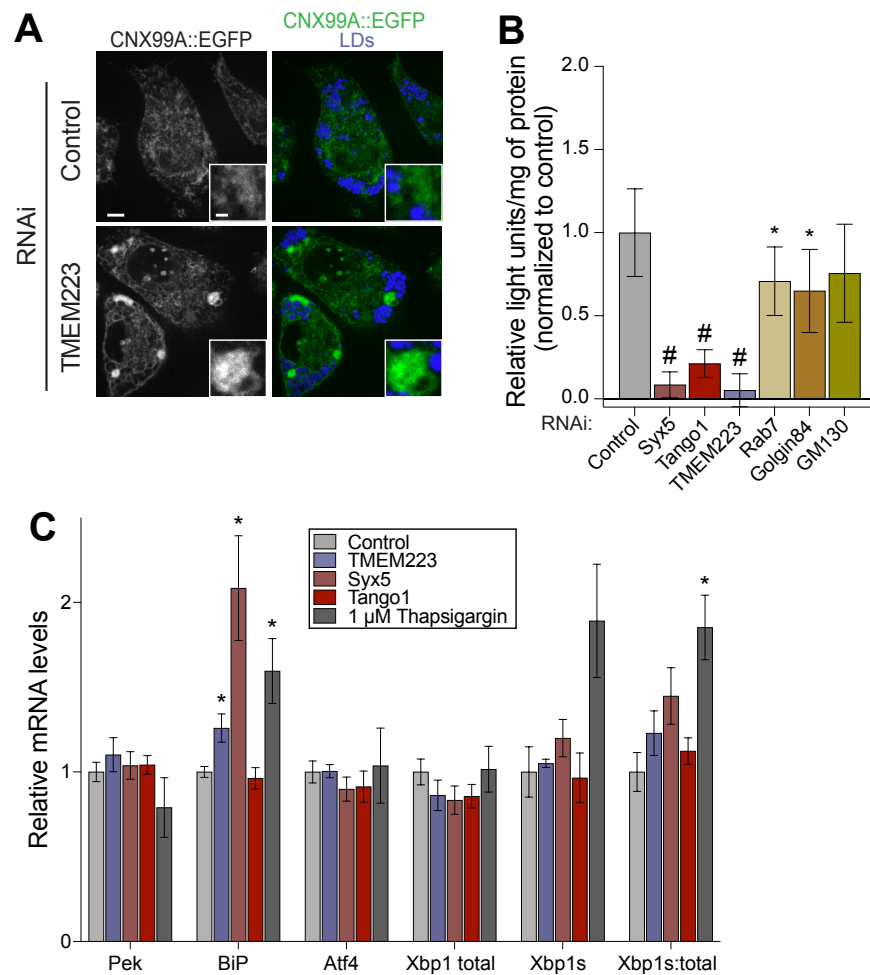


Figure 3.6: (A) TMEM223 depletion in *Drosophila* S2 R+ cells with endogenously tagged Calnexin99A (CNX99A::EGFP)¹⁰³ is characterized by ER aggregates of Calnexin99A compared to control knockdown after incubation with oleic acid for 21 hours. LDs marked by MDH. Scale bar 5 μ m and for inlay 1 μ m. (B) Quantification of ssHRP secreted into media through the ERES and Golgi with depletion of Syx5, Tango1 or TMEM223 is significantly impaired compared to control knockdown or depletion of components of other membrane trafficking pathways (Rab7, Golgin84, GM130). Data are represented as mean \pm SD of the results from at least 2 independent experiments. Two-tailed unpaired t test, * p <0.05, # p <0.0001 compared to control. (C) Wildtype *Drosophila* S2 R+ cells were subjected to dsRNA for 5 days and RNA was extracted for qPCR to detect gene expression of ER stress response components. Multiple t test with Bonferroni-Dunn multiple comparisons test, * p <0.05 compared to control.

ERES for their function. As general controls we included Rab7, Golgin84 and GM130, which are proteins involved in other cellular membrane trafficking processes. Strikingly, TMEM223 depletion impaired protein secretion from the ERES and through the Golgi to the same level as Syx5 and Tango1 depletion: close to no secretion (Figure 3.6B). These observations suggest that TMEM223 depletion at the mitochondria affects ER morphology; we can imagine that, consequently, impaired ER morphology affects protein secretion as in Syx5 and Tango1 knockdown cells. Finally, we tested if depletion in TMEM223 caused ER stress. We observe that, while not as dramatic as cells treated with Thapsigargin to induce ER stress, TMEM223 depletion slightly increased levels of the ER chaperone, BiP, to a lesser extent than Syx5 depletion (Figure 3.6C). Of note, Tango1 depletion does not appear to induce ER stress.

3.7 TMEM223 IS REQUIRED FOR CELLULAR LIPID HOMEOSTASIS

Based on the dramatic effects TMEM223 depletion at the mitochondria has on ER morphology and ERES derived protein secretion, we hypothesized that the common culprit could be changes in lipids, particularly phospholipids. Phospholipid balance is important for LD formation and expansion as well as LD protein targeting^{110,232}. While the ER is known to be a major site of phospholipid biosynthesis in the cell, the mitochondria also contributes to the synthesis of phospholipids such as phosphatidylcholine and phosphatidylethanolamine (PC and PE)^{48,134,221}. PE produced at high levels at the mitochondria, for example, can be transferred to the ER for downstream conversion to PC¹³⁴. Dysregulation in PC synthesis has been shown by previous members of our laboratory to cause defects in LD homeostasis¹¹³.

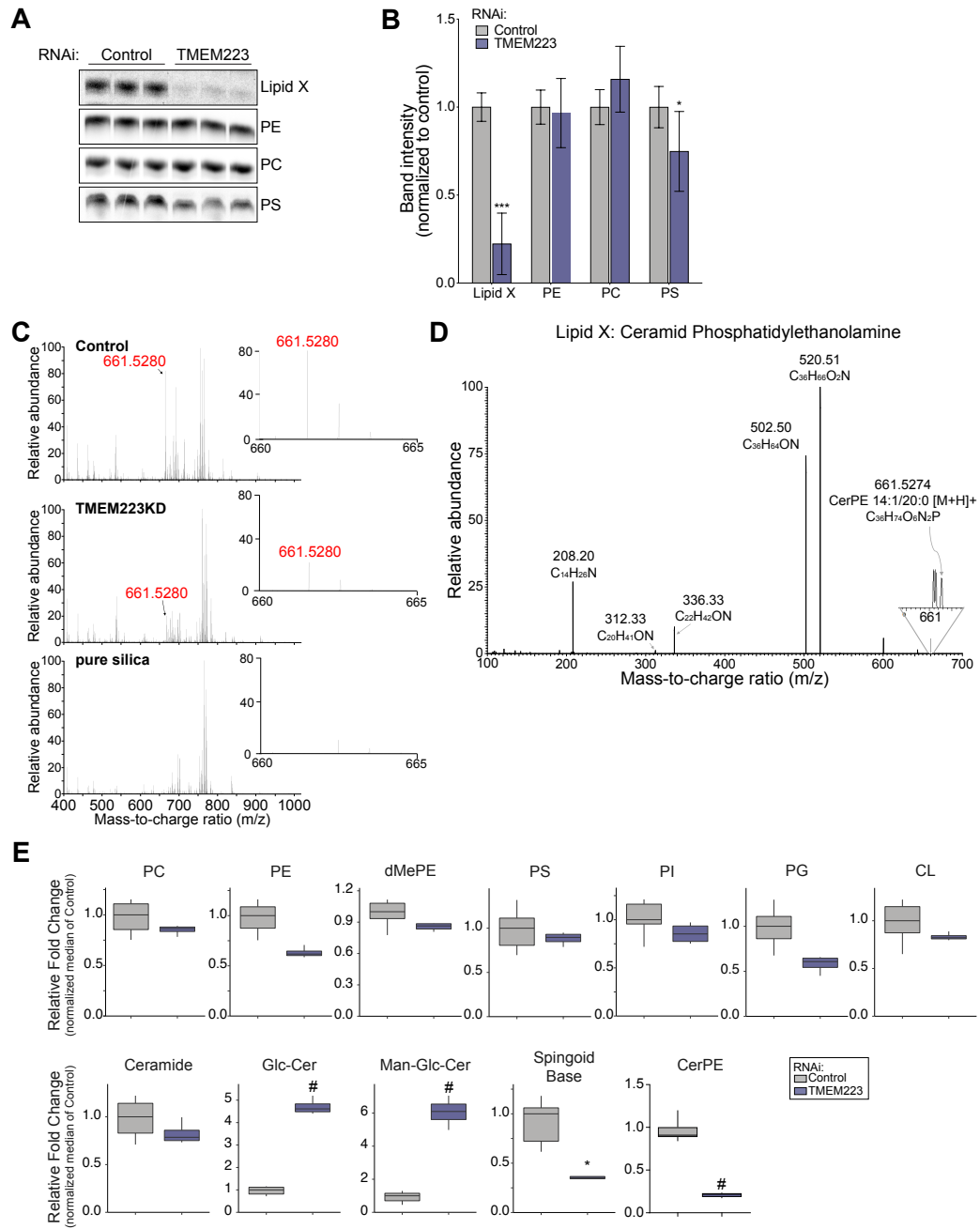
As mitochondria and the ER are known to exchange phospholipids^{1,36,161,219}, we sought to determine if TMEM223 depletion affected cellular lipid profiles that could subsequently affect ERTOLD protein targeting. In studies of intact *Drosophila* S2 R+ cells incubated with radio-labeled [¹⁴C] oleate overnight, phospholipid changes with TMEM223 depletion were observed. Strikingly, an unknown phospholipid running at a height between phosphatidylcholine (PC) and phosphatidylethanolamine (PE) was depleted with TMEM223 knockdown compared to control knockdown (Figure 3.7, A-B). To determine the identity of the unknown Lipid X, unlabeled cells were run alongside radiolabeled cells to determine the localization of the unknown phospholipid when separated on silica plates by thin layer chromatography (TLC). Silica plates were scraped at the location of Lipid X from cells treated with either control or TMEM223 dsRNA and incubated overnight in oleate, back extracted in 2:1 Chloroform:Methanol and lipids were directly diffused into the mass spectrometer (Figure 3.7C-D). As a control, an empty silica lane was extracted from wildtype S2 R+ cells. By comparing the intensity of all identified lipids in the control knockdown sample and the TMEM223 knockdown compared to the silica control, the sphingolipid ceramide phosphoethanolamine (CerPE) was identified as the most abundant lipid detected that was depleted in TMEM223 knockdown samples⁷⁸.

To corroborate our finding, we took an unbiased approach, using whole cell lipidomics of S2 R+ cells treated with dsRNA against control or TMEM223 and incubated with oleate overnight. Interestingly, TMEM223 knockdown specifically affected sphingolipids, leading to a dramatic accumulation of glucosylceramides as well as decreases in sphingoid bases and partial decrease detected in CerPE, thereby confirming our identification of the phospholipid depleted with TMEM223 depletion (Figure 3.7E).

CerPE is the *Drosophila* equivalent to mammalian sphingomyelin, which plays a key role in membrane structure^{21,183}. CerPE is synthesized in two locations: at the Golgi Apparatus by ceramide phosphoethanolamine synthase (CPES), or minimally at the ER by sphingomyelin synthase related-

Figure 3.7 (following page): (A) Wildtype *Drosophila* S2 R+ cells were subjected to dsRNA against control or TMEM223 for 4 days before addition of oleate spiked with radiolabeled oleate for 21 hours. On day 5 of knockdown, incorporation of [¹⁴C] oleate into phospholipids phosphatidylethanolamine (PE), phosphatidylserine (PS) and phosphatidylcholine (PC) were measured. Lipids were extracted from cells and separated by TLC. Representative autoradiographs are shown. The unknown phospholipid, Lipid X, is depleted with TMEM223 knockdown (B) Quantification of Lipid X, PE, PC and PS reveal that the unknown lipid is dramatically decreased with TMEM223 depletion. Data are represented as mean +/- SD of 4 independent experiments. n=3 per knockdown. Multiple t test with Bonferroni-Dunn multiple comparisons test, *p<0.05, **p<0.01, #p<0.0001 compared to control. (C) Similar experiment to that in (A) was performed with unlabeled oleate, and the silica plate was scraped at the location of Lipid X. Lipids were extracted from silica in 2:1 Methanol:Chloroform and directly infused into a mass spectrometer and measured spectra are presented for one of the most abundant ceramide phosphoethanolamine species detected in control cells that was decreased in TMEM223 knockdown cells (CerPE[14:1/20:0]); n=2. As a control an empty silica lane was used. (D) Fragmentation pattern after higher-energy collision dissociation of the ion 661.52 identified in (C) to determine the identified lipid is Ceramide Phosphatidylethanolamine (CerPE) (E) Whole cell lipidomics was performed on wildtype *Drosophila* S2 R+ cells subjected to dsRNA against control or TMEM223 for 4 days then incubated with oleic acid for 21 hours. Lipids were extracted on day 5 of dsRNA treatment and separated on an LC/MS revealing changes in sphingolipids. Relative fold change represented as normalized median of control +/- SD. TMEM223KD, n = 4; Control KD, n = 6. Multiple t test with Bonferroni-Dunn multiple comparisons test, *p<0.05, #p<0.0001 compared to control.

Figure 3.7: (continued)



1 (SMSr)^{148,217}. Interestingly, studies in *Drosophila* cells have shown a connection between depletion of SMSr at the ER and accumulation of ceramide and glucosylceramides that impairs ERES²¹⁶. We wondered if the depletion of CerPE or the accumulation of glucosylceramide with TMEM223 knockdown was specific to TMEM223 depletion or was more broadly related to mitochondrial function.

3.8 DEPLETION OF MICOS COMPONENTS QIL1 AND CHCHD3 EXHIBIT PHENOTYPES SIMILAR TO TMEM223 DEPLETION

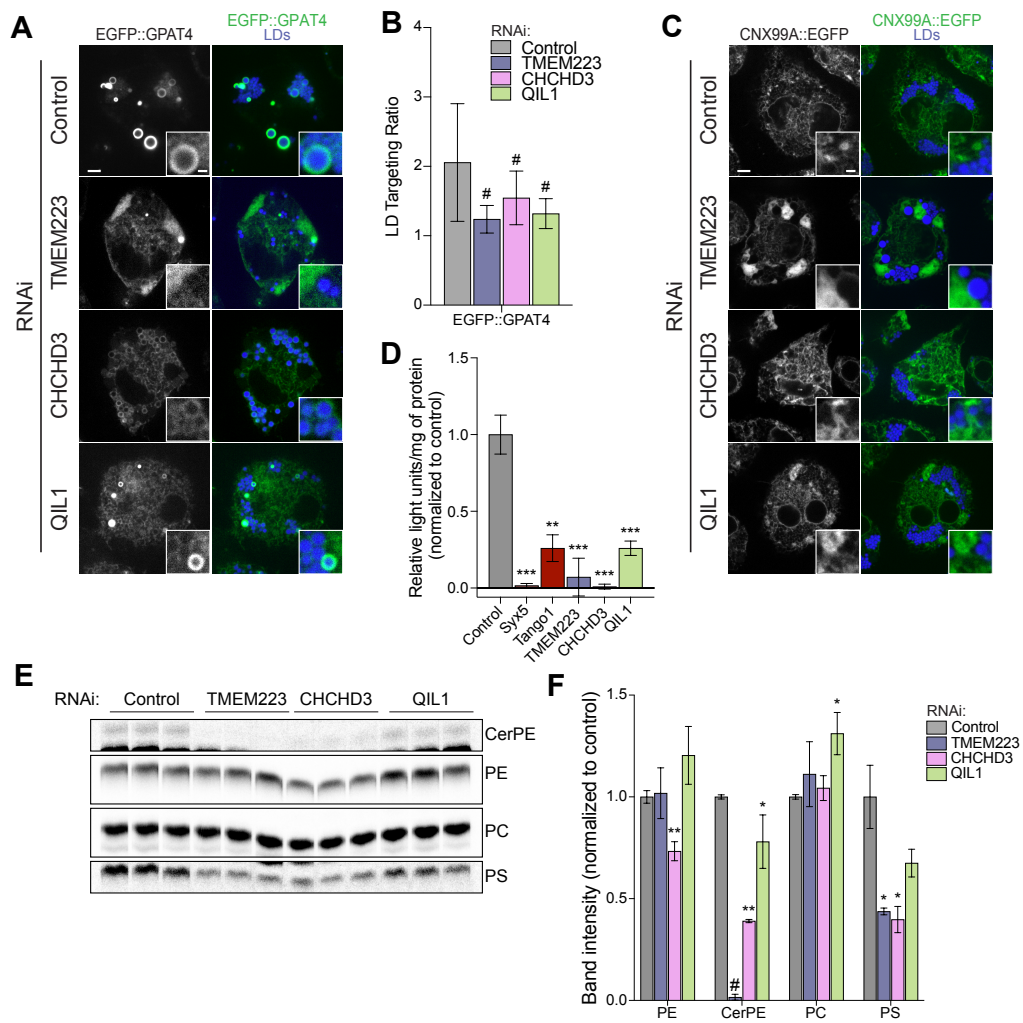
Returning to the results from our genome wide screen, pathway analysis of other mitochondrial genes that decrease targeting of GPAT₄ targeting with knockdown revealed two key components of the mitochondrial contact site and cristae organizing system (MICOS). To test if TMEM₂₂₃ functions similarly to components of MICOS, QIL₁ and CHCHD₃ that were strong hits in the screen, I confirmed the effect of CHCHD₃ and QIL₁ depletion on GPAT₄ targeting using a spinning disk confocal for higher resolution (Figure 3.8, A-B). As MICOS has previously been implicated in phospholipid transport between the ER and the mitochondria¹, we used the aforementioned CNX_{99A}-EGFP knock-in cells to investigate changes in ER morphology. Neither QIL₁ or CHCHD₃ depletion caused disruption in ER morphology to the same extent as TMEM₂₂₃ knockdown, however ER aggregates were observed in some cells with QIL₁ knockdown (Figure 3.8C). Using the ssHRP construct packaged at the ERES for secretion, we observed that both CHCHD₃ and QIL₁ dramatically impaired protein secretion to the extent of TMEM₂₂₃ depletion (Figure 3.8D). Most strikingly, we found that cells treated with CHCHD₃ and, to a lesser extent, QIL₁ dsRNA had decreased CerPE levels, similar to TMEM₂₂₃ depletion (Figure 3.8, E-F). These observations suggest that TMEM₂₂₃ and MICOS at the mitochondria have similar effects that alter ERTOLD protein targeting.

3.9 TMEM223 DEPLETION IN MAMMALIAN CELLS RESULTS IN SIMILAR PHENOTYPES

As TMEM₂₂₃ is highly conserved from *Drosophila* to humans we tested if TMEM₂₂₃ is also required in mammalian cells for ERTOLD protein targeting. We first determined if the mitochondrial localization was conserved between organisms. We confirmed that TMEM₂₂₃ also localizes to mitochondria in the human breast cancer carcinoma cell line, SUM159 cells, by generating a cell

Figure 3.8 (following page): (A) Representative images of EGFP::GPAT4 knock in *Drosophila* S2 R+ cells were treated with dsRNA against CG12935, CHCHD3, QIL1 or control for 5 days, incubated in oleic acid for 21 hours, then stained with MDH and imaged by confocal microscopy. Scale bar 5 μ m and for inlay 1 μ m. (B) Quantification of LD targeting ratio from images represented by (A) reveal QIL1 and CHCHD3 depletion also impair ERTOLD protein targeting. n=25-45 cells per knockdown. Two-tailed unpaired t test, #p<0.0001 compared to control. (C) Representative images of CNX99A::EGFP knock in *Drosophila* S2 R+ cells were treated with dsRNA against CG12935, CHCHD3, QIL1 or control for 5 days, incubated in oleic acid for 21 hours, then stained with MDH and imaged by confocal microscopy. CNX99A aggregates are observed with QIL1 and TMEM223 depletion, and mildly with CHCHD3 depletion. Scale bar 5 μ m and for inlay 1 μ m. (D) Quantification of ssHRP secreted into media through the ERES and Golgi with depletion of Syx5, Tango1, TMEM223, CHCHD3 or QIL1 is significantly impaired compared to control knockdown. Data are represented as mean +/- SD. Two-tailed unpaired t test, **p<0.01, ***p<0.001 compared to control. (E) Wildtype *Drosophila* S2 R+ cells were subjected to dsRNA against control or TMEM223 for 4 days before addition of oleate spike with radiolabeled oleate for 21 hours. On day 5 of knockdown, incorporation of [¹⁴C] oleate into phospholipids phosphatidylethanolamine (PE), ceramide phosphoethanolamine (CerPE), phosphatidylcholine (PC), and phosphatidylserine (PS) were measured. Lipids were extracted from cells and separated by TLC. Representative autoradiographs are shown. (F) Quantification of PE, CerPE, PC and PS reveal that CerPE is dramatically decreased with TMEM223 or CHCHD3 depletion, and significantly decreased with QIL1 depletion. Data are represented as mean +/- SD. n=3 per knockdown. Multiple t test with Bonferroni-Dunn multiple comparisons test, *p<0.05, **p<0.01, #p<0.0001 compared to control.

Figure 3.8: (continued)



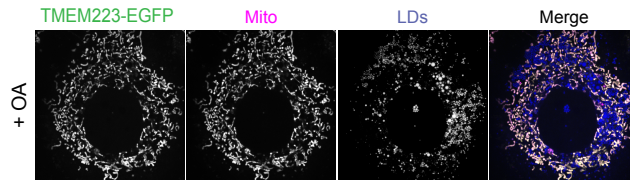


Figure 3.9: TMEM223-EGFP expressed in Huh7 cells also localizes to the mitochondria (MitoTracker Red CMXRos). Cells incubated with 0.5 mM oleic acid for 21 hours to form LDs visualized by LipidTox Deep Red. Scale bar 5 μ m and for inlay 1 μ m.

line stably expressing TMEM223 tagged with EGFP at the AAVS1 locus (Figure 3.10A). We also confirmed localization to the mitochondria in another cell line, Huh7, by exogenous overexpression of fluorescently tagged TMEM223 (Figure 3.9).

While localization of TMEM223 to the mitochondria had been proposed in the literature^{122,130,172} and confirmed here, the sublocalization within the mitochondria is unknown. This information would shed light on its potential function. To address this, we took advantage of the conservation of TMEM223 localization in mammalian cells, as there are more tools for mitochondria assays in mammalian cells. To determine if TMEM223 is an integral membrane protein, we isolated mitochondria from these cells and subjected them to increasing pH of sodium bicarbonate. An antibody against GFP was used to determine the localization of TMEM223 between the supernatant and pellet fractions. Similar to Tom40, TMEM223 (GFP) remained in the pellet fraction even with increasing pH. Peripheral membrane matrix proteins mtHSP70 and ClpP become strongly enriched in the supernatant fraction with increasing pH. Mic60, an integral membrane protein that localizes in the pellet fraction until the highest pH level, pH 12.0. (Figure 3.10B).

To determine the sublocalization of TMEM223 between the outer and inner mitochondrial membranes, we subjected cells to increasing levels of digitonin followed by Proteinase K treatment. Mitochondrial fission factor (Mff), Tom40, Tom 20 and Opa1 were used as markers of the outer mi-

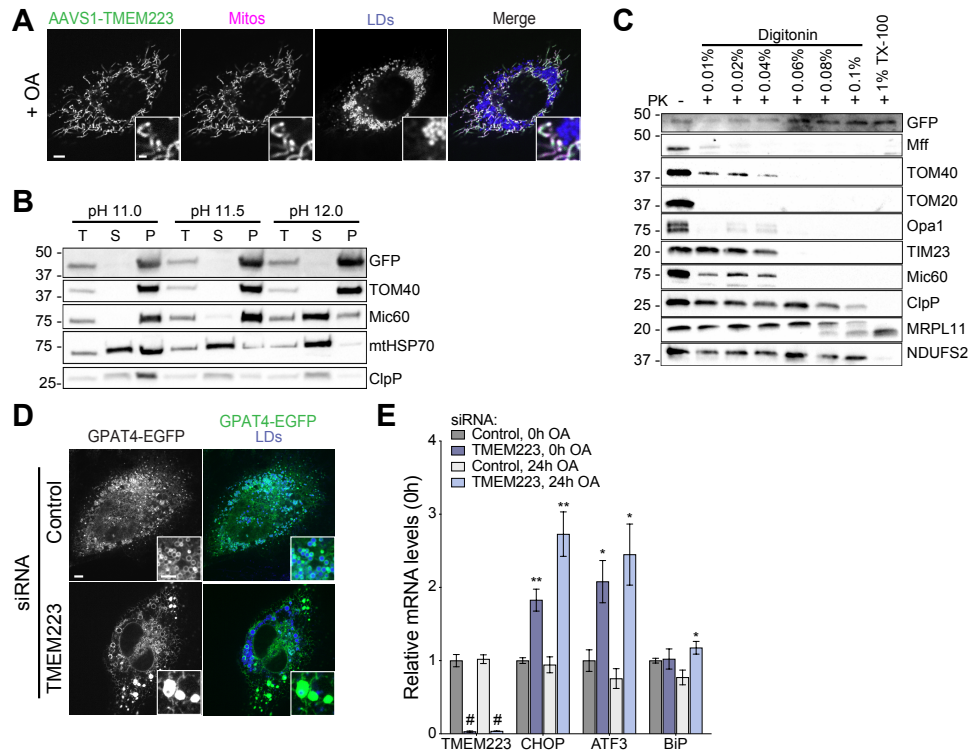


Figure 3.10: (A) AAVS1 Safe Harbor targeting method of EGFP conjugated to the C-terminus hTMEM223 under a TK promoter allowed stable integration into SUM159 (AAVS1-TMEM223). AAVS1-TK-TMEM223-EGFP localizes to mitochondria (MitoTracker Red CMXRos). Cells incubated with 0.5 mM oleic acid for 21 hours to form LDs visualized by LipidTox Deep Red. Scale bar 5 μ m and for inset 1 μ m. (B) Sodium bicarbonate extraction of mitochondrial membrane proteins with increasing pH. Antibodies against endogenous TOM40, MIC60, mtHSP70 and ClpP were used to identify the outer and inner membrane and matrix compartments respectively. Antibody against GFP was used to identify AAVS1-TK-TMEM223-EGFP and is shown in the mitochondrial membrane fraction. T = 10% of total input, S = supernatant, P = pellet. (C) TMEM223 localizes to the inner membrane compartment with termini likely facing toward the matrix. Increasing digitonin in the presence of Proteinase K was used to digest the outer membrane, then inner membrane proteins. Addition of TritonX-100 was used to access matrix proteins, though the mitoribosome component, MRPL11, and TMEM223 remained protected. Antibodies against endogenous Mff, TOM40, TOM20 and Opa1 marked the outer membrane, TIM23 and MIC60 marked the inner membrane, and ClpP, MRPL11 and NDUFS2 marked the matrix compartment. Molecular mass markers (kDa) are shown on the left for panels (B) and (C). (D) Wildtype SUM159 cells were treated with siRNA against control (NC1 sequence) or TMEM223 for two days, transfected with and EGFP-GPAT4 construct and treated with oleic acid for 24 hours before being stained with LipidTox Deep Red to visualize LDs. GPAT4 aggregates in the ER in cells treated with TMEM223 siRNA and does not fully enrich around LDs. (E) ER stress increases with depletion of TMEM223 by siRNA compared to control in presence or absence of oleic acid (OA) treatment. qPCR analysis of indicated genes where data represents mean \pm SD; n=3. Multiple t test with Bonferroni-Dunn multiple comparisons test, *p<0.05, **p<0.01, #p<0.0001 compared to control.

tochondrial membrane (OMM). These proteins were all degraded at the lowest levels of digitonin. Inner mitochondrial membrane (IMM) proteins Tim23 and Mic60 were degraded at higher levels of digitonin (0.04%). Matrix markers ClpP, MRPL11 and NDUFS2 were all protected even at the highest digitonin concentration. ClpP and NDUFS2 were both degraded with the addition of TritonX-100. MRPL11 was partially degraded, its association with the membrane and mitoribosomes may have protected it. Similar to MRPL11, TMEM223 (GFP) was also protected from Proteinase K digestion, even with TritonX-100 (Figure 3.10C). A recent paper posited the TMEM223 was homologue of yeast Mrx15 which is known to associate with the mitoribosome as well, which could explain our observations¹⁷². We reveal here that TMEM223 is a bona fide integral membrane protein that localizes to the inner mitochondrial membrane.

To test the effect of TMEM223 depletion in SUM159 cells on ERTOLD protein targeting, we used siRNA against TMEM223 in SUM159 cells, and exogenously expressed fluorescently tagged GPAT4 in knockdown cells before addition of oleate overnight. Similar to *Drosophila* S2 cells, depletion of TMEM223 by siRNA mediated knockdown impairs GPAT4 targeting to LDs at later time points, 24 hours after incubation with oleate (Figure 3.10D). In TMEM223 knockdown cells, GPAT4 instead localizes to the ER and aggregates around the larger LDs. Sheet-like patches of GPAT4 are also observed in the cell periphery (Figure 3.10D). The late onset of both phenotypes indicates a role of TMEM223 in ER homeostasis that begets the LD-related phenotypes observed. Furthermore, knock down of TMEM223 in SUM159 cells results in increased ER stress both in the presence and absence of oleate, suggesting TMEM223 depletion disrupts ER homeostasis (Figure 3.10E). Together these observations support our findings in *Drosophila* cells and reveal a conserved requirement for a mitochondria inner membrane protein in ERTOLD protein targeting.

3.10 DISCUSSION

Our current understanding of ER-LD bridge formation for protein targeting of ER to LDs highlight a role of proteins typically involved in ER-Golgi trafficking. Interestingly, additional strong hits in the screen whose depletion impaired GPAT₄ targeting – Tango₁ – are proteins involved in organizing the ER exit site, a specialized ER site for vesicle formation for ER-Golgi trafficking for protein secretion^{8,168}. Furthermore, membrane fusion proteins proposed to be required for ER-LD membrane fusion are also involved in ER to Golgi protein and phospholipid trafficking by vesicles, including Rint₁ and Syx₅. This model suggests that the proposed ER-LD bridges may also form at that ERES in a repurposing of machinery known to participate in membrane fusion for cargo transport. It is known that formation of these specialized ER domains for ER to Golgi trafficking involves a fencing of Tango₁ proteins and may depend on specific lipids to create or maintain these domains^{8,168}. Furthermore, a sphingolipid gradient is a characteristic of the secretory pathway from the ER to the Golgi¹⁰¹.

While studies have shown that a majority of CerPE is synthesized by CPES at the Golgi, additional investigations of the role of SMSr have revealed it plays a key role in modulating ER ceramide and glucosylceramide levels at the ER that are important for ER to Golgi trafficking. Depletion of SMSr, an enzyme known to synthesize a fraction of the CerPE in *Drosophila*, has been shown to disrupt ERES organization and transitional ER (tER)-Golgi units²¹⁶. This observation correlated with ceramide and glucosylceramide accumulation observed with depletion of TMEM223. However, depletion of CPES *Drosophila* cells only mildly impaired ERTOLD protein targeting despite completely depleting CerPE levels (Figure 3.11, A & C). SMSr depletion does not decrease CerPE levels, as previously reported²¹⁶, or ERTOLD protein targeting, but does dramatically increase glucosylceramide levels as previously reported²¹⁶ (Figure 3.11, B-C). Interestingly, double knock down of CPES and SMSr together does not impair ERTOLD protein targeting despite completely deplet-

ing CerPE levels. This suggests that CerPE itself is not the culprit but a downstream consequence. We hypothesize that the dramatic decrease in CerPE and accumulation of glucosylceramides with TMEM223 depletion is due to impaired ER-Golgi trafficking, as we observed ER-Golgi trafficking was clearly disrupted (Figure 3.6B), and this prevents normal trafficking of ceramide to the Golgi for CerPE synthesis. Of note, trafficking of ceramide from the ER to the Golgi for conversion to CerPE in *Drosophila* and sphingomyelin in mammalian cells is ATP-dependent via the cytosolic protein CERT^{118,213}. We suspect that the apoptotic and detrimental effects of ceramide accumulation in the ER is mitigated by conversion to glucosylceramides, hence the accumulation of glucosylceramide species.

However, these observations still beget the question of how does mitochondrial TMEM223 affect the fundamental process of protein targeting from the ER to LDs? Further studies need to be carried out to directly test the function of TMEM223 at the mitochondria. While TMEM223 depletion does not disrupt oxygen consumption in *Drosophila* S2 R+ cells, we clearly noted increased cell death with TMEM223 depletion. This could indicate that cellular energy levels are impaired with TMEM223 depletion. We propose to measure levels of energy molecules such as ATP/ADP and NAD/NADH ratios to complete our investigation of a role for TMEM223 in mitochondria function. As previously mentioned, the posited yeast homologue of TMEM223, Mrx15, was shown to have synthetic genetic interactions with the mitoribosome protein Mba1 (mammalian and *Drosophila* MRPL45); while depletion of Mrx15 alone did not have respiratory growth defects, Mrx15Δ on an Mba1Δ background exacerbated Mba1 respiratory growth defects on glycerol¹³⁷. Similarly, Mrx15Δ alone does not affect electron transport chain complex activity, but Mrx15Δ on an Mba1Δ background further depletes Complex IV protein levels and Complex IV activity¹³⁷. These studies as well as the evolutionary relationship between TMEM223 and TMEM186 and TMEM70, which are both involved in the assembly of Complex I or V, suggests TMEM223 may be involved in mitochondrial oxidative phosphorylation complex assembly. This can be directly

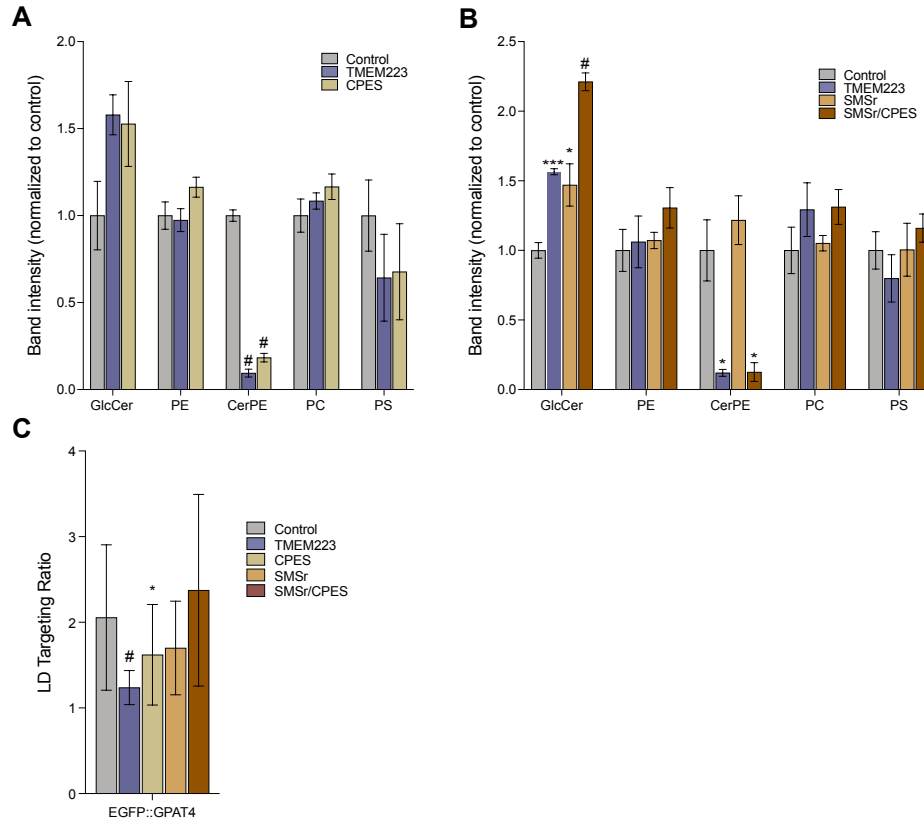


Figure 3.11: (A) Wildtype *Drosophila* S2 R+ cells were subjected to dsRNA against control, TMEM223 or CPES for 4 days before addition of oleate spike with radiolabeled oleate for 21 hours. On day 5 of knockdown, incorporation of [¹⁴C] oleate into phospholipids glucosylceramide (GlcCer), phosphatidylethanolamine (PE), ceramide phosphoethanolamine (CerPE), phosphatidylcholine (PC), and phosphatidylserine (PS) were measured. Lipids were extracted from cells and separated by TLC and quantification reveals trending increases in glucosylceramides and dramatic decreases in CerPE with either TMEM223 or CPES depletion. Data are represented as mean +/- SD. n=3 per knockdown. Multiple t test with Bonferroni-Dunn multiple comparisons test, #p<0.0001 compared to control. (B) Wildtype *Drosophila* S2 R+ cells were subjected to dsRNA against control, TMEM223, SMSr, or a combination of SMSr/CPES for 4 days before addition of oleate spike with radiolabeled oleate for 21 hours. On day 5 of knockdown, incorporation of [¹⁴C] oleate into phospholipids glucosylceramide (GlcCer), phosphatidylethanolamine (PE), ceramide phosphoethanolamine (CerPE), phosphatidylcholine (PC), and phosphatidylserine (PS) were measured. Lipids were extracted from cells and separated by TLC and quantification reveals increases in glucosylceramides with either TMEM223, SMSr or SMSr/CPES depletion. Dramatic decreases in CerPE were only observed with TMEM223 or SMSr/CPES depletion. Data are represented as mean +/- SD. n=3 per knockdown. Multiple t test with Bonferroni-Dunn multiple comparisons test, *p<0.05, ***p<0.001, #p<0.0001 compared to control. (C) EGFP::GPAT4 knock in *Drosophila* S2 R+ cells were treated with dsRNA against TMEM223, CPES, SMSr, SMSr/CPES or control for 5 days, incubated in oleic acid for 21 hours, then stained with MDH, imaged by confocal microscopy and the LD targeting ratio was quantified. n = 25-45 cells per knockdown, n = 13 for CPES/SMSr knockdown. *p<0.05, #p<0.0001 compared to control.

tested by assaying for individual activity of each of the complexes as has been previously reported in *Drosophila* S2 cells¹⁶⁶.

As MICOS is known to play a key role in cristae architecture, and displays similar phenotypes to TMEM223, electron microscopy of *Drosophila* cells subjected to dsRNA against control, TMEM223, CHCHD3 and QIL1 will reveal if TMEM223 similarly impairs mitochondrial morphology. Electron microscopy studies will also elucidate if the physical relationship between the ER and the mitochondria is disrupted with loss of either TMEM223 or MICOS components, CHCHD3 and QIL1.

Our current model is that MICOS and TMEM223 are required for mitochondrial function and that impaired energy production impairs ATP-dependent SNARE complex disassembly key for membrane fusion in membrane trafficking between the ER and Golgi⁷⁶ and posited to be important for ER-LD membrane fusion. Consequently, impaired ER-Golgi trafficking disrupts ER morphology, ER protein export and most likely ceramide transfer, resulting in the observed CerPE depletion and glucosylceramide accumulation and strikingly, impaired ERTOLD protein targeting. Ultimately, these studies suggest a previously unexplored role for the mitochondria in ERTOLD protein targeting and identifies an important mitochondrial factor for maintenance of membrane lipid composition, further illustrating how LD phenotypes can be sensitive markers for ER membrane dysfunction.

3.11 MATERIALS AND METHODS

3.11.1 ANTIBODIES

Antibodies used in this study are listed in Table A1

3.11.2 PLASMIDS

Plasmids were generated by first PCR amplifying the insert using PfuUltra II Fusion Hotstart DNA Polymerase (Agilent Technologies, #600672) following the manufacturer's protocol. PCR product were gel purified using a NucleoSpin Gel and PCR Clean-up Kit (Macherey-Nagel, #740609.250). Purified PCR products were cloned into an entry vector using the pENTR/D-TOPO Cloning Kit (Invitrogen, #K240020) and then using the the Gateway LR clonase Enzyme mix (Invitrogen, #11791019) cloned into a destination vector from the *Drosophila* Gateway vector collection system (Murphy Laboratory, Carnegie Mellon University). Information on PCR templates and primers can be found in Table A2.

For mammalian constructs, PCR of inserts for cloning was performed using Q5 Hot Start High-Fidelity DNA Polymerase (New England Biolabs, #M0493S). PCR products were purified with a NucleoSpin Gel and PCR Clean-up Kit (Macherey-Nagel, #740609.250). PCR products and vectors were digested with enzymes from New England Biolabs and then ligated with the Rapid DNA Dephos & Ligation Kit (Sigma-Aldrich, #4898117001). pTK-hGPAT₄-EGFP was developed by F. Wilfling²³⁴. The synthetic DNAs (gBlock, Integrated DNA Technologies) used in this study and cloning strategies of the other plasmids are summarized in Table A3.

3.11.3 *DROSOPHILA* CELL CULTURE AND TRANSFECTION

The *Drosophila* S2 R+ cells (sex: male) used were provided by Professor Norbert Perrimon (Harvard Medical School). Additional knock in cell lines used in this study (S2R+-Cnx99a-GFP-4, S2R+-Gmap-GFP-4, S2R+-Tom20-GFP-2) were kind gifts the lab of Professor Norbert Perrimon¹⁰³. EGFP::GPAT₄ knock in cells were developed by Jiunn Song (manuscript in preparation). Seipin knockout (SeipinKO) cells were previously developed by Wang et al²²⁷. Cells were cultured at 26 °C in Schneider's *Drosophila* Medium (Gibco, #21720001) with 10% fetal bovine serum (Gibco,

#16140-071) and 50 µg/mL streptomycin and 50 units/mL penicillin. Where noted, cells were incubated with 1 mM oleic acid complexed with 0.5% essentially fatty acid free BSA (Sigma Aldrich). Cells were maintained by splitting 1:3-1:12 every 2-4 days. Transfection of *Drosophila* S2 R+ cells was performed with Effectene Transfection Reagent (Qiagen, #301425) following the manufacturer's protocol. Any further treatments, such as addition of oleic acid, took place after 26 hours after transfection.

3.11.4 CRISPR-CAS9 KNOCK-IN CELL LINE GENERATION

Knock-in cell lines were generated using CRISPR-Cas9 and following protocols published by Housden et al^{91,90,92}. Guide RNA sequence and PCR primer sequences for donor construct cloning can be found in Table X. 1 week after transfection, cells were suspended in 1x DPBS supplemented with 1% fetal bovine serum and sorted by fluorescence-activated cell sorting (FACS Aria-561 with 100µm gating) to single cells into a 96-well plate containing conditioned media (media collected from confluent cells combined with equal volume of fresh *Drosophila* Schneider's medium with 20% fetal bovine serum). After near 3 weeks, viable monoclonal colonies were expanded and subjected to microscopy, western blot and genomic sequencing of PCR-amplified gRNA target regions subcloned into PCR Blunt II TOPO vector (Thermo Fisher Scientific) for verification of proper insertion by genome editing.

3.11.5 dsRNA SYNTHESIS FOR RNAi AND RNAi

Genomic DNA of wildtype *Drosophila* S2 R+ cells was isolated using GenElute Genomic DNA Miniprep Kit (Sigma-Aldrich, #G1N350-1KT). PCR amplification of genomic DNA was performed by Q5 Hot Start High-Fidelity DNA Polymerase (New England Biolabs, #M0493S) using primers with a T7 promoter (TAATACGACTCACTATAGGG) on both forward and reverse

primers. PCR products were separated using 1% agarose gel in Tris-acetate-EDTA buffer and PCR products of the expected size were excised from the gel for purification using a NucleoSpin Gel and PCR Clean-up Kit (Macherey-Nagel, #740609.250). Purified PCR products were used as a template for RNA transcription with the MEGAscript T7 Transcription Kit (Invitrogen, #AM1334). Synthesized dsRNA was then treated with TurboDNase from the MEGAscript T7 Transcription Kit (Invitrogen, #AM1334) before purification with the RNeasy Mini Kit (Qiagen, #74104). Expected size and quality of synthesized dsRNA were confirmed using a 1% agarose gel with Tris-Borate-EDTA buffer before use. PCR primer sequences for dsRNA are listed in Table A1.

For knockdown by RNAi, cells were spun down at 1,200 RPM for 5 minutes and resuspended in Schneider's *Drosophila* Medium (Gibco, #21720001) without serum supplementation or antibiotics at 6×10^4 cells/mL. Cells were plated in enough volume to cover the bottom of the plate and dsRNA was added at 20 ng/ μ L. After carefully rotating the plate to mix the contents, plates were sealed with parafilm and placed in a wet chamber composed of damp paper towels lining an airtight container, and stored in a 26 °C incubator to prevent evaporation. After 50 minutes, serum-supplemented medium with antibiotics (50 units/mL of penicillin, and 50 μ g/mL of streptomycin) was added carefully to avoid detaching cells at 3 volumes to the initial volume of cells plated. Plates were sealed again with parafilm and incubated in the wet chamber for 4-5 days prior to further treatment. If RNAi treated cells were used for transfection or imaging, cells were transferred to a new plate before following the transfection protocol or before imaging.

3.11.6 IMMUNOFLUORESCENCE

For standard immunofluorescence experiments, cells treated with RNAi were re-plated at 50% density on a glass-bottomed 24 well plate, each well coated manually with 0.1 mg/mL Concanavalin A. After one hour of settling at 26 °C, 1 mM oleic acid was added to cells where indicated. After 21 hours treatment with oleic acid, cells were fixed in 4% paraformaldehyde (Electron Microscopy Sci-

ences 15710) for 10 minutes. Cells were washed with Dulbecco's phosphate buffered saline (DPBS) (Gibco, #14190-144) 3 times then permeabilized for 3 minutes in 0.05% saponin (Sigma, #47036-50G-F), 0.1% bovine serum albumin (BSA) (Chem Cruz, #sc-2323) in 1x DPBS. Cells were washed three times in DPBS and then blocked for 1 hour in 0.05% saponin and 5% Normal Goat Serum (Cell Signaling Technologies, #5425S). Primary and secondary antibody dilutions were performed in the same solution. We used anti-dSec16 (gift from Professor Catherine Rabouille, Hubrecht Institute) at a 1:800 dilution to detect tER. We used Alexa Fluor 647-conjugated secondary antibodies (Life Technologies). In between first and secondary antibody incubations and after incubation with the secondary antibody, cells were washed 3x for 5 min each with 0.05% saponin and 0.2% BSA in DPBS). LDs were stained with MDH in DPBS before imaging.

3.11.7 IMAGING AND IMAGE ANALYSIS

Drosophila S2 R+ that underwent transfection or RNAi treatment in 24-well plates were resuspended in their current medium and plated at a 50% density on a glass-bottomed 24 well plate or plated with equal volume of fresh medium on a 35 mm dish with 14 mm No. 1.5 coverslip bottom (Matek Life Sciences, #P35G-1.5-14-C); each well was coated manually with 0.1 mg/mL Concanavalin A prior to plating. After one hour of settling at 26 °C, 1 mM oleic acid was added to cells where indicated. SUM159 mammalian cells were plated a 35 mm dish with 14 mm No. 1.5 coverslip bottom (Matek Life Sciences, #P35G-1.5-14-C). Imaging was carried out in Life Technologies Fluorobrite DMEM (Life Technologies) supplemented with SUM159 maintenance media components and, where indicated, treated with 0.5 mM oleic acid. Unless otherwise indicated, cells were imaged 21 hours after addition of oleic acid. LDs were stained with either 100 μ M monodansylpentane (MDH) (AUTODot; Abcepta, #SM100b), 0.5 μ g/ml BODIPY 493/503 (Life Technologies) or HCS LipidTOX Deep Red Neutral Lipid Stain (Thermo Fisher Scientific) at least 15 minutes before imaging. Mitochondria were stained with 25 nM MitoTracker Red CMXRos (Thermo Fisher,

#M-7512) or MitoTracker Deep Red FM (Thermo Fisher, #M22426) at least 15 minutes before imaging. Specific dyes used in each experiment are specified in the figure legends.

Live cell imaging was performed on a Nikon Eclipse Ti inverted microscope equipped with a CSU-X1 spinning disk confocal head (Yokogawa); 405-, 488-, 561-, or 639-nm laser lines; 100x ApoTIRF 1.4 NA objective (Nikon, Melville, NY); and iXon Ultra 897 electron-multiplying charge-coupled device (EMCCD) or Zyla 4.2 Plus scientific complementary metal-oxide semiconductor (sCMOS) cameras (Andor, Belfast, UK). Cells were annually tested for mycoplasma contamination by Universal Mycoplasma Detection Kit (American Type Culture Collection).

3.11.8 QUANTIFICATION OF LD TARGETING RATIO

Confocal images were quantified using FIJI software¹⁷⁴ to calculate LD targeting ratios. Cell boundaries were drawn manually based on fluorescence from the channel of the fluorescently tagged protein whose LD targeting was being measured. Cells were then individually cropped out and used as Mask 1. LD regions were distinguished by using the Otsu method of automatic thresholding to the monodansylpentane channel within each cropped cell. The LD signal was dilated by 1 pixel to include LD surfaces, serving as Mask 2. LD targeting ratios were determined by dividing the mean intensity of the fluorescent protein channel image in Mask 2 and dividing this value by the mean intensity of fluorescent protein signal in Mask 1 that in Mask 2. For quantification of CCT1 LD targeting ratio, nuclei were separately distinguished by manually drawing the nuclear boundary visible in the mCherry-CCT1 channel, which was also excluded from Mask 1 in the denominator of the previously described equation.

3.11.9 OXYGEN CONSUMPTION

Drosophila S2 R+ cells that underwent transfection or RNAi treatment in 24-well plates were resuspended and counted. 200,000 cells per 100 μ L *Drosophila* Schneider's medium without serum or antibiotics were seeded in 24-well assay plates coated with 22.4 μ g/mL Cell-Tak (Corning, #354240) following manufacturer's protocol. Seeded cells were spun for 20 seconds at 200 g in both directions to adhere *Drosophila* S2 R+ cells. After 30 minutes 400 μ L *Drosophila* Schneider's medium without serum or antibiotics was added to the cells and cells were loaded into an XF24 extracellular analyzer (Seahorse Bioscience, North Billerica, USA) to measure oxygen consumption rates (OCR) at 25 °C. Basal oxygen consumption rates were measured four times, then cells were exposed in sequence to 2.5 μ M oligomycin (Sigma-Aldrich, # O4876-5MG), 1 μ M carbonylcyanide p-trifluoromethoxyphenylhydrazone (FCCP) (Santa Cruz Biotechnology, #sc-203578), and 5 μ M Rotenone (Sigma-Aldrich, #R8875-1G) and 5 μ M Antimycin A (Sigma-Aldrich, #A8674-25MG) combined. After each injection the medium was mixed for 90 seconds, OCR was measured for 3 minutes, and then there was a wait period of 90 seconds before the cycle was repeated again 3 more times.

3.11.10 PROTEIN SECRETION ASSAY

Drosophila S2 R+ wildtype cells that had been treated with dsRNA in triplicate were re-plated to a new 96 well plate and transfected with pMT-BiP-ssHRP-C-V5-His, a gift from Professor Vivek Malhotra⁸. After 4 days of dsRNA treatment of 2 days after transfection, cells were incubated for 24 hours in 100 μ L *Drosophila* Schneider medium with FBS, antibiotics and 500 μ M copper sulfate (Sigma-Aldrich, #C1297-100G). 10 μ L of the supernatant was transferred into a receptacle plate in duplicate for each sample and HRP secretion was detected by incubating with 75 μ L ECL reagent SuperSignal West Dura Extended Duration Substrate (VWR, #34075) for 20 minutes and lumi-

nescence was measured using a plate reader. Protein concentration of each sample was measured by a DC Protein Assay (Bio-Rad, #5000112). As a control, supernatant from cells transfected with ssHRP, but not incubated with copper sulfate overnight were used to gauge background signal. For analysis, background signal was subtracted from each reading. Each reading was then normalized to protein concentration and then to control. Any negative readings after background subtraction were adjusted to zero.

3.11.11 RNA EXTRACTION AND REAL-TIME QPCR

Total RNA was isolated from cells using the RNeasy Kit (Qiagen #74104) following the manufacturer's protocol. cDNA was synthesized using the iScript cDNA synthesis kit (Bio-Rad, #1708891), and qPCR was performed in duplicates on biological triplicates using the Power SYBR Green PCR Master Mix Kit (Applied Biosystems, #4368702). Where indicated, cells were treated with 1 μ M Thapsigargin (Tocris, #1138) for 24 hours. Sequences of the PCR primers used for qPCR can be found in Table A1.

3.11.12 [¹⁴C] OLEIC ACID LABELING OF LIPIDS, LIPID EXTRACTION, AND TLC

Drosophila S2 R+ wildtype cells that had been treated with dsRNA for 4.5 days were pulse labeled with [¹⁴C] oleic acid (25 μ Ci/ μ mol) in combination with 1 mM oleic acid. After 21 hours of oleic acid incubation, cells were washed once with PBS and lipids were extracted in hexane/isopropanol (3:2) and protein was extracted in 0.3 N sodium hydroxide (Millipore Sigma, #221465) and 0.1 % SDS (Thermo Fisher, #AM9820) for 2 hours before protein was measured with a DC Protein Assay (Bio-Rad, #5000112) following the manufacturer's protocol. Lipids were normalized to protein concentration before loading onto thin layer chromatography (TLC) plates (Analtech, #43911). Phospholipids were separated in CHCl₃/CH₃OH/H₂O (65/25/4). Standards resuspended in

chloroform were run on TLC plates alongside samples to identify lipids: phosphatidylethanolamine [16:0/18:1] (Avanti, #850757), phosphatidylcholine [16:0/18:1] (Avanti, #850457), phosphatidylserine [16:0/18:1] (Avanti, #840060), C12 Glucosyl(β) Ceramide [d18:1/12:0] (Avanti, #860543), Brain CPE (Avanti, #860066). TLC plates were exposed to imaging screens and scanned in a Typhoon FLA 7000 (GE Healthcare) to visualize radioactive compounds. Standards were visualized by incubating plates with iodine chips. Quantification of TLC plates was performed using FIJI software. A rectangular region of interest was drawn around the band of a specific lipid type for each sample and band intensity was measured for each sample and each lipid on the TLC.

3.11.13 LIPIDOMICS ANALYSIS BY MASS SPECTROMETRY

Drosophila S2 R+ wildtype cells subjected to dsRNA for 4.5 days were incubated in 1 mM oleic acid for 21 hours. At 5 days treatment with dsRNA and 21 hours treatment with oleic acid, cells were pelleted at 1,200 RPM for minutes, medium was removed and cell pellets were washed once with DPBS. Cell pellets were then resuspended in 300 μ L water and subjected to a freeze-thaw cycle in liquid nitrogen for 5 seconds and ultrasonic water bath sonicator at room temperature for 5 minutes for a total of three cycles. 50 μ L of ruptured cell lysate was removed from each sample and incubated on a rotating table with 0.1 % digitonin for 2 hours, while the rest of the ruptured cells were kept in tubes on dry ice. Protein concentration for each sample was determined with a DC Protein Assay (Bio-Rad, #5000112) following the manufacturer's protocol. Equal amounts of ruptured cell lysate were then transferred to lipid extraction glass tubes containing 1 μ L of SPLASH LIPIDOMIX Mass Spec Standard (Avanti, #330707) and volumes were brought up to 300 μ L with water. Lipids were then extracted in chloroform/methanol (2/1, v/v) on ice, vortexed briefly, and the caps of the glass tubes were wrapped in parafilm and set to shake at 4 °C for 1.5 hours. 4 volumes of 0.88% sodium chloride (w/v) was added and samples were vortexed. Samples were then centrifuged at 1,100 RPM for 30 minutes at 4 °C and the lower organic phase was transferred to clean

glass tubes using a sterile glass pipette. Extracted lipids were dried under nitrogen stream and stored at -80 °C. Dried lipids were later resuspended in a small volume of chloroform/methanol (2/1, v/v) for lipidomic analysis.

Lipidomic analysis by LC-MS/MS was performed as described in detail in Gluchowski et al⁶¹. In brief, 5 µL of each sample was analyzed separately by liquid chromatography-mass spectrometry separated by the UHPLC system (consisting of Thermo Acclaim C₃₀ reverse-phase column connected to a Dionex UltiMate 3000 UHPLC system) over 60 minutes of increasing gradient from stationary phase (60/40 water/acetonitrile (v/v), 10 mM ammonium formate and 0.1% formic acid) to mobil phase (90/10 2-propanol/acetonitrile, 10 mM ammonium formate and 0.1% formic acid). Data for each sample were acquired in the positive and negative ionization modes. The UHPLC system was connected to a Q-Exactive Orbitrap mass spectrometer equipped with an electrospray ion source (Thermo Fisher), which generate MS spectra of lipids using the full scan/data-dependent MS₂ mode.

LipidSearch version 4.1 SP (Thermo Fisher Scientific) was used to analyze the MS data. Only identified species with grade A or B were validated and quantified using the R-script developed in-house. Additional sphingolipids not identifiable by LipidSearch were analyzed by LipidXplorer⁸².

To identify ceramide phosphatidyl ethanolamine as Lipid X, *Drosophila* S2 R+ cells were subjected to dsRNA against control or TMEM223 and incubated in 1 mM unlabeled oleic acid for 21 hours. Lipids were extracted and separated by TLC as previously described. The silica plate was scraped at the known migration location of Lipid X. Lipids were extracted with 5 mL of chloroform/methanol (2/1) for 2 hours shaking in glass tubes at 4 °C. Samples were then centrifuged at 1,100 RPM for 15 minutes to pellet silica and the solvents were transferred to clean glass tubes using a sterile glass pipette. Lipids were dried under a nitrogen stream and resuspended in 7.5 mM ammonium acetate in chloroform/ methanol/propanol (1:2:4 vol:vol:vol). Shotgun lipidomics analyses were performed on a Q-Exactive mass spectrometer (Thermo Fisher Scientific) equipped with a

robotic nanoflow ion source TriVersa NanoMate (Advion BioSciences). Briefly, samples were analyzed in both positive and negative ion modes with a resolution of $R_{m/z=200}=280,000$ for MS and $R_{m/z=200}=17,500$ for MS/MS experiments, in a single acquisition. MS/MS was triggered by an inclusion list encompassing corresponding MS mass ranges scanned in 1 Da increments.

Ten microliters of sample, thermostatted to 10°C in a 96-well plate, were infused via 4.1 µm spraying nozzles for 6 min. Backpressure was set to 0.95 psi and ionization voltage to 1.25 kV. After 30 s of spray stabilization, FT-MS spectra in the range of m/z 400 to 1,000 were acquired for 1 min in profile mode with an AGC setting of 1E6 and maximum ion time of 200 ms. For the next 2 min, product ion scans in centroid mode were acquired in data-independent analysis mode, using a precursor list starting at m/z 400.25, with increments of m/z 1.001, until m/z 999.849, with a resolution setting of 17,500 (FWHM at m/z 200), an AGC setting of 1E5, a normalized collision energy of 20, an isolation window of m/z 1, and a fixed first mass of m/z 80. Samples were analyzed first in positive, then switch to negative, ion mode for next 3 min, using lock masses of common background ions (m/z 536.16536 and m/z 680.48022 in positive ion mode, and m/z 529.46262 in negative ion mode) in full scan mode. Both MS and MS/MS data were combined to identify CerPE using LipidXplorer software^{83,176}.

3.11.14 MAMMALIAN CELL CULTURE AND TRANSFECTION

SUM159 cells (RRID:CVCL_5423) were obtained from the laboratory of Professor Tomas Kirchausen (Harvard Medical School) and were maintained in DMEM/F-12 GlutaMAX (Life Technologies) with 5 µg/ml insulin (Cell Applications), 1 µg/ml hydrocortisone (Sigma), 5% FBS (Gibco #10082147; Thermo Fisher), 50 µg/mL streptomycin and 50 units/mL penicillin. Where noted, cells were incubated with media containing 500 µM oleic acid complexed with 0.5% essentially fatty acid free BSA (Sigma Aldrich). Transfection of plasmids into SUM159 cells was performed with FuGENE HD transfection reagent (Promega) 18-24 h before imaging. siRNA treatment was

performed 48 hours prior to addition of oleic acid by reverse transfection using Lipofectamine RNAiMAX (Thermo Fisher Scientific, #13778075) following the manufacturer's instructions. siRNA against TMEM223 was purchased from Dharmacon (#L-032704-02-0005). siRNA for Negative Control was purchased from IDT DNA Technologies (Forward: rCrGrUrUrArArUrCrGrCrGrUrArUrArArUrArCrGrCrGrUAT; Reverse: rArUrArCrGrCrGrUrArUrUrArUrArCrGrCrGrArUrUrArArCrGrArC) and annealed by heating equal molar amounts of each oligo strand in 1x siRNA Buffer (Horizon Discovery, #B-002000-UB-100) to 90 °C and then incubating at 37 °C for 1 hour²¹⁵.

3.11.15 STABLE CELL LINE GENERATION

The AAVS1 Safe Harbor Targeting method (System Biosciences) was used to generate a SUM159 cell line stably expressing TMEM223-EGFP under a TK promoter. In brief, donor plasmids of AAVS1-TK-TMEM223-EGFP were co-transfected with simultaneously transfected with hCas9 plasmid (Addgene plasmid #41815) and gRNA-AAVS1-T2 plasmid (Addgene plasmid #41818) into wildtype SUM159 cells using FuGENE HD transfection reagent (Promega) following the manufacturer's protocol. Cells were selected with 1.5 µg/mL puromycin for 48 hours and single-cell FACS sorting was performed with 488-nm excitation with 100 µm gating at the flow cytometry core facility (Harvard, Division of Immunology). Positive clones were confirmed by fluorescence microscopy and by western blot with anti-GFP antibody.

3.11.16 MITOCHONDRIAL AND MICROSOME ISOLATION

To isolate mitochondria from AAVS1-TK-TMEM223-EGFP SUM159 cells a modified protocol from Guarani et al. was used⁶⁹. In brief, cells were pelleted and washed once with DBPS. Cells were then resuspended in mito-isolation buffer (250 mM sucrose, 1 mM EDTA, 10 mM MOPS-KOH,

pH 7.2) and ruptured by douncing 40 times in a 2 mL Wheaton tissue grinder (DWK Life Sciences, #358029). Homogenized cellular extract was then centrifuged at 600 x g for 5 minutes at 4 °C to obtain a post-nuclear supernatant. Mitochondria were then pelleted by centrifugation at 8,000 x g for 10 minutes at 4 °C. The mitochondria pellet was then washed twice with mito-isolation buffer. Concentration of mitochondria was determined with a DC Protein Assay Kit (Bio-Rad, #5000112). To further isolate microsomes, the supernatant after centrifugation at 8,000 x g for 10 minutes was transferred to a new tube and subjected to ultracentrifugation in a TLA-45 rotor (Beckman) for 30 min at 100,000 x g at 4 °C. The remaining supernatant was assayed as the cytosol.

3.11.17 BICARBONATE EXTRACTION AND PROTEINASE K TREATMENT

Isolated mitochondria were subjected to alkaline extraction in freshly prepared 0.1 M sodium bicarbonate at pH 11, 11.5, or 12. Membranes were then pelleted at 100,000 x g for 30 minutes at 4 °C in a TLA-45 rotor (Beckman). Supernatants were transferred to a new tube and 100% trichloroacetic acid was added to a final concentration of 12.5% for 30 minutes to precipitate proteins. The membrane pellet was immediately resuspended in 1x Laemmli Sample Buffer diluted in mito-isolation buffer. After 30 minutes incubation in trichloroacetic acid, the supernatants were spun down at 18,000 x g for 30 minutes at 4 °C and washed once with cold acetone. After treatments, 100% of the soluble (S, supernatant) and insoluble (P, pellet) and 10% of the input (T, total) were analyzed by SDS-PAGE and immunoblotting (see following section) using antibodies against Tom40, Mic60, mtHSP70, ClpP and GFP (see Table A1 for antibodies).

For subcellular localization within the mitochondria, equal amounts of isolated mitochondria were divided into eight tubes on ice and brought to a total reaction volume of 50 µL with mito-isolation buffer with increasing amounts of digitonin (0.01%, 0.02%, 0.04%, 0.06%, 0.08% and 0.1%) from a 1% digitonin stock solution (Sigma-Aldrich, #D141-500MG) or 1% TritonX-100 (Thermo Fisher Scientific, #28314). Each sample was incubated with 0.2 mg/mL Proteinase K

(Thermo Fisher Scientific, #17916) for 30 minutes on ice after which the reaction was stopped with 4 mM Phenylmethylsulfonyl fluoride (PMSF) (Sigma-Aldrich, #11359061001) for 10 minutes on ice. Laemmli Sample Buffer was added to samples to a final concentration of 1X and samples were boiled for 5 minutes at 95 °C prior to SDS-PAGE and immunoblotting analysis (see following section) using antibodies against GFP, Mff, Tom40, Tom20, Opa1, Tim23, Mic60, ClpP, MRPL11, and NDUFS2 (see Table A1 for antibodies).

3.11.18 IMMUNOBLOTTING

For analysis of proteins from organelle isolation and mitochondria treatments, Laemmli Sample Buffer was added to samples to a final concentration of 1X. Samples were incubated for 10 minutes at 70 °C prior to SDS-PAGE. Proteins were separated on a 4-15% SDS-PAGE gel (Bio-Rad, #4568086) in 1X Tris/Glycine/SDS buffer (Bio-Rad, #161-0772) and transferred to 0.2 µm nitrocellulose membranes (Bio-Rad, #1620112) in 1X Tris/glycine transfer buffer (Bio-Rad, #161-0771) with 20% methanol for 2 hours at 70 V in an ice water bath. The membranes were incubated in 5% non-fat dry milk (Santa Cruz Biotechnology, #sc-2325) in TBS-T (20mM Tris at pH 7.6, 150mM NaCl, 0.1% Tween-20) for 1 hour and subsequently incubated overnight in primary antibodies at 4 °C. Membranes were washed three times in TBS-T for 5 minutes and then incubated at room temperature with 1:5000 dilutions either anti-mouse or anti-rabbit HRP-conjugated secondary antibodies (Santa Cruz Biotechnology, #sc-2357 and #sc-516192) in 5% non-fat dry milk in TBS-T. Signal was analysed by chemiluminescence with SuperSignal West Pico, Dura or Femto reagents (Thermo Fisher Scientific).

3.11.19 STATISTICAL ANALYSIS

All statistical analysis was performed in GraphPad Prism 9. Information about the significance test and results are provided in detail in each figure legend.

3.12 AUTHOR CONTRIBUTIONS

Experiments designed by CBKJ, JS, RVF, TCW. Plasmid and knock in *Drosophila* cell line generation carried out by JS. Original RNAi screen carried out by JS. Experiments carried out by CBKJ. Lipidomics carried out by ZWL and YA.

Now this is not the end. It is not even the beginning of the end. But it is, perhaps, the end of the beginning.

Winston Churchill

4

Concluding remarks

By combining both targeted studies of Rab18 and deeper investigations of an unbiased genome-wide screen, this work reveals that these two approaches can complement each other in uncovering requirements for cellular pathways such as ERTOLD protein targeting. In testing the hypothesis that Rab18 is required for ERTOLD protein targeting, we revealed that Rab18 is not required for protein targeting in general, nor for LD biogenesis or turnover in the human mammary carcinoma cell line, SUM159⁹⁹. These findings were corroborated by the RNAi genome wide screen in

Drosophila, where Rab18 was not identified as a modulator of ERTOLD protein targeting. Instead, much of the same machinery proposed to interact with Rab18 for ER-LD membrane tethering²³⁷ were identified in the screen along with the Rab GTPase Rab1. Further studies on the membrane fusion machinery identified in the screen and proposed to mediate the connections between the ER and LDs for protein targeting are described in the thesis and manuscript of J. Song.

In addition to protein machinery required for membrane fusion for ERTOLD protein targeting, this screen provided a wealth of information to explore. Of great interest was the identification of numerous mitochondrial proteins whose depletion impaired ERTOLD protein targeting. We focused on one such hit, TMEM223 and confirmed its localization to the mitochondria. We further determined that TMEM223 depletion not only impairs ERTOLD protein targeting, but also dramatically alters lipid metabolism, ER morphology and ER function, namely protein secretion. These observations strengthen a model in which ERTOLD protein targeting follows similar principles to ER-Golgi trafficking: ATP dependent, SNARE mediated membrane fusion for protein and lipid transport in the context of ER-Golgi trafficking and in the context of ERTOLD protein targeting, for protein targeting to LDs. These studies also highlight a previously underappreciated role of mitochondrial proteins in ERTOLD protein targeting.

What remains to be discovered is how TMEM223 depletion affects mitochondria. We predict that the increased cell death with TMEM223 depletions hits to an effect on cellular energy levels and would be unsurprised if TMEM223 depletion impairs cellular energy currency in the forms of ATP or NADH. Interestingly, of the 896 hits whose depletion impaired GPAT4 protein targeting, 19 were mitochondrial hits, including 10 subunits of the oxidative phosphorylation (OXPHOS) complexes. As other members of the TMEM70/TMEM186/TMEM223 family are involved in the assembly of Complex I and V¹⁷², and the role of the potential yeast homologue of TMEM223, Mrx15 in binding mitoribosomes¹³⁷, we speculate that TMEM223 may play a role in the translation or assembly of OXPHOS complexes; therefore depletion of TMEM223 would alter cellular

energy levels originating from the mitochondria that ultimately are important for ER-Golgi trafficking and ERTOLD protein targeting.



Methods Supplementary Tables

Table A1

Reagent or Resource	Source	Identifier
Antibodies		
Rabbit polyclonal anti-GFP	Abcam	Cat# ab290; RRID: AB_303395
Rabbit polyclonal anti-dSec16 antibody 764	Ivan et al., 2008(Ivan et al., 2008)	N/A
Rabbit polyclonal anti-TOMM40	Proteintech	Cat# 18409-1-AP
Rabbit polyclonal anti-Mitofilin (MIC60)	Proteintech	Cat# 10179-1-AP
Rabbit polyclonal anti-MFF	Proteintech	Cat# 17090-1-AP
Rabbit polyclonal anti-CLPP	Proteintech	Cat# 15698-1-AP
Mouse anti-OPA1 Clone 19	BD biosciences	Cat# 612606
Mouse anti-Tim23	BD biosciences	Cat# 611222
Rabbit mAb anti-MRPL11 (D68F2) XP #2066	Cell Signaling Technology	Cat# D68F2
Mouse monoclonal anti-NDUFS2 [7A12BE5AD5]	Abcam	Cat# ab110249
Mouse monoclonal anti-mtHSP70 (JG1)	Invitrogen	Cat# MA3-028
Mouse anti-tom20 clone 29	BD biosciences	Cat# 612278
Mouse anti-IgG kappa binding protein-HRP	Santa Cruz Biotechnology	Cat# sc-516102; RRID: AB_2687626
Mouse monoclonal anti-rabbit IgG-HRP	Santa Cruz Biotechnology	Cat# sc-2357; RRID: AB_628497
dsRNA sequences		
dsRNA target	Forward primer	Reverse primer
pBlueScript KS II+	TAAATTGTAAAGCGTTAATATTTTGTAAAA	CCCTGGCGTTACCCAACCTTAATCGCCTTGC
Scipin	ACGCCCTGCACCTTTCC	ACTATGGCCGACAATACGG
CG12935/TMEM 223	ATGAGCAATCTGCTGAATTTGCC	CTTGAAAAGTATTATGTCCITGGGG
GM130	CAATCGCAGGCACAAATCAAGGAC	CTCGCTGGTTTCTTCCTTGGATG
Golgin84	GTGCTGGAAGCTCTGGTAAAAAGTC	CAACTCCTTTGCTAGTGTTCCTCG
Rab7	GACACTGCTGGTCAGGAACGCT	CTCCAACCTTAACGCATTCTTGGC
Syx5	CACACAAACCTGCCAGCTAAGTG	GGTCIGTTTGATGAAGGCGTCTTC
Tango1	ATTGCCAAAATCACCTACGCCATTG	CAGAGGCGTTAAGAACAGGCTGC
CHCHD3	CGTGAGCACGCAGCCGCTGCCGAG	GTCACCTTCGACGACTCTGGTTCC
QIL1	AACCGTCTACTACACACAAAAGGT	ACTTCGGCCGACTGGACTCCGCAC
CPES	GACCACACCAACCACTACC	GTGAAGCTGATCAGTTCTT

SMSr1**	TTAATACGACTCACTATAGGGAGA AGAA ACAGCCAGAAGAACATCG	TTAATACGACTCACTATAGGGAGA TAGCACGACCACCCAAATG
GlcT1	CAGAACATGTCCGAGAAGCA	GACTACCGCAGGCTCTAACG
qPCR primers		
Target	Forward primer	Reverse primer
dRpL19	AGGTGGGACTGCTTAGTGACC	CGCAAGCTTATCAAGGATGG
dAtf4	GGAGTGGCTGTATGACGATAAC	CATCACTAAGCAACTGGAGAGAA
dBiP	CCACCAACGGTGATACTCATT	GTCCITGCCCTTCTTCTTCTT
dGPAT4	CCCAAGACTGACGACAAAACA	GCGTCCCTGGTAATCAATGT
dXbp1_total	TGGGAGGAGAAAAGTGCAAAG	TCCGTTCGTCTGTTCAGCTC
dXbp1_short	ACCAACCTTGGATCTGCCG	CGCCAAGCATGTCTTGTAAGA
dPek	TACTAGGTCCAGTGGTGC	GCTTGTCCAGGTGGGAAGCTA
dTMEM223	GCATTATGACCGTGCCATTAAA	CACGCATATCCAGGACGTAATA
dCPES	CCCTGAAATCAGCCCGATAA	AGAAGATGATCAGCAGGAACAG
hTMEM223	AGCGAGACCTTGTCTCTATTIAC	AGGGATGACTGCTCCITTTATTI
hCHOP	AGA ACC AGG AAA CGG AAA CAG A	TCT CCT TCA TGC GCT GCT TT
hATF3	GGA GTG CCT GCA GAA AGA GT	CCA TTC TGA GCC CGG ACA AT
hBiP	GACATCAAGTTCTTGCCGTCA	CITTTGTTTGCCACCTCCAATA

Table A2

Plasmid	PCR template	Primer Forward	Primer Reverse
pAEGFP-GPAT4	pAC-GPAT4(Wilfling et al., 2013)	CACC ATGATCGCCGTGCTGTTGGACATATTC	TTAGGTGGAGTCCGACTTCAGCCG
pA-TMEM223-EGFP	gBlock Gene Fragment Synthesis (Integrated DNA Technologies): CACC+gene sequence from flybase.org (FBgn0033547) excluding the stop codon		
pA-Ldsdh1-EGFP	gBlock Gene Fragment Synthesis (Integrated DNA Technologies): CACC+gene sequence from flybase.org (FBgn0029994) excluding the stop codon		
pA-HSD17B11-EGFP	gBlock Gene Fragment Synthesis (Integrated DNA Technologies): CACC+gene sequence from flybase.org (FBgn0032910) excluding the stop codon		
pA-LDAH-EGFP	gBlock Gene Fragment Synthesis (Integrated DNA Technologies): CACC+gene sequence from flybase.org (FBgn0035206) excluding the stop codon		
pAEGFP-Ubx8	gBlock Gene Fragment Synthesis (Integrated DNA Technologies): CACC+gene sequence from flybase.org (FBgn0025608)		
pAmCherry-Lsd1	pAC-Lsd1(Kory et al., 2015)	CACC ATGGCAACTGCAACCAGCGGCAGTG	CTAGTAGACGCCGTTGATGTTATTGTG
pA-CGI58-mCherry	pA-CGI-58-C(Kory et al., 2015)	CACC ATGCTGCGTGCCGTGGAGAAGAAG	CTTCGGTTTGATGTTCCGCCAG
pAmCherry-CCT1	pAC-CCT1(Kory et al., 2015)	CACC ATGGCCACCTCATCGATACTCGCC	TCAATTGCTTCGACGCTCGTACTCC
CRISPR-Cas9 genome editing of TMEM223-EGFP knock-in cells			
Plasmid	PCR template	Primer Forward	Primer Reverse
PI18 (Cas9 and guide)(Housden et al., 2016)	S2 genomic DNA	GTTTCG CGAGTTATTTCGATTACACGG	AAAC CCGTGTAATCGAATAACTCG C
pBH-donor vector DNA (using BsaI)(Housden and Perrimon, 2016)	S2 genomic DNA (left homology arm)	TAGT GGTCTC T GACCGCCGGTFACTTCCACGATAAAGAG	TAGT GGTCTC T GAAC AATGCGACGCTTGAGGCCCGCC
	EGFP C-tag insert with GGGGS*3 linker	TAGT GGTCTC T GTTT TA <u>ggtgcccagggtcctctgaggccggagccgagg</u> <u>gggtgctca</u> ATGGTGAGCAAGGGCGAGGAGCT	TAGT GGTCTC T GCCC CTACTTGTACAGCTCGTCCATGCCGAG
	S2 genomic DNA (right homology arm)	TAGT GGTCTC T GGGC AGGGCAAGTTTGTGTTTGTAGCT	TAGT GGTCTC T TATA ACGGGCAAGCTCCTTATTCAT ACT

Table A3

Plasmid	PCR template	Primer Forward	Primer Reverse	Vector backbone	Enzyme sites
pTK-hTMEM223-EGFP	TMEM223 gBlock	GCACAGAGCTCGCCACCATGGC GGCGCCTTGAGG	GCACAGGTACCCACAAGCTCCG GTAGGCACC	pTK-EGFP-N1	SacI/KpnI
AAVS1-TK-hTMEM223-EGFP	pTK-TMEM223-EGFP	GCACA ATGCAT GAAATGAGTCT TCGGACCTCGCGGG	GCACA TCTAGA TTACTTGTACA GCTCGTCCATGCCGAG	AAVS1_puro-PGK1-3XFLAG-Twin_S tep	NsiI/XbaI
pTK-EGFP-GPAT1	GPAM cDNA	GCACAGAGCTCGAATGGATGAA TATGCACTGACCCCTGGTAC	GCACAGGTACCCTACAGCACCAC CAGAATATAATTC	pTK-EGFP-C1	SacI/KpnI
pHalo-GPAT1	GPAM cDNA	GCACATCCGGAATGGATGAATA TGCACTGACCCCTGGTAC	GCACACTGCAGCTACAGCACCA CAAACTCAGAATATAATTC	pHalo-C1	BspEI/PstI
pEGP-GPAT1	GPAM cDNA	GCACAGAGCTCGAATGGATGAA TATGCACTGACCCCTGGTAC	GCACAGGTACCCTACAGCACCAC CAGAATATAATTC	pEGFP-C1	SacI/KpnI
pTK-Halo-PLIN3	pEGFP-PLIN3(C hung et al., 2019)	CACC ATGGCAACTGCAACCAGCGGCA GTG	CTAGTAGACGCCGTTGATGTTA TTGTG	pTK-Halo-C1	KpnI/BamHI
pTK-mCherry-FIS1	gBlock	GCACAGGTACCATGGAGGCCGT GCTGAAC	CTGTGGGATCCTCAGGATTTGG ACTTG	pTK-mCherry-C1	KpnI/BamHI
p-ACSL1-Halo	ACSL1 cDNA	GCACA GAATTC GCCACC ATGCAAGCCCATGAGCTGTTCCG G	GCACA GGATCC TT AACCTTGATAGTGGAAATAGAGG TCATC	pHalo-N1	EcoRI/BamHI
p-AGPAT5-EGFP	AGPAT5 gBlock	GCACA GAGCTC CTGCTGTCCCTGGTCTCCAC	GCACA GGTACC CTATGCTTTAATAGTAACCCACA GGCAGC	pEGFP-N1	SacI/KpnI
pTK-EGFP-GPAT1-catalytic +TMD1 +2	pTK-EGFP-GPAT1	GCACAGAGCTCGAATGGATGAA TATGCACTGACCCCTGGTAC	CTGTCTGGTA GGTACC CTA CCCCAGTCCCCTCTGTTCAGAA CTGC	pTK-EGFP-C1	SacI/KpnI
pTK-EGFP-GPAT1-catalytic +TMD1	pTK-EGFP-GPAT1	GCACAGAGCTCGAATGGATGAA TATGCACTGACCCCTGGTAC	CTGTCTGGTA GGTACC CTA TCCCAGCAGCTGTATGGCATGC	pTK-EGFP-C1	SacI/KpnI
pTK-EGFP-GPAT1-catalytic	pTK-EGFP-GPAT1	GCACAGAGCTCGAATGGATGAA TATGCACTGACCCCTGGTAC	CTGTCTGGTA GGTACC CTA TGGTAAACAACGCTTGCTCCAGG	pTK-EGFP-C1	SacI/KpnI
pTK-EGFP-GPAT1-C-term +TMD1 +2	pTK-EGFP-GPAT1	GCACAGAGCTCTAAGAAATGCA ACAGATGAATCCCTACGAAGG	GCACAGGTACCCTACAGCACCAC CAGAATATAATTC	pTK-EGFP-C1	SacI/KpnI

*For of all sad words of tongue or pen,
The saddest are these: "It might have been!"*

John Greenleaf Whittier

B

GPAT_I is specific for endogenous fatty acid incorporation into triacylglycerol

B.1 INTRODUCTION

Triglyceride (TG) synthesis and storage is integral to energy homeostasis in eukaryotic cells. Dysregulation of this process has been implicated in metabolic diseases including obesity and nonalco-

holic fatty liver disease. While the majority of the TG synthesis pathway resides at the endoplasmic reticulum (ER), a specific isoform of the rate-limiting step, glycerol-3-phosphate acyltransferase 1 (GPAT₁), localizes to mitochondria. The connection between GPAT₁ at the mitochondria and the remainder of the TG synthesis pathway at the ER is incompletely understood. Unexpectedly, we show that GPAT₁ can localize around LDs in addition to mitochondria during conditions of fatty acid incubation. Members of the TG synthesis pathway have also been identified on LDs, suggesting GPAT₁ may play a role in connecting mitochondria and LDs to efficiently contribute to TG synthesis. We and others have observed increased mitochondria-LD associations during anabolic conditions; however, the mechanism by which mitochondria-LD associations are mediated, particularly to facilitate TG synthesis, is incompletely understood. Therefore, the goal of this project was to address how GPAT₁ localizes to LDs and to test if LD localization is important for TG storage.

This study aimed to provide mechanistic insight into how inter-organelle pathways are connected and how GPAT₁ efficiently contributes to TG synthesis and storage. The rate-limiting step of TG synthesis is GPAT. There are four major isoforms of GPAT: GPAT₃ and GPAT₄ are mainly ER-localized isoforms, and GPAT₁ and GPAT₂ are mitochondrial isoforms^{231,242}. While the ER-localized GPATs constitute the majority of GPAT activity in most tissues, GPAT₁ is known to make up 30-50% of the GPAT activity in liver⁴². Interestingly, in murine models of genetic and diet-induced obesity, GPAT₁ activity levels are higher in adipocytes and hepatocytes^{98,128}. Contrastingly, overexpression of GPAT₁ in rat liver leads to the development of fatty liver, hyperlipidemia and insulin resistance¹³⁹. These observations indicate the importance of GPAT₁ in regulating TG levels, and a potential role of GPAT₁ in the development of metabolic diseases. However, given that GPAT₁ localizes to the mitochondria, it remains unclear how LPA produced by GPAT₁ is transported to the remainder of the TG synthesis pathway and thus how it efficiently contributes to TG storage.

B.2 GPAT_I LOCALIZATION

GPAT_I is an 828 amino acid protein, localizing at the outer mitochondrial membrane (OMM)⁶³. The catalytic domain of GPAT_I is located near the N terminus exposed to the cytosol; it is conserved across glycerolipid acyltransferases and consists of four motifs involved in substrate binding and catalysis³⁹. Most of the work to determine the localization and orientation of GPAT_I relied on biochemical methods^{63,150}. By these methods, GPAT_I was identified in both pure mitochondria fraction and mitochondria associated membranes (MAM)¹⁵¹, the domain where mitochondria and ER form contact sites¹⁶⁴, indicating GPAT_I may have some localization to sites of interorganelle contact. Studies have shown that GPAT_I can target mitochondria independent of microsomes, suggesting GPAT_I targets from the cytosol¹⁵¹; however, the mechanism of GPAT_I targeting to mitochondria is unknown. Gonzalez-Baró et al claim that GPAT_I contains two transmembrane domains (TMD) in the middle of the protein responsible for GPAT_I localization to the OMM⁶³. Intriguingly, TMD prediction algorithms do not consistently predict two TMDs and the hydrophobicity of predicted TMDs is low compared to bona fide OMM proteins with TMD(s). Furthermore, little cell biology has been done to confirm and study the dynamics of the localization of GPAT_I.

B.3 GPAT_I REGULATION

GPAT_I levels are sensitive to nutrient and hormonal state: high insulin or carbohydrates increases GPAT_I mRNA levels, while fasting decreases mRNA, protein and activity levels in adipocytes and hepatocytes^{10,124,230}. Increase in GPAT_I mRNA in response to insulin is mediated by SREBP-1, sterol regulatory element sites and carbohydrate response elements^{44,100}. While GPAT_I expression is not detected in pre-adipocytes, GPAT_I mRNA levels increase with adipocyte differentiation, mediated by SREBP₁/ADD₁⁴⁴.

GPAT_I activity may also be regulated by post-translational modifications. AMPK is able to in-

activate GPAT_I in vitro and treatment of hepatocytes with AICAR to activate AMPK decrease GPAT_I activity¹³⁸. Interestingly, when hepatic GPAT_I activity decreases with AICAR treatment, a concomitant increase in fatty acid oxidation (FAO) is observed, pointing to reciprocal regulation of the two pathways¹³⁸. Similarly, overexpressing GPAT_I in rat hepatocytes greatly decreases FAO¹²⁸, suggesting that GPAT_I at the mitochondria is directing FAs into TG synthesis over beta-oxidation. Overexpression of GPAT_I also increases the basal level of TGs as well as the incorporation of exogenous FAs into diacylglycerol (DAG) and TG^{95,128}. However, the mechanism by which GPAT_I efficiently channels its substrate to the remainder of TG synthesis at the ER during times of FA overload remains to be elucidated.

B.4 GPAT_I IN PHYSIOLOGY

Studies in primary hepatocytes from GPAT_I^{-/-} mice indicate GPAT_I depletion affects incorporation of endogenously synthesized FAs into TG, with no effect on exogenous FA incorporation²³⁰. Furthermore, GPAT_I depletion increased levels of FAO and acyl-carnitines, supporting a hypothesis that GPAT_I on the mitochondria competes with CPT_I - the rate limiting step of FAO - for substrate^{75,95,230}. In general, GPAT_I^{-/-} mice weigh less, have lower hepatic TG content, plasma TG and very low-density lipoprotein secretion, and have decreased gonadal fat pad weights compared to controls⁷⁴. Furthermore, these mice have increased hyperinsulinemia and reduced glucose tolerance on high fat or high sucrose diet⁷⁵. Interest in GPAT_I as a therapeutic target has developed due to studies implicating GPAT_I as the primary GPAT isoform for de novo lipogenesis (DNL). Increased DNL contributes to the development of NAFLD³¹, which is currently the most common liver disease in the US and associated with other metabolic diseases^{60,155}. Therefore, it is important to understand the mechanism by which GPAT_I is involved in TG synthesis to better understand the pathways contributing to metabolic disease manifestation.

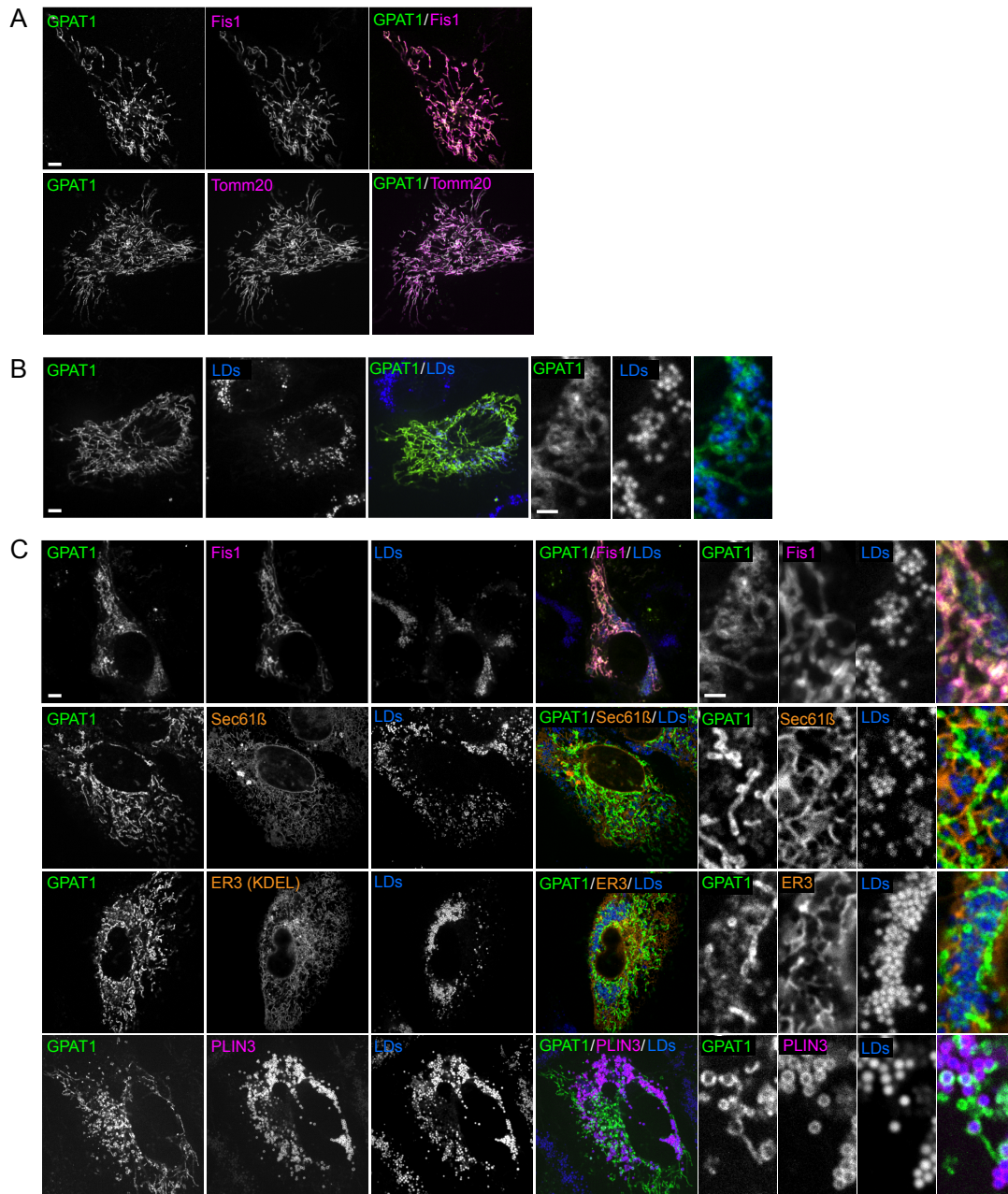
Taken together, current knowledge demonstrate GPAT_I is critical for committing and channeling FAs into TG synthesis, however the question remains: how does mitochondrial localized GPAT_I coordinate with the terminal enzymes in the TG synthesis pathway known to localize to the ER and LDs for efficient TG synthesis and storage?

B.5 GPAT_I CAN LOCALIZE TO MITOCHONDRIA AND LDs

To initially address this question, we sought to confirm the localization of GPAT_I in cells. We expressed GPAT_I along with Fis_I and Tomm20, both known OMM proteins, in SUM_I59 cells under basal conditions and observed that GPAT_I colocalized with mitochondria markers (Figure B.1A). Intriguingly, upon incubating cells expressing GPAT_I with the FA oleate (OA) to induce LD for-

Figure B.1 (following page): (A) GPAT1 localizes to mitochondria marked by co-transfection with Fis1 or Tomm20 under basal conditions. Scale bar 5 μm , for inlay 1 μm . (B) After incubation with 500 μM OA overnight, GPAT1 localizes around LD structures stained with LipidTox. Scale bar 5 μm , for inlay 1 μm . (C) GPAT1 localizes around LDs distinct from mitochondria marker Fis1, ER markers Sec61 β and ER3 (KDEL), and colocalizes with LD protein PLIN3 around LDs. Scale bar 5 μm , for inlay 1 μm .

Figure B.1: (continued)



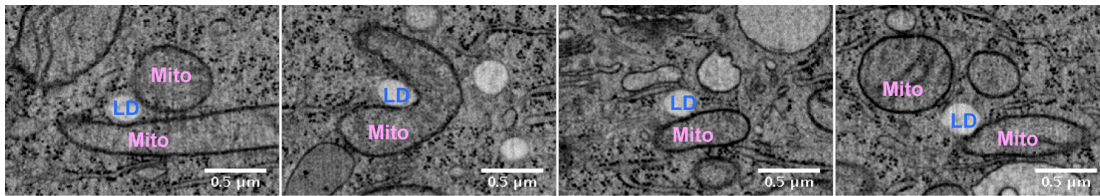


Figure B.2: Mitochondria and LD are observed in close contact with OA incubation by FIB-SEM (Chung, unpublished).

mation, we observed a portion of the GPAT_I population surrounding LDs (Figure B.1B). To determine if this localization of GPAT_I was distinct from other membranes, we expressed GPAT_I along with known mitochondria, ER and LD markers (Figure B.1C). GPAT_I localized around the LDs distinct from the ER luminal and membrane markers KDEL and Sec61 β , and colocalized with PLIN₃, a bona fide LD protein that associates with LDs by an amphipathic helix (Figure B.1C).

Interestingly, focused ion beam-scanning electron microscopy (FIB-SEM) studies in our lab have identified association of mitochondria and LDs in cells incubated with OA (Figure B.2). Furthermore, protein correlation profiles of GPAT_I in hepatocytes from mice on low fat or high fat diet reveal that GPAT_I's localization changes after high fat diet to have some localization in the LD fraction¹¹⁵ (Figure B.3A). This localization pattern is consistent with the profiles of other proteins identified to localize to contact sites between LDs and other organelles, such as VPS13A and Mfn2^{18,119} (Figure B.3B). These observations strongly suggest the formation of mitochondria-LD membrane contact sites during anabolic conditions. However, the mechanism by which mitochondria-LD associations are mediated, particularly to facilitate TG synthesis, is incompletely understood. I sought to test the hypothesis that GPAT_I localizes at mitochondria-LD contact sites to efficiently contribute to TG synthesis from DNL derived FAs and storage in LDs.

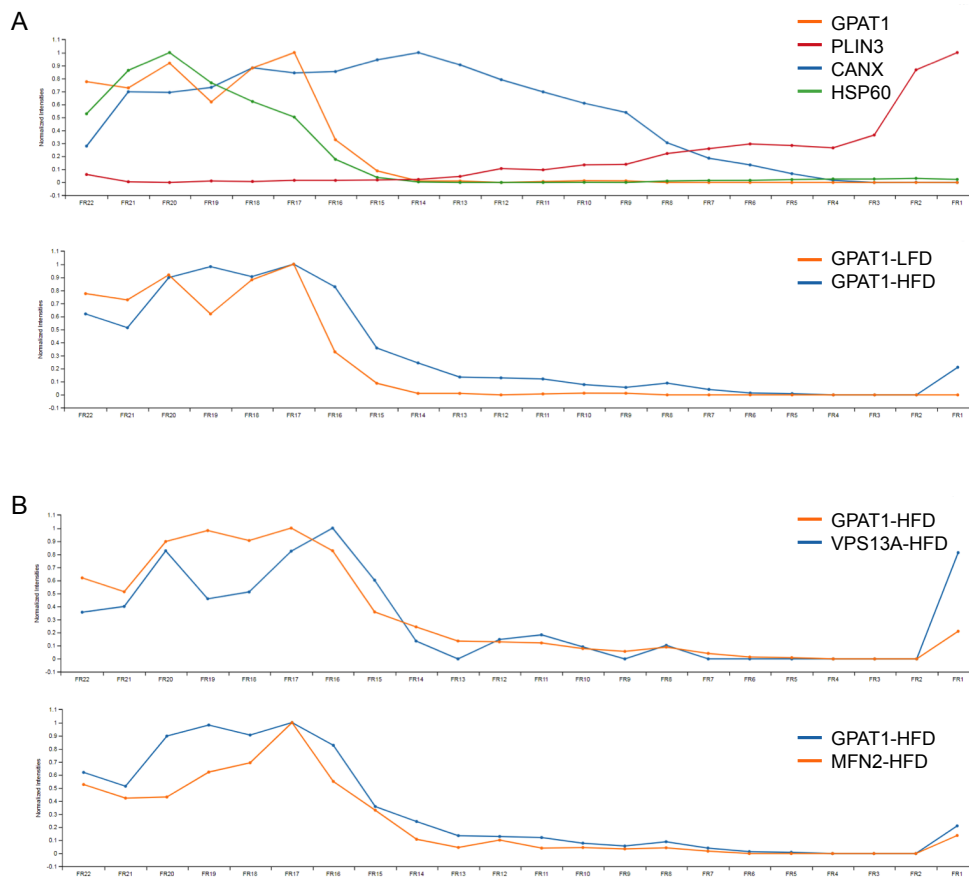


Figure B.3: (A) GPAT1 protein correlation profile from hepatocytes of mice on a low fat diet (LFD) plotted against the profiles of known organelle markers¹¹⁵. Perilipin3 (PLIN3) marks LDs, Tomm20 marks mitochondria, and calnexin (CANX) marks the ER. GPAT1 profile after high fat diet (HFD) exhibits a peak of GPAT1 identified in the LD fraction. (B) GPAT1 profile plotted against predicted LD protein and mitochondria-ER contact site protein, VPS13A, and mitochondria-LD contact site protein, Mitofusin2 (MFN2) under HFD conditions.

B.6 GPAT₁ IS SPECIFIC FOR THE INCORPORATION OF DE NOVO LIPOGENESIS (DNL) DERIVED FAS

To first determine the role of GPAT₁ in handling of FAs from exogenous and endogenous sources for TG synthesis and storage, I tested the effects of GPAT₁ depletion or overexpression on the incorporation of radiolabeled [¹⁴C] acetate into TG. I verified in SUM159 cells that GPAT₁ depletion by siRNA knockdown decreases [¹⁴C] acetate incorporation into TG (Figure B.4, A-B). An inhibitor of the first step of DNL, Acetyl-CoA Carboxylase 1 (ACC1), was used as a control to abolish [¹⁴C] acetate incorporation via DNL. Using a GPAT_{3/4} inhibitor, I showed that the effect of GPAT₁ knockdown on [¹⁴C] acetate incorporation is not further affected by inhibition of GPAT₃ and GPAT₄ (Figure B.4, A-B). Further supporting the model that GPAT₁ is specific for the incorporation of DNL derived FAs, incorporation of [¹⁴C] oleate is most impaired by GPAT_{3/4} inhibition (Figure B.4, C-D). Depletion of GPAT₁ by siRNA on top of GPAT_{3/4} inhibition does not further decrease [¹⁴C] oleate incorporation indicating that GPAT₃ and GPAT₄ are the dominant isoform for incorporation of exogenous FAs into TG, while GPAT₁ is the dominant isoform for incorporation of endogenous (DNL derived) FAs into TG.

B.7 GPAT₁ N-TERMINUS, AND NOT THE TRANSMEMBRANE DOMAINS, IS NECESSARY FOR MITOCHONDRIA LOCALIZATION

I next sought to understand how GPAT₁ localizes to mitochondria and LDs. Studies have shown that GPAT₁ can target mitochondria independent of microsomes, suggesting GPAT₁ targets from the cytosol¹⁵¹; however, the mechanism of GPAT₁ targeting to mitochondria is unknown. Gonzalez-Baró et al claim that GPAT₁ contains two transmembrane domains (TMD) in the middle of the protein responsible for GPAT₁ localization to the OMM⁶³. Intriguingly, TMD prediction al-

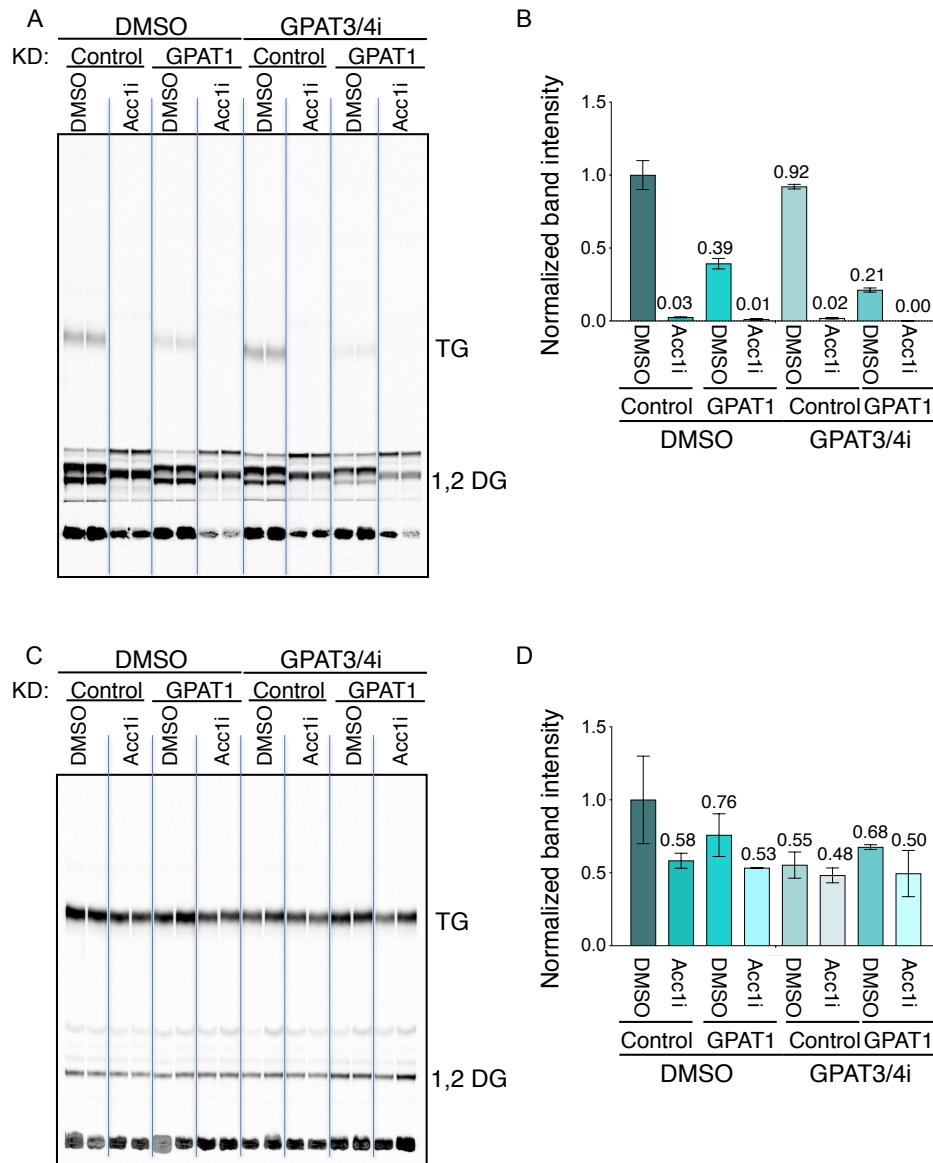


Figure B.4: (A) Thin layer chromatography incorporation reveals GPAT1 knockdown impairs the incorporation of [^{14}C] acetate derived fatty acids into TG and is not further impaired by inhibition of GPAT3 and GPAT4. (B) Quantification of TLC triglyceride (TG) band. (C) Thin layer chromatography incorporation reveals GPAT1 knockdown does not affect the incorporation of [^{14}C] oleate into TG to the extent of inhibition of GPAT3 and GPAT4. (D) Quantification of TLC triglyceride (TG) band.

gorithms do not consistently predict two TMDs and the hydrophobicity of predicted TMDs is low compared to bona fide OMM proteins with TMD(s)¹¹⁷ (Figure B.6A). To address the lack of molecular understanding of GPAT_I localization, I showed that the N-terminus alone prior to the predicted transmembrane domains can localize to mitochondria (Figure B.5).

I also determined that the transmembrane domains of GPAT_I are not necessary for mitochondria targeting, as expression of a GPAT_I construct without the two transmembrane domains (GPAT_IΔTM) localizes to the mitochondria (Figure B.6B). The C-terminus of GPAT_I harbors two predicted α-helices (AHs) which are motifs known to recognize packing defects in the LD monolayer and facilitate LD localization¹⁵⁶. To test if either of both of these AHs were necessary and/or sufficient for LD association of GPAT_I, I first generated a truncated construct of GPAT_I including only the two AHs (AH₁ and AH₂) and the remaining C-terminus (Figure B.6, C-D). This construct mostly localizes to LDs, though intriguingly, some mitochondria localization was observed. A truncation construct of just AH₂ and the remaining C-terminus localized solely to LDs, revealing that AH₂ is sufficient for LD localization (Figure B.6, C-D). I next generated deletion constructs removing either both AHs (GPAT_I^{AHΔ1-2}) or just AH₂ (GPAT_I^{AHΔ2}) (Figure B.6, C and E). GPAT_I^{AHΔ1-2} does not localize around LDs, localizing only to the mitochondria (Figure B.6E). Intriguingly, however, GPAT_I^{AHΔ2} localizes either to the cytosol or around LDs (Figure B.6E).

B.8 ENDOGENOUS GPAT_I MAY LOCALIZE TO LDs ONLY UNDER SPECIFIC METABOLIC CONDITIONS WHERE GPAT_I EXPRESSION IS UPREGULATED

GPAT_I expressed in SUM159, HepG2, Huh7, and Cos7 cells has the capacity to localize to both mitochondria and LDs (Figure B.7). Interestingly, the distribution of GPAT_I between the two subcellular compartments varies per cell line. To further characterize the localization of GPAT_I, I generated an endogenously Super-Folder GFP (sfGFP) tagged GPAT_I cell line in the human breast

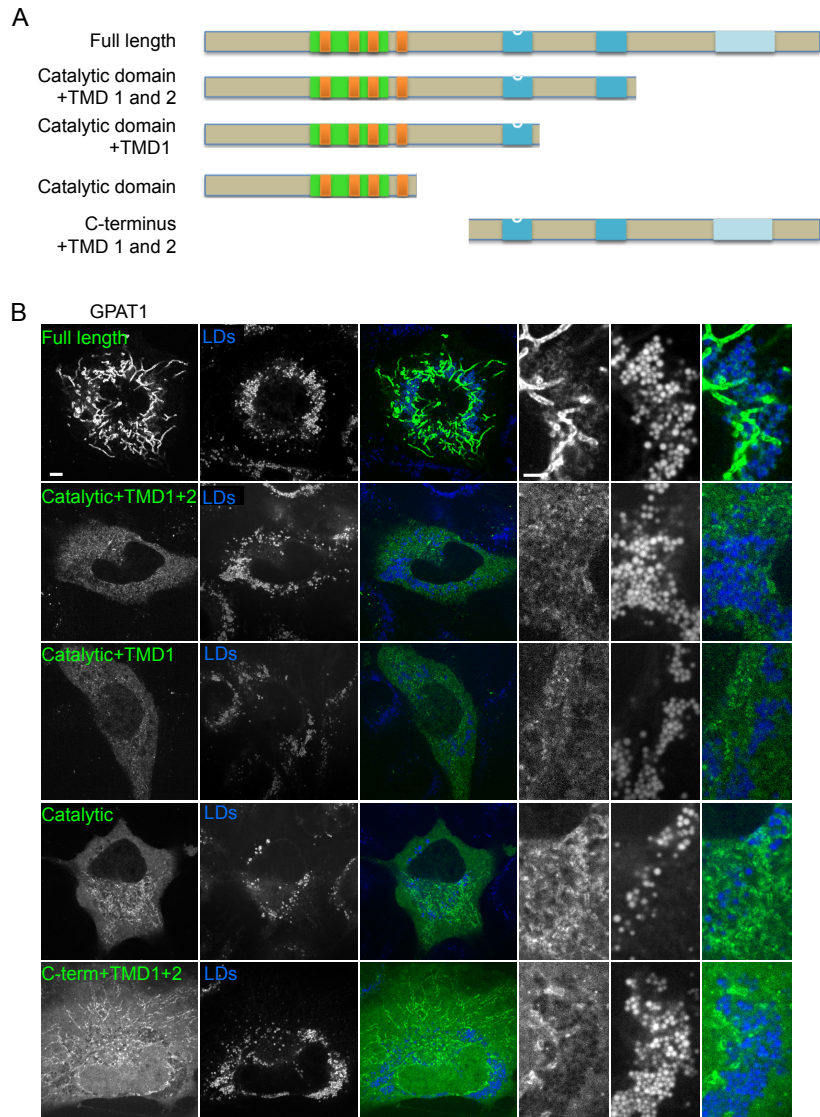


Figure B.5: (A) Graphical models of GPAT1 truncations; the catalytic site is green, catalytic motifs in orange, predicted transmembrane domains are in blue. (B) GPAT1 truncations were expressed in cells and imaged after incubating with oleate overnight. LDs are stained with LipidTox. Scale bar 5 μm , for inlay 1 μm .

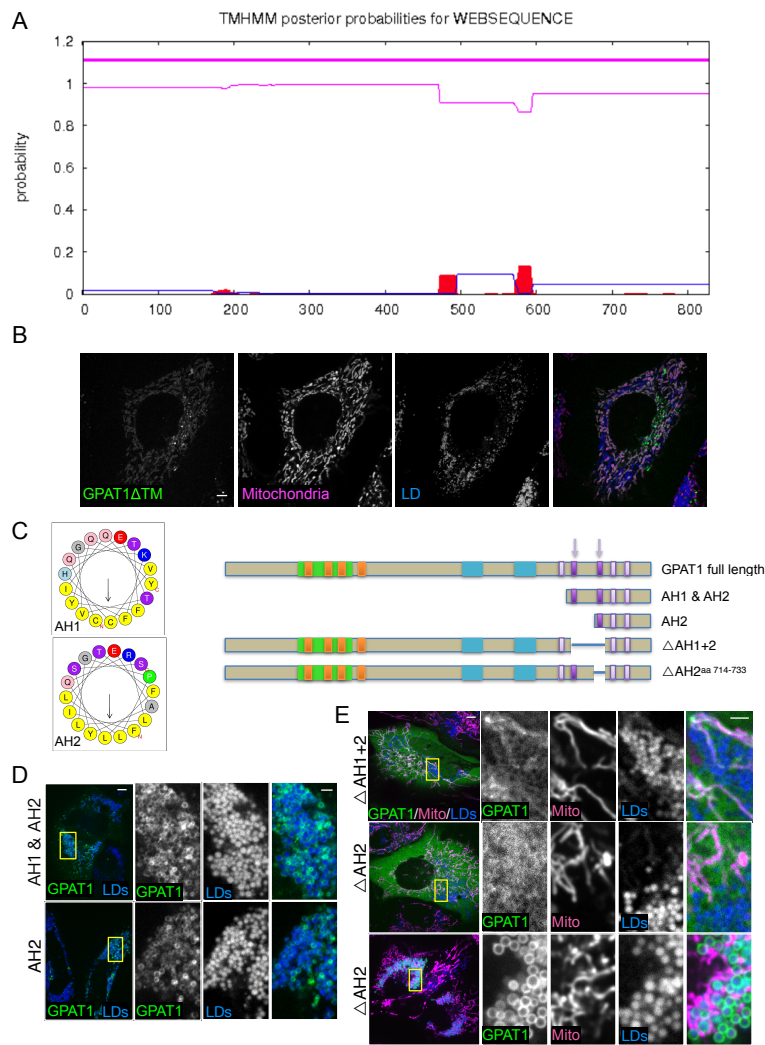


Figure B.6: (A) GPAT1 is weakly predicted to have two transmembrane domains (TMHMM algorithm)^{188,117}. (B) GPAT1 lacking transmembrane domains (GPAT1 Δ TM) is able to localize to mitochondria. Mitochondria are stained with Mito-Tracker CMX ROS. Scale bar 5 μ m. (C) GPAT1 has two alpha helices at the C-terminus predicted by HELIQUEST⁵⁴ that were altered to determine sufficiency. (D) Truncations to observe the C-terminus with both or one of the alpha helices reveal AH2 is sufficient for LD localization. Scale bar 5 μ m, for inlay 1 μ m. (E) GPAT1 truncation constructs removing both alpha helices or just AH2 reveal LD targeting is complex and may involve both alpha helices. Scale bar 5 μ m, for inlay 1 μ m.

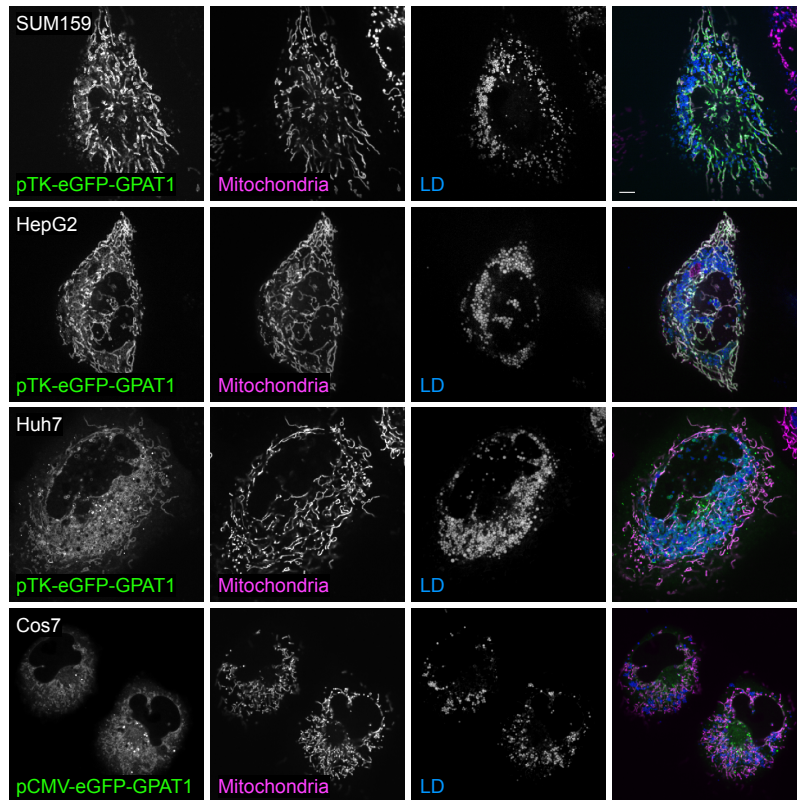


Figure B.7: GPAT1 localizes to the mitochondria and LDs in breast cancer carcinoma (SUM159), liver (HepG2 and Huh7) and kidney (Cos7) cell lines. Mitochondria are stained with MitoTracker Deep Red, LDs are stained with AutoDot. Scale bar 5 μm .

carcinoma cell SUM159. While preliminary imaging of the polyclonal population indicated endogenously tagged GPAT1 localizes to mitochondria under basal conditions and around LDs upon addition of the fatty acid oleate (OA) (Figure B.8A), this was not observed in the single clones isolated. Western blot (WB) of verified homozygous sfGFP GPAT1 single clone indicated high levels of free GFP (Figure B.8B). The levels of free GFP were also apparent by confocal imaging, making the localization of sfGFP GPAT1 unclear with background GFP signal in the cytosol (Figure B.8C).

To address this, I generated a new $^{sfGFP-HA}$ GPAT1 cell line that includes an increased linker

with an HA-tag – in the event that cleavage of the sfGFP was occurring – and with a kozak sequence before the sfGFP – as genomic editing may have destroyed the endogenous kozak sequence. The levels of free GFP were reduced in this cell line as detected by both WB for GFP and confocal imaging, and GPAT₁ signal that does not colocalize with mitochondria signal is observed near some LDs (Figure B.8, D-E). Because GPAT₁ most clearly localizes to LDs during conditions of overexpression, identifying conditions under which GPAT₁ expression is enhanced may be necessary for GPAT₁ localization to LDs. In support of this, exogenous expression of GPAT₁ in the sfGFP-HA-GPAT₁ cell line localized around LDs and promoted localization of sfGFP-HA-GPAT₁ to LDs as well (Figure B.8F).

Ultimately, we concluded that GPAT₁ may localize to LDs under certain metabolic states of the cell, such as those that promote de novo lipogenesis. We propose that this dual localization may be for substrate channeling. However, our lab is not best poised to test this hypothesis, which was proposed in the literature at the same time we were arriving at this conclusion³⁸. Therefore, we did not pursue this project further.

B.9 FUTURE DIRECTIONS

A striking observation is that GPAT₃ and GPAT₄ are unable to compensate for loss of GPAT₁ in incorporating FAs derived from DNL into TG²³⁰ (Figure B.4, A-B). This indicates that there is some specificity of GPAT₁ for DNL derived FAs. A hypothesis that has been previously posed to the field is that GPAT₁ accomplishes this specificity via substrate channeling³⁸. Supporting this hypothesis, I have observed colocalization of GPAT₁ with DGAT₂ around LDs, suggesting LDs may be the site at which GPAT₁ delivers LPA to the downstream enzymes in TG synthesis that normally localize to the ER, but have been observed on LDs as well²³³ (Figure B.9A). Interestingly, the immediate next step in TG synthesis, AGPAT₅, does not colocalize with GPAT₁ around LDs (Fig-

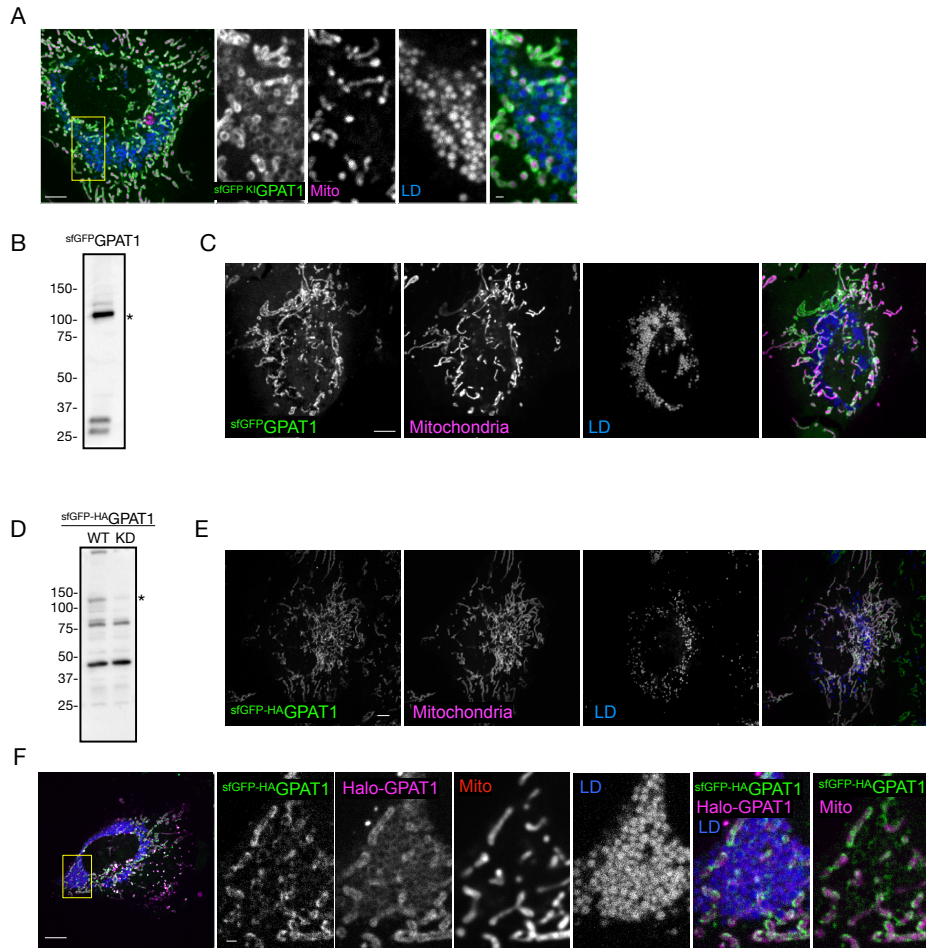


Figure B.8: (A) $sfGFP$ GPAT1 polyclonal knock in cells have GPAT1 localization to mitochondria and LDs after incubation with oleate for 48 hours. Mitochondria stained with MitoTracker CMX ROS, LDs stained with LipidTox Deep Red. Scale bar 5 μ m, inlay scale bar 1 μ m. (B) Western blot against GFP of single clone $sfGFP$ GPAT1 reveals high levels of free GFP. $sfGFP$ GPAT1 as detected by anti-GFP antibody marked by asterisk. (C) $sfGFP$ GPAT1 single clone cell line localizes to the mitochondria after incubation with oleate for 18 hours. Mitochondria stained with MitoTracker CMX ROS, LDs stained with LipidTox Deep Red. Scale bar 5 μ m. (D) Western blot of single clone $sfGFP$ - HA GPAT1 cells with 48 hours siRNA against control or GPAT1. $sfGFP$ - HA GPAT1 marked by asterisk. (E) $sfGFP$ - HA GPAT1 single clone cell line localizes to the mitochondria after incubation with oleate for 18 hours. Mitochondria stained with MitoTracker CMX ROS, LDs stained with LipidTox Deep Red. Scale bar 5 μ m. (F) Exogenous expression of GPAT1 in $sfGFP$ - HA GPAT1 single clone cells promotes localization of endogenous $sfGFP$ - HA GPAT1 to the LDs after incubation with oleate for 18 hours. Mitochondria stained with MitoTracker Deep ed, LDs stained with AutoDot. Scale bar 5 μ m, inlay scale bar 1 μ m.

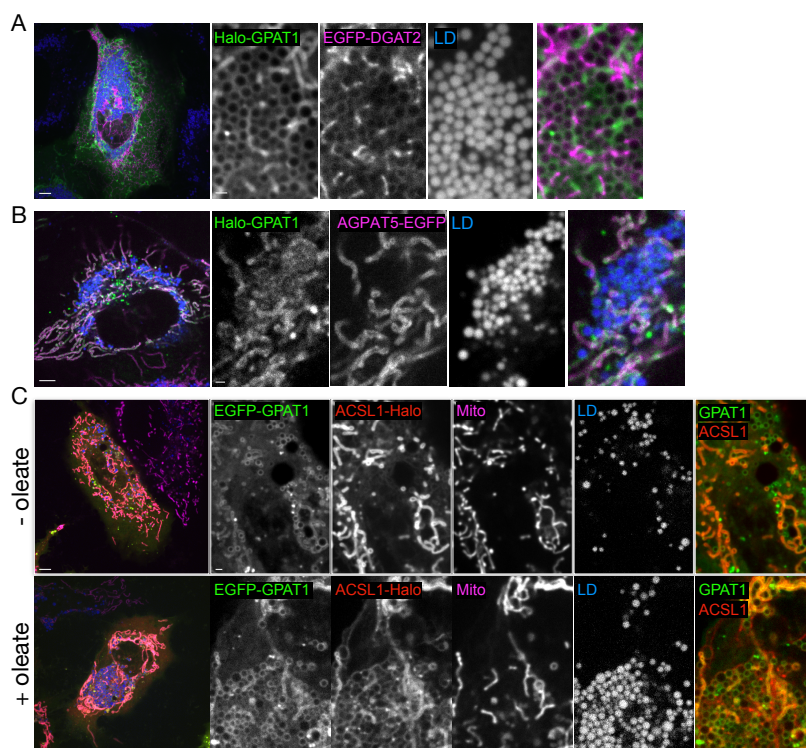


Figure B.9: (A) Exogenously expressed GPAT1 and DGAT2 in SUM159 cells colocalize to some LDs after incubation with oleate for 16 hours. LDs stained with LipidTox Deep Red. Scale bar 5 μm , inlay scale bar 1 μm . (B) Exogenously expressed GPAT1 and AGPAT5 in SUM159 cells colocalize to the mitochondria after incubation with oleate for 18 hours. LDs stained with LipidTox Deep Red. Scale bar 5 μm , inlay scale bar 1 μm . (C) Exogenously expressed GPAT1 and ACSL1 in Huh7 liver cells colocalize to the mitochondria under basal conditions and to some LDs after incubation with oleate for 24 hours. Mitochondria stained with MitoTracker Deep Red, LDs stained with AutoDot. Scale bar 5 μm , inlay scale bar 1 μm .

ure B.9B). Furthermore, ACSL₁, which synthesizes fatty acyl-CoAs from free FAs just upstream of GPAT₁ colocalizes with GPAT₁ at the mitochondria under basal conditions in Huh7 cells (Figure B.9C). However, upon the addition of oleate to enhance LD formation, ACSL₁ colocalizes with GPAT₁ around LDs, suggesting that LDs may be a hub for substrate channeling through GPAT₁ (Figure B.9C).

The interactome of GPAT₁ has not been studied and could provide insight into how GPAT₁ localizes to mitochondria and contributes to TG synthesis from its mitochondrial localization. With

the newly developed SUM159^{sfGFP-HA}GPAT1 cell line, it will be possible to fish for interactors of GPAT1 during different metabolic conditions. Identifying conditions that upregulate GPAT1 similar to during conditions of DNL in liver^{10,124,230} has been a challenge. Ultimately, the ideal system would be to endogenously tag GPAT1 in the CRISPR mouse and then isolate tagged GPAT1 from mouse liver under conditions of fasting versus feeding to identify interactors of GPAT1 unique to DNL conditions. Simultaneous isolation of hepatocytes from these mice could allow the localization of GPAT1 during different conditions as well to test if the physiological relevance of GPAT1 localization to LDs versus to mitochondria only. To address this from a different angle, I have generated a SUM159 cell line that stably over expresses EGFP-GPAT1 under a pTK promoter using the safe-harbor locus in which GPAT1 stably overexpressed localizes faintly to LDs; the majority of the GFP signal remaining localized to the mitochondria. As a control, I generated a SUM159 cell line that stably over expresses EGFP-MAVS (mitochondrial antiviral signal) under a pTK promoter. Immunoprecipitation by GFP can be used to identify candidates that interact with GPAT1 specifically under basal conditions versus candidates that are uniquely identified with OA incubation. Interaction of GPAT1 with these candidates can be confirmed by co-IP. Co-expressing fluorescently tagged candidates in^{sfGFP-HA}GPAT1 cells will allow determination of co-localization by confocal microscopy. Interactors of GPAT1 will inform hypotheses as to how GPAT1 localizes to mitochondria or LDs, the specificity of DNL derived FAs for GPAT1, and the mechanism by which GPAT1 can contribute to ER localized TG synthesis.

B.10 MATERIALS AND METHODS

B.10.1 ANTIBODIES

Antibodies used in this study are listed in Table A1

B.10.2 CELL CULTURE AND TRANSFECTION

SUM159 cells (RRID:CVCL_5423) were obtained from the laboratory of Tomas Kirchhausen (Harvard Medical School) and were maintained in DMEM/F-12 GlutaMAX (Life Technologies, #10565-042) with 5 µg/ml insulin (Cell Applications), 1 µg/ml hydrocortisone (Sigma), 5% FBS (Gibco 10082147; Thermo Fisher), 50 µg/mL streptomycin and 50 units/mL penicillin. HepG2 (ATCC, #HB-8065), Cos7 (ATCC, #CRL-1651) and Huh7 cells were maintained in Gibco DMEM, High Glucose (Life Technologies, #11-965-118), 10% FBS (Gibco #10082147; Thermo Fisher), 50 µg/mL streptomycin and 50 units/mL penicillin. Cells were annually tested for mycoplasma contamination by Universal Mycoplasma Detection Kit (American Type Culture Collection).

Where noted, cells were incubated with media containing 500 µM oleic acid complexed with 0.5% essentially fatty acid free BSA (Sigma Aldrich). Transfection of plasmids into SUM159 cells was performed with FuGENE HD transfection reagent (Promega) 18-24 h before imaging. siRNA treatment was performed 48 hours prior to addition of oleic acid by reverse transfection using Lipofectamine RNAiMAX (Thermo Fisher Scientific, #13778075) following the manufacturer's instructions. Control siRNA (siGENOME RISC-Free Control, Dharmacon, #D-001220-01-05) was used, and siRNA against GPAT1 was purchased from Dharmacon (#L-009946-00-0005).

B.10.3 [¹⁴C] LABELING OF LIPIDS, LIPID EXTRACTION, AND TLC

SUM159 cells subjected to siRNA against GPAT1 or control for 48 hours were treated with an inhibitor against GPAT3 and GPAT4 (Eli Lilly, #3216874), which was a kind gift from Craig Hammond and Jianliang Lu, 3 hours prior to oleate or acetic acid loading and an inhibitor against ACC1 (Sigma-Aldrich, #PF-05175157) or DMSO for 1.5 hours prior to oleate loading, and DMSO. Cells were then pulse labeled with either [¹⁴C] oleic acid (25 µCi/µmol) in combination with 0.5 mM oleic acid or [¹⁴C] acetic acid (25 µCi/µmol) for 2 hours. After 2 hours of treatment, cells were

washed three times with DPBS and lipids were extracted in hexane/isopropanol (3:2) twice and then dried, and protein was extracted in 0.3 N sodium hydroxide (Millipore Sigma, #221465) and 0.1 % SDS (Thermo Fisher, #AM9820) for 2 hours before protein was measured with a DC Protein Assay (Bio-Rad, #5000112) following the manufacturer's protocol. Lipids were normalized to protein concentration before loading onto thin layer chromatography (TLC) plates (Analtech, #43911). Lipids were separated in hexane/diethyl ether/acetic acid (80/20/1). Standards resuspended in chloroform were run on TLC plates alongside samples to identify lipids: Triolein (18:1 TG) (Avanti, #8701100-1mg), 1,2-dioleoyl-sn-glycerol (1,2-DG) (Avanti, #870520P-5mg). TLC plates were exposed to imaging screens and scanned in a Typhoon FLA 7000 (GE Healthcare) to visualize radioactive compounds. Standards were visualized by incubating plates with iodine chips. Quantification of TLC plates was performed using FIJI software. A rectangular region of interest was drawn around the band of a specific lipid type for each sample and band intensity was measured for each sample and each lipid on the TLC.

B.10.4 PLASMIDS

PCR of inserts for cloning was performed using Q5 Hot Start High-Fidelity DNA Polymerase (New England Biolabs, #M0493S). PCR products were purified with a NucleoSpin Gel and PCR Clean-up Kit (Macherey-Nagel, #740609.250). PCR products and vectors were digested with enzymes from New England Biolabs and then ligated with the Rapid DNA Dephos & Ligation Kit (Sigma-Aldrich, #4898117001). The synthetic DNAs (gBlock, Integrated DNA Technologies) used in this study and cloning strategies of the other plasmids are summarized in Table A3). pTK-EGFP-C1, pTK-EGFP-N1, pTK-Halo-C1, pTK-Halo-PLIN3 were developed by Chung et al³⁵. pTK-EGFP-DGAT2 was developed by Wilfling et al²³⁴. mCherry-ER-3 (ER3) was a gift from Michael Davidson (Addgene plasmid #55041 ; <http://n2t.net/addgene:55041> ; RRID:Addgene_55041). mApple-TOMM20-N-10 was a gift from Michael Davidson (Addgene plasmid #54955 ;

<http://n2t.net/addgene:54955> ; RRID:Addgene_54955). GPAT₁ was amplified from GPAM cDNA (Dharmacon, #MHS6278-202806915). ACSL₁ was amplified from ACSL₁ cDNA (Dharmacon, #MHS6278-202808193).

B.10.5 GENERATION OF KNOCK-IN CELLS WITH CRISPR/CAS9- MEDIATED GENOME EDITING

Endogenous tagging of the N-terminus of GPAT₁ with superfolderGFP (sfGFP) were generated by simultaneously transfecting a repair template donor plasmid (pSMART) containing homology arms around 800 nucleotides upstream and downstream of the target site with an annealed gRNA (top: 5'-CACCg GGG AATTACACTTTGTGACA-3' and bottom 5'-AAAC TGTCACAAAGTG-TAATTCCC c-3') using FuGene HD transfection reagent (Promega, #E2311). Cells were selected with 1.5 µg/mL puromycin for 48 hours and single-cell FACS sorting was performed with 488-nm excitation with 100µm gating at the flow cytometry core facility (Harvard, Division of Immunology). Positive clones were confirmed by fluorescence microscopy, western blot with anti-GFP antibody, and genomic sequencing of PCR-amplified gRNA target regions subcloned into pCR Blunt II TOPO vector (Thermo Fisher Scientific) for verification of proper insertion by genome editing. Primer and plasmid design for knock in constructs are in Table A3.

B.10.6 STABLE CELL LINE GENERATION

The AAVS₁ Safe Harbor Targeting method (System Biosciences) was used to generate SUM159 cell lines stably expressing EGFP-GPAT₁ or EGFP-MAVS under a TK promoter. In brief, donor plasmids of AAVS₁-TK-TMEM223-EGFP were co-transfected with simultaneously transfected with hCas9 plasmid (Addgene plasmid #41815) and gRNA-AAVS₁-T2 plasmid (Addgene plasmid #41818) into wildtype SUM159 cells using FuGENE HD transfection reagent (Promega) follow-

ing the manufacturer's protocol. Cells were selected with 1.5 µg/mL puromycin for 48 hours and single-cell FACS sorting was performed with 488-nm excitation with 100µm gating at the flow cytometry core facility (Harvard, Division of Immunology). Positive clones were confirmed by fluorescence microscopy and by western blot with anti-GFP antibody. The cloning strategies (including primers) of the mentioned plasmids are summarized in Table A3.

B.10.7 IMMUNOBLOTTING

For analysis of protein lysate, cells were lysed in 1% SDS lysis buffer (50 mM Tris, pH 8.0, 150 mM NaCl, 1% SDS and cOmplete Mini EDTA-Free Protease Inhibitor Cocktail tablet (Sigma-Aldrich, #11836170001)) with 100 units of Benzonase nuclease (MilliporeSigma, #E1014). Protein concentration was determined using either a Pierce BCA Protein Assay Kit (Thermo Fisher Scientific, #23225) or a DC Protein Assay Kit (Bio-Rad, #5000112). Laemmli Sample Buffer was added to samples to a final concentration of 1X. Samples were incubated for 15 minutes at 60 °C prior to SDS-PAGE. Proteins were separated on a 4-15% SDS-PAGE gel (Bio-Rad, #4568086) in 1 X Tris/Glycine/SDS buffer (Bio-Rad, #161-0772) and transferred to Immun-Blot PVDF membranes (Bio-Rad, #1620177) in 1 X Tris/glycine transfer buffer (Bio-Rad, #161-0771) with 20% methanol for 2 hours at 70 V in an ice water bath. The membranes were incubated in 5% non-fat dry milk (Santa Cruz Biotechnology, #sc-2325) in TBS-T for 1 hour and subsequently incubated overnight in primary antibodies at 4 °C. Membranes were washed three times in TBS-T for 5 minutes and then incubated at room temperature with 1:5000 dilutions either anti-mouse or anti-rabbit HRP-conjugated secondary antibodies (Santa Cruz Biotechnology, #sc-2357 and #sc-516192) in 5% non-fat dry milk in TBS-T. Signal was analysed by chemiluminescence with SuperSignal West Pico, Dura or Femto reagents (Thermo Fisher Scientific).

B.10.8 IMAGING AND IMAGE ANALYSIS

Live cell imaging was performed on a Nikon Eclipse Ti inverted microscope equipped with CSU-X1 spinning disk confocal head (Yokogawa), 405-, 488-, 561-, or 639- nm laser lines, 100x ApoTIRF 1.4 NA objective (Nikon, Melville, NY), and iXon Ultra 897 EMCCD or Zyla 4.2 Plus sCMOS cameras (Andor, Belfast, UK). Cells were annually tested for mycoplasma contamination by Universal Mycoplasma Detection Kit (ATCC). For quantification of ER morphology, 3 μm Z stacks with 0.25 μm steps were acquired.

Imaging experiments of SUM159 cells were carried out in Gibco Fluorobrite DMEM (Life Technologies) supplemented with SUM159 maintenance media components. Imaging experiments of HepG2, Huh7, and Cos7 cells were carried out in Gibco Fluorobrite DMEM (Life Technologies) supplemented with 10% FBS and antibiotics. LDs were stained with either 100 μM monodansylpentane (MDH) (AUTODOT; Abcepta, #SM100b), 0.5 $\mu\text{g}/\text{ml}$ BODIPY 493/503 (Life Technologies) or HCS LipidTOX Deep Red Neutral Lipid Stain (Thermo Fisher Scientific) at least 15 minutes before imaging. Mitochondria were stained with 25 nM MitoTracker Red CMXRos (Thermo Fisher, #M-7512) or MitoTracker Deep Red FM (Thermo Fisher, #M22426) at least 15 minutes before imaging. Specific dyes used in each experiment are specified in the figure legends.

B.11 AUTHOR CONTRIBUTIONS

Experiments designed by CBKJ, RVF, and TCW. Many plasmids used were developed by JC. Experiments carried out by CBKJ.

References

- [1] Aaltonen, M. J., Friedman, J. R., Osman, C., Salin, B., Paul, J., Nunnari, J., Langer, T., & Tatsuta, T. (2016). MICOS and phospholipid transfer by Ups2 – Mdm35 organize membrane lipid synthesis in mitochondria. *Journal of Cell Biology*, 213(5), 525–534.
- [2] Abel, E. D. (2010). Free fatty acid oxidation in insulin resistance and obesity. *Heart and Metabolism*, 48, 5–10.
- [3] Adeyo, O., Horn, P. J., Lee, S. K., Binns, D. D., Chandrabhas, A., Chapman, K. D., & Goodman, J. M. (2011). The yeast lipin orthologue Pah1p is important for biogenesis of lipid droplets. *Journal of Cell Biology*, 192(6), 1043–1055.
- [4] Ameer, F., Scandiuizzi, L., Hasnain, S., Kalbacher, H., & Zaidi, N. (2014). De novo lipogenesis in health and disease. *Metabolism: Clinical and Experimental*, 63(7), 895–902.
- [5] Aon, M. A., Bhatt, N., & Cortassa, S. (2014). Mitochondrial and cellular mechanisms for managing lipid excess. *Frontiers in Physiology*, 5 JUL(July), 1–13.
- [6] Arakel, E. C. & Schwappach, B. (2018). Correction: Formation of COPI-coated vesicles at a glance [J. Cell Sci, 131, (jcs209890)] doi:10.1242/jcs.209890. *Journal of Cell Science*, 131(7).
- [7] Ayyappan, J. P., Paul, A., & Goo, Y. H. (2016). Lipid droplet-associated proteins in atherosclerosis (Review). *Molecular Medicine Reports*, 13(6), 4527–4534.
- [8] Bard, F., Casano, L., Mallabiabarrena, A., Wallace, E., Saito, K., Kitayama, H., Guizzunti, G., Hu, Y., Wendler, F., DasGupta, R., Perrimon, N., & Malhotra, V. (2006). Functional genomics reveals genes involved in protein secretion and Golgi organization. *Nature*, 439(7076), 604–607.
- [9] Barr, F. A. (2013). Rab GTPases and membrane identity: Causal or inconsequential? *Journal of Cell Biology*, 202(2), 191–199.
- [10] Bates, E. J. & Saggerson, E. D. (1979). A study of the glycerol phosphate acyltransferase and dihydroxyacetone phosphate acyltransferase activities in rat liver mitochondrial and microsomal fractions. Relative distribution in parenchymal and non-parenchymal cells, effects of N-ethylmaleimide, p. *The Biochemical journal*, 182(3), 751–62.

- [11] Becuwe, M., Bond, L. M., Pinto, A. F., Boland, S., Mejhert, N., Elliott, S. D., Cicconet, M., Graham, M. M., Liu, X. N., Ilkayeva, O., Saghatelian, A., Walther, T. C., & Farese, R. V. (2020). FIT2 is an acyl-coenzyme A diphosphatase crucial for endoplasmic reticulum homeostasis. *Journal of Cell Biology*, 219(10).
- [12] Beller, M., Sztalryd, C., Southall, N., Bell, M., Jäckle, H., Auld, D. S., & Oliver, B. (2008). COPI Complex Is a Regulator of Lipid Homeostasis. *PLOS Biology*, 6(11), e292.
- [13] Ben M'barek, K., Ajjaji, D., Chorlay, A., Vanni, S., Forêt, L., & Thiam, A. R. (2017). ER Membrane Phospholipids and Surface Tension Control Cellular Lipid Droplet Formation. *Developmental Cell*, 41(6), 591–604.
- [14] Bi, J., Xiang, Y., Chen, H., Liu, Z., Grönke, S., Kühnlein, R. P., & Huang, X. (2012). Opposite and redundant roles of the two Drosophila: Perilipins in lipid mobilization. *Journal of Cell Science*, 125(15), 3568–3577.
- [15] Binns, D., Januszewski, T., Chen, Y., Hill, J., Markin, V. S., Zhao, Y., Gilpin, C., Chapman, K. D., Anderson, R. G. W., & Goodman, J. M. (2006). An intimate collaboration between peroxisomes and lipid bodies. *Journal of Cell Biology*, 173(5), 719–731.
- [16] Bohnert, M. (2020). Tethering Fat: Tethers in Lipid Droplet Contact Sites. *Contact*, 3, 251525642090814.
- [17] Bombardier, J. P. & Munson, M. (2015). Three steps forward, two steps back: Mechanistic insights into the assembly and disassembly of the SNARE complex. *Current Opinion in Chemical Biology*, 29, 66–71.
- [18] Boutant, M., Kulkarni, S. S., Joffraud, M., Ratajczak, J., Valera-Alberni, M., Combe, R., Zorzano, A., & Cantó, C. (2017). Mfn2 is critical for brown adipose tissue thermogenic function. *The EMBO Journal*, 36(11), 1543–1558.
- [19] Brasaemle, D. L., Dolios, G., Shapiro, L., & Wang, R. (2004). Proteomic analysis of proteins associated with lipid droplets of basal and lipolytically stimulated 3T3-L1 adipocytes. *Journal of Biological Chemistry*, 279(45), 46835–46842.
- [20] Brasaemle, D. L. & Wolins, N. E. (2012). Packaging of fat: An evolving model of lipid droplet assembly and expansion. *Journal of Biological Chemistry*, 287(4), 2273–2279.
- [21] Breslow, D. K. & Weissman, J. S. (2010). Membranes in Balance: Mechanisms of Sphingolipid Homeostasis. *Molecular Cell*, 40(2), 267–279.
- [22] Bulankina, A. V., Deggerich, A., Wenzel, D., Mutenda, K., Wittmann, J. G., Rudolph, M. G., Burger, K. N. J., & Höning, S. (2009). TIP47 functions in the biogenesis of lipid droplets. *Journal of Cell Biology*, 185(4), 641–655.

- [23] Bussell, R. (2005). Helix periodicity, topology, and dynamics of membrane-associated - Synuclein. *Protein Science*, 14(4), 862–872.
- [24] Camus, G., Vogt, D. A., Kondratowicz, A. S., & Ott, M. (2013). *Lipid Droplets and Viral Infections*, volume 116. Elsevier Inc., 1 edition.
- [25] Carpanini, S. M., McKie, L., Thomson, D., Wright, A. K., Gordon, S. L., Roche, S. L., Handley, M. T., Morrison, H., Brownstein, D., Wishart, T. M., Cousin, M. A., Gillingwater, T. H., Aligianis, I. A., & Jackson, I. J. (2014). A novel mouse model of Warburg Micro syndrome reveals roles for RAB18 in eye development and organisation of the neuronal cytoskeleton. *Disease Models & Mechanisms*, 7(6), 711–722.
- [26] Carr, R. M. & Ahima, R. S. (2016). Pathophysiology of lipid droplet proteins in liver diseases. *Experimental Cell Research*, 340(2), 187–192.
- [27] Carvalho, F. A., Carneiro, F. A., Martins, I. C., Assuncao-Miranda, I., Faustino, A. F., Pereira, R. M., Bozza, P. T., Castanho, M. A. R. B., Mohana-Borges, R., Da Poian, A. T., & Santos, N. C. (2012a). Dengue Virus Capsid Protein Binding to Hepatic Lipid Droplets (LD) Is Potassium Ion Dependent and Is Mediated by LD Surface Proteins. *Journal of Virology*, 86(4), 2096–2108.
- [28] Carvalho, M., Sampaio, J. L., Palm, W., Brankatschk, M., Eaton, S., & Shevchenko, A. (2012b). Effects of diet and development on the Drosophila lipidome. *Molecular Systems Biology*, 8(600), 1–17.
- [29] Chan, E. Y. & McQuibban, G. A. (2012). Phosphatidylserine decarboxylase 1 (Psd1) promotes mitochondrial fusion by regulating the biophysical properties of the mitochondrial membrane and alternative topogenesis of mitochondrial genome maintenance protein 1 (Mgm1). *Journal of Biological Chemistry*, 287(48), 40131–40139.
- [30] Chen, Y. A. & Scheller, R. H. (2001). SNARE-mediated membrane fusion. *Nature reviews. Molecular cell biology*, 2(2), 98–106.
- [31] Chiu, S., Mulligan, K., & Schwarz, J. M. (2018). Dietary carbohydrates and fatty liver disease: De novo lipogenesis. *Current Opinion in Clinical Nutrition and Metabolic Care*, 21(4), 277–282.
- [32] Chorlay, A., Monticelli, L., Verissimo Ferreira, J., Ben M'barek, K., Ajjaji, D., Wang, S., Johnson, E., Beck, R., Omrane, M., Beller, M., Carvalho, P., & Rachid Thiam, A. (2019). Membrane Asymmetry Imposes Directionality on Lipid Droplet Emergence from the ER. *Developmental Cell*, 50(1), 25–42.
- [33] Choudhary, V., Golani, G., Joshi, A. S., Cottier, S., Schneiter, R., Prinz, W. A., & Kozlov, M. M. (2018). Architecture of Lipid Droplets in Endoplasmic Reticulum Is Determined by Phospholipid Intrinsic Curvature. *Current Biology*, 28(6), 915–926.

- [34] Choudhary, V., Ojha, N., Golden, A., & Prinz, W. A. (2015). A conserved family of proteins facilitates nascent lipid droplet budding from the ER. *Journal of Cell Biology*, 211(2), 261–271.
- [35] Chung, J., Wu, X., Lambert, T. J., Lai, Z. W., Walther, T. C., & Farese, R. V. (2019). LDAF1 and Seipin Form a Lipid Droplet Assembly Complex. *Developmental Cell*, 51(5), 551–563.
- [36] Cockcroft, S. & Raghu, P. (2018). Phospholipid transport protein function at organelle contact sites. *Current Opinion in Cell Biology*, 53, 52–60.
- [37] Cohen, A. W., Razani, B., Schubert, W., Williams, T. M., Wang, X. B., Iyengar, P., Brasaemle, D. L., Scherer, P. E., & Lisanti, M. P. (2004). Role of Caveolin-1 in the Modulation of Lipolysis and Lipid Droplet Formation. *Diabetes*, 53(5), 1261–1270.
- [38] Coleman, R. A. (2019). It takes a village: Channeling fatty acid metabolism and triacylglycerol formation via protein interactomes. *Journal of Lipid Research*, 60(3), 490–497.
- [39] Coleman, R. A. & Lee, D. P. (2004). Enzymes of triacylglycerol synthesis and their regulation. *Progress in Lipid Research*, 43(2), 134–176.
- [40] Čopič, A., Antoine-Bally, S., Giménez-Andrés, M., La Torre Garay, C., Antonny, B., Manni, M. M., Pagnotta, S., Guihot, J., & Jackson, C. L. (2018). A giant amphipathic helix from a perilipin that is adapted for coating lipid droplets. *Nature Communications*, 9(1), 1–16.
- [41] Datta, S., Liu, Y., Hariri, H., Bowerman, J., & Henne, W. M. (2019). Cerebellar ataxia disease-associated Snx14 promotes lipid droplet growth at ER-droplet contacts. *Journal of Cell Biology*, 218(4), 1335–1351.
- [42] Dircks, L. K. & Sul, H. S. (1997). Mammalian mitochondrial glycerol-3-phosphate acyltransferase. *Biochimica et Biophysica Acta - Lipids and Lipid Metabolism*, 1348(1-2), 17–26.
- [43] Duncan, J. G. (2008). Lipotoxicity: what is the fate of fatty acids? *Journal of Lipid Research*, 49(7), 1375–1376.
- [44] Ericsson, J., Jackson, S. M., Kim, J. B., Spiegelman, B. M., & Edwards, P. A. (1997). Identification of glycerol-3-phosphate acyltransferase as an adipocyte determination and differentiation factor. *J Biol. Chem.*, 272(11), 7298–7305.
- [45] Farese, R. V. & Walther, T. C. (2009). Lipid Droplets Finally Get a Little R-E-S-P-E-C-T. *Cell*, 139(5), 855–860.
- [46] Feldmann, A., Bekbulat, F., Huesmann, H., Ulbrich, S., Tatzelt, J., Behl, C., & Kern, A. (2017). The RAB GTPase RAB18 modulates macroautophagy and proteostasis. *Biochemical and Biophysical Research Communications*, 486(3), 738–743.

- [47] Flanagan, L., Van Weelden, K., Ammerman, C., Ethier, S. P., & Welsh, J. E. (1999). SUM-159PT cells: A novel estrogen independent human breast cancer model system. *Breast Cancer Research and Treatment*, 58(3), 193–204.
- [48] Flis, V. V. & Daum, G. (2013). Lipid Transport between the Endoplasmic. *Cold Spring Harb Perspect Biol*, 5(6), 1–22.
- [49] Formosa, L. E., Muellner-Wong, L., Reljic, B., Sharpe, A. J., Beilharz, T. H., Lazarou, M., Stroud, D. A., & Ryan, M. T. (2019). Dissecting the Roles of Mitochondrial Complex I Intermediate Assembly (MCIA) Complex Factors in the Biogenesis of Complex I. *bioRxiv*, (pp. 808311).
- [50] Friedman, J. R., Mourier, A., Yamada, J., Mccaffery, J. M., & Nunnari, J. (2015). MICOS coordinates with respiratory complexes and lipids to establish mitochondrial inner membrane architecture. *eLife*, (pp. 1–25).
- [51] Fukasawa, Y., Tsuji, J., Fu, S.-C., Tomii, K., Horton, P., & Imai, K. (2015). MitoFates: Improved Prediction of Mitochondrial Targeting Sequences and Their Cleavage Sites. *Molecular and Cellular Proteomics*, 14(4), 1113–1126.
- [52] Fukushima, A. & Lopaschuk, G. D. (2016). Cardiac fatty acid oxidation in heart failure associated with obesity and diabetes. *Biochimica et Biophysica Acta - Molecular and Cell Biology of Lipids*, 1861(10), 1525–1534.
- [53] Gabler, F., Nam, S. Z., Till, S., Mirdita, M., Steinegger, M., Söding, J., Lupas, A. N., & Alva, V. (2020). Protein Sequence Analysis Using the MPI Bioinformatics Toolkit. *Current Protocols in Bioinformatics*, 72(1), 1–30.
- [54] Gautier, R., Douguet, D., Antonny, B., & Drin, G. (2008). HELIQUEST: A web server to screen sequences with specific α -helical properties. *Bioinformatics*, 24(18), 2101–2102.
- [55] Gerondopoulos, A., Bastos, R. N., Yoshimura, S. I., Anderson, R., Carpanini, S., Aligianis, I., Handley, M. T., & Barr, F. A. (2014). Rab18 and a Rab18 GEF complex are required for normal ER structure. *Journal of Cell Biology*, 205(5), 707–720.
- [56] Gillingham, A. K., Sinka, R., Torres, I. L., Lilley, K. S., & Munro, S. (2014). Toward a comprehensive map of the effectors of rab GTPases. *Developmental cell*, 31(3), 358–373.
- [57] Giraudo, C. G., Hu, C., You, D., Slovic, A. M., Mosharov, E. V., Sulzer, D., Melia, T. J., & Rothman, J. E. (2005). SNAREs can promote complete fusion and hemifusion as alternative outcomes. *Journal of Cell Biology*, 170(2), 249–260.
- [58] Girusse, a. & Langin, D. (2012). Adipocyte lipases and lipid droplet-associated proteins: insight from transgenic mouse models. *International Journal of Obesity*, 36(4), 581–594.

- [59] Glatz, J. F., Luiken, J. J., & Bonen, A. (2010). Membrane fatty acid transporters as regulators of lipid metabolism: Implications for metabolic disease. *Physiological Reviews*, 90(1), 367–417.
- [60] Gluchowski, N. L., Becuwe, M., Walther, T. C., & Farese, R. V. (2017). Lipid droplets and liver disease: from basic biology to clinical implications. *Nature Reviews Gastroenterology & Hepatology*, 14(6), 343–355.
- [61] Gluchowski, N. L., Gabriel, K. R., Chitraju, C., Bronson, R. T., Mejhert, N., Boland, S., Wang, K., Lai, Z. W., Farese, R. V., & Walther, T. C. (2019). Hepatocyte Deletion of Triglyceride-Synthesis Enzyme Acyl CoA: Diacylglycerol Acyltransferase 2 Reduces Steatosis Without Increasing Inflammation or Fibrosis in Mice. *Hepatology*, 70(6), 1972–1985.
- [62] Gomes, S., Soares, V. C., & Ferreira, A. C. (2020). Lipid droplets fuel SARS-CoV-2 replication and production of inflammatory mediators. *bioRxiv*, (pp. 1–19).
- [63] Gonzalez-Baró, M. R., Granger, D. A., & Coleman, R. A. (2001). Mitochondrial Glycerol Phosphate Acyltransferase Contains Two Transmembrane Domains with the Active Site in the N-terminal Domain Facing the Cytosol. *Journal of Biological Chemistry*, 276(46), 43182–43188.
- [64] Grahn, T. H. M., Kaur, R., Yin, J., Schweiger, M., Sharma, V. M., Lee, M. J., Ido, Y., Smas, C. M., Zechner, R., Lass, A., & Puri, V. (2014). Fat-specific protein 27 (FSP27) interacts with adipose triglyceride lipase (ATGL) to regulate lipolysis and insulin sensitivity in human adipocytes. *Journal of Biological Chemistry*, 289(17), 12029–12039.
- [65] Grippa, A., Buxó, L., Mora, G., Funaya, C., Idrissi, F. Z., Mancuso, F., Gomez, R., Muntanya, J., Sabidó, E., & Carvalho, P. (2015). The seipin complex Fld1/Ldb16 stabilizes ER-lipid droplet contact sites. *Journal of Cell Biology*, 211(4), 829–844.
- [66] Grönke, S., Mildner, A., Fellert, S., Tennagels, N., Petry, S., Müller, G., Jäckle, H., & Kühnlein, R. P. (2005). Brummer lipase is an evolutionary conserved fat storage regulator in *Drosophila*. *Cell Metabolism*, 1(5), 323–330.
- [67] Gross, D. A. & Silver, D. L. (2014). Cytosolic lipid droplets: From mechanisms of fat storage to disease. *Critical Reviews in Biochemistry and Molecular Biology*, 49(4), 304–326.
- [68] Gross, D. A., Zhan, C., & Silver, D. L. (2011). Direct binding of triglyceride to fat storage-inducing transmembrane proteins 1 and 2 is important for lipid droplet formation. *Proceedings of the National Academy of Sciences*, 108(49), 19581–19586.
- [69] Guarani, V., McNeill, E. M., Paulo, J. A., Huttlin, E. L., Gygi, S. P., Vactor, D. V., & Harper, J. W. (2015). QIL1 is a novel mitochondrial protein required for MICOS complex stability and cristae morphology. *eLife*, (pp. 1–23).

- [70] Guerrero-Castillo, S., Baertling, F., Kownatzki, D., Wessels, H. J., Arnold, S., Brandt, U., & Nijtmans, L. (2017). The Assembly Pathway of Mitochondrial Respiratory Chain Complex I. *Cell Metabolism*, 25(1), 128–139.
- [71] Guo, Y., Walther, T. C., Rao, M., Stuurman, N., Goshima, G., Terayama, K., Wong, J. S., Vale, R. D., Walter, P., & Farese, R. V. (2008). Functional genomic screen reveals genes involved in lipid-droplet formation and utilization. *Nature*, 453(7195), 657–661.
- [72] Gusdon, A. M., Song, K.-X., & Qu, S. (2014). Nonalcoholic Fatty liver disease: pathogenesis and therapeutics from a mitochondria-centric perspective. *Oxidative medicine and cellular longevity*, 2014, 637027.
- [73] Gustafsson, M. G., Shao, L., Carlton, P. M., Wang, C. J., Golubovskaya, I. N., Cande, W. Z., Agard, D. A., & Sedat, J. W. (2008). Three-dimensional resolution doubling in wide-field fluorescence microscopy by structured illumination. *Biophysical Journal*, 94(12), 4957–4970.
- [74] Hammond, L. E., Gallagher, P. A., Wang, S., Hiller, S., Kluckman, K. D., Posey-Marcos, E. L., Maeda, N., & Coleman, R. A. (2002). Mitochondrial Glycerol-3-Phosphate Acyltransferase-Deficient Mice Have Reduced Weight and Liver Triacylglycerol Content and Altered Glycerolipid Fatty Acid Composition. *Molecular and Cellular Biology*, 22(23), 8204–8214.
- [75] Hammond, L. E., Neschen, S., Romanelli, A. J., Cline, G. W., Ilkayeva, O. R., Shulman, G. I., Muoio, D. M., & Coleman, R. A. (2005). Mitochondrial glycerol-3-phosphate acyltransferase-1 is essential in liver for the metabolism of excess acyl-CoAs. *Journal of Biological Chemistry*, 280(27), 25629–25636.
- [76] Hay, J. C., Chao, D. S., Kuo, C. S., & Scheller, R. H. (1997). Protein interactions regulating vesicle transport between the endoplasmic reticulum and Golgi apparatus in mammalian cells. *Cell*, 89(1), 149–158.
- [77] Heaton, N. S., Perera, R., Berger, K. L., Khadka, S., LaCount, D. J., Kuhn, R. J., & Randall, G. (2010). Dengue virus nonstructural protein 3 redistributes fatty acid synthase to sites of viral replication and increases cellular fatty acid synthesis. *Proceedings of the National Academy of Sciences of the United States of America*, 107(40), 17345–17350.
- [78] Hebbar, S., Sahoo, I., Matysik, A., Argudo Garcia, I., Osborne, K. A., Papan, C., Torta, F., Narayanaswamy, P., Fun, X. H., Wenk, M. R., Shevchenko, A., Schwudke, D., & Kraut, R. (2015). Ceramides and stress signalling intersect with autophagic defects in neurodegenerative drosophila blue cheese (bchs) Mutants. *Scientific Reports*, 5(December), 1–18.
- [79] Heden, T. D., Johnson, J. M., Ferrara, P. J., Eshima, H., Verkerke, A. R., Wentzler, E. J., Siripoksup, P., Narowski, T. M., Coleman, C. B., Lin, C. T., Ryan, T. E., Reidy, P. T., de Castro Brás, L. E., Karner, C. M., Burant, C. F., Alan Maschek, J., Cox, J. E., Mashek,

- D. G., Kardon, G., Boudina, S., Zeczycki, T. N., Rutter, J., Shaikh, S. R., Vance, J. E., Drummond, M. J., Darrell Neuffer, P., & Funai, K. (2019). Mitochondrial PE potentiates respiratory enzymes to amplify skeletal muscle aerobic capacity. *Science Advances*, 5(9), 1–12.
- [80] Hejzlarová, K., Tesarřová, M., Vrbacká-Čížková, A., Vrbacký, M., Hartmannová, H., Kaplanová, V., Nosková, L., Kratochvílová, H., Buzková, J., Havlíčková, V., Zeman, J., Kmoch, S., & Houšťek, J. (2011). Expression and processing of the TMEM70 protein. *Biochimica et Biophysica Acta - Bioenergetics*, 1807(1), 144–149.
- [81] Herms, A., Bosch, M., Reddy, B. J. N., Schieber, N. L., Fajardo, A., Rupérez, C., Fernández-Vidal, A., Ferguson, C., Rentero, C., Tebar, F., Enrich, C., Parton, R. G., Gross, S. P., & Pol, A. (2015). AMPK activation promotes lipid droplet dispersion on deetyrosinated microtubules to increase mitochondrial fatty acid oxidation. *Nature communications*, 6(May), 7176.
- [82] Herzog, R., Schuhmann, K., Schwudke, D., Sampaio, J. L., Bornstein, S. R., Schroeder, M., & Shevchenko, A. (2012). LipidXplorer: A software for consensual cross-platform lipidomics. *PLoS ONE*, 7(1), 15–20.
- [83] Herzog, R., Schwudke, D., Schuhmann, K., Sampaio, J. L., Bornstein, S. R., Schroeder, M., & Shevchenko, A. (2011). A novel informatics concept for high-throughput shotgun lipidomics based on the molecular fragmentation query language. *Genome Biology*, 12(1), 1–25.
- [84] Hiraoka, Y., Sedat, J. W., & Agard, D. A. (1990). Determination of three-dimensional imaging properties of a light microscope system. Partial confocal behavior in epifluorescence microscopy. *Biophysical Journal*, 57(2), 325–333.
- [85] Hodges, B. D. & Wu, C. C. (2010). Proteomic insights into an expanded cellular role for cytoplasmic lipid droplets. *Journal of Lipid Research*, 51(2), 262–273.
- [86] Holthuis, J. C., Pomorski, T., Raggars, R. J., Sprong, H., & Van Meer, G. (2001). The organizing potential of sphingolipids in intracellular membrane transport. *Physiological Reviews*, 81(4), 1689–1723.
- [87] Hong, W. (2005). SNAREs and traffic. *Biochimica et biophysica acta*, 1744(3), 493–517.
- [88] Hönscher, C., Mari, M., Auffarth, K., Bohnert, M., Griffith, J., Geerts, W., van der Laan, M., Cabrera, M., Reggiori, F., & Ungermann, C. (2014). Cellular metabolism regulates contact sites between vacuoles and mitochondria. *Developmental Cell*, 30(1), 86–94.
- [89] Hoppins, S., Collins, S. R., Cassidy-Stone, A., Hummel, E., DeVay, R. M., Lackner, L. L., Westermann, B., Schuldiner, M., Weissman, J. S., & Nunnari, J. (2011). A mitochondrial-focused genetic interaction map reveals a scaffold-like complex required for inner membrane organization in mitochondria. *Journal of Cell Biology*, 195(2), 323–340.

- [90] Housden, B. E., Hu, Y., & Perrimon, N. (2016). Design and generation of *Drosophila* single guide RNA expression constructs. *Cold Spring Harbor Protocols*, 2016(9), 782–788.
- [91] Housden, B. E., Lin, S., & Perrimon, N. (2014). *Cas9-based genome editing in drosophila*, volume 546. Elsevier Inc., 1 edition.
- [92] Housden, B. E. & Perrimon, N. (2016). Design and generation of donor constructs for genome engineering in *Drosophila*. *Cold Spring Harbor Protocols*, 2016(9), 789–793.
- [93] Huguenoth, M. & Bohnert, M. (2020). Come a little bit closer! Lipid droplet-ER contact sites are getting crowded. *Biochimica et Biophysica Acta - Molecular Cell Research*, 1867(2), 118603.
- [94] Hutagalung, A. H. & Novick, P. J. (2011). Role of Rab GTPases in Membrane Traffic and Cell Physiology. *Physiological Reviews*, 91(1), 119–149.
- [95] Igal, R. A., Wang, S., Gonzalez-Baró, M. R., & Coleman, R. A. (2001). Mitochondrial Glycerol Phosphate Acyltransferase Directs the Incorporation of Exogenous Fatty Acids into Triacylglycerol. *Journal of Biological Chemistry*, 275(45), 42205–42212.
- [96] Jacquier, N., Choudhary, V., Mari, M., Toulmay, A., Reggiori, F., & Schneider, R. (2011). Lipid droplets are functionally connected to the endoplasmic reticulum in *Saccharomyces cerevisiae*. *Journal of Cell Science*, 124(14), 2424–2437.
- [97] Jacquier, N., Mishra, S., Choudhary, V., & Schneider, R. (2013). Expression of oleosin and perilipins in yeast promotes formation of lipid droplets from the endoplasmic reticulum. *Journal of Cell Science*, 126(22), 5198–5209.
- [98] Jamdar, S. C. & Fang Cao, W. (1995). Triacylglycerol biosynthetic enzymes in lean and obese Zucker rats. *Biochimica et Biophysica Acta (BBA)/Lipids and Lipid Metabolism*, 1255(3), 237–243.
- [99] Jayson, C., Arlt, H., Fischer, A. W., Weng Lai, Z., Farese, R. V., & Walther, T. C. (2018). Rab18 is not necessary for lipid droplet biogenesis or turnover in human mammary carcinoma cells. *Molecular Biology of the Cell*, 29(17), 2045–2054.
- [100] Jerkins, A., Liu, W. R., Lee, S., & Sul, H. S. (1995). Characterization of the Murine Mitochondrial Glycerol-3-phosphate Acyltransferase promoter. *The Journal of Biological Chemistry*, 270(3), 1416–1421.
- [101] Jiménez-Rojo, N., Leonetti, M. D., Zoni, V., Colom, A., Feng, S., Iyengar, N. R., Matile, S., Roux, A., Vanni, S., Weissman, J. S., & Riezman, H. (2020). Conserved Functions of Ether Lipids and Sphingolipids in the Early Secretory Pathway. *Current Biology*, 30(19), 3775–3787.

- [102] Joiner, A. M. N., Phillips, B. P., Yugandhar, K., Sanford, E. J., Smolka, M. B., Yu, H., Miller, E. A., & Fromme, J. C. (2020). Structure and mechanism of TRAPP3-mediated Rab1 activation. *Biorxiv*.
- [103] Kanca, O., Zirin, J., Garcia-Marques, J., Knight, S. M., Yang-Zhou, D., Amador, G., Chung, H., Zuo, Z., Ma, L., He, Y., Lin, W. W., Fang, Y., Ge, M., Yamamoto, S., Schulze, K. L., Hu, Y., Spradling, A. C., Mohr, S. E., Perrimon, N., & Bellen, H. J. (2019). An efficient CRISPR-based strategy to insert small and large fragments of DNA using short homology arms. *eLife*, 8, 1–22.
- [104] Kassan, A., Herms, A., Fernández-Vidal, A., Bosch, M., Schieber, N. L., Reddy, B. J., Fajardo, A., Gelabert-Baldrich, M., Tebar, F., Enrich, C., Gross, S. P., Parton, R. G., & Pol, A. (2013). Acyl-CoA synthetase 3 promotes lipid droplet biogenesis in ER microdomains. *Journal of Cell Biology*, 203(6), 985–1001.
- [105] Khaldoun, S. A., Emond-Boisjoly, M.-A., Chateau, D., Carrière, V., Lacasa, M., Rousset, M., Demignot, S., & Morel, E. (2014). Autophagosomes contribute to intracellular lipid distribution in enterocytes. *Molecular biology of the cell*, 25(1), 118–32.
- [106] Khandelia, H., Duelund, L., Pakkanen, K. I., & Ipsen, J. H. (2010). Triglyceride blisters in lipid bilayers: Implications for lipid droplet biogenesis and the mobile lipid signal in cancer cell membranes. *PLoS ONE*, 5(9), 1–8.
- [107] Kloska, A., Węsierska, M., Malinowska, M., Gabig-Cimińska, M., & Jakóbkiewicz-Banecka, J. (2020). Lipophagy and lipolysis status in lipid storage and lipid metabolism diseases. *International Journal of Molecular Sciences*, 21(17), 1–33.
- [108] Koizumi, K., Higashida, H., Yoo, S., Islam, M. S., Ivanov, A. I., Guo, V., Pozzi, P., Yu, S. H., Rovescalli, A. C., Tang, D., & Nirenberg, M. (2007). RNA interference screen to identify genes required for *Drosophila* embryonic nervous system development. *Proceedings of the National Academy of Sciences of the United States of America*, 104(13), 5626–5631.
- [109] Kojima, R., Kakimoto, Y., Furuta, S., Itoh, K., Sesaki, H., Endo, T., & Tamura, Y. (2019). Maintenance of Cardiolipin and Crista Structure Requires Cooperative Functions of Mitochondrial Dynamics and Phospholipid Transport. *CellReports*, 26(3), 518–528.
- [110] Kory, N., Farese, R. V., & Walther, T. C. (2016). Targeting Fat: Mechanisms of Protein Localization to Lipid Droplets. *Trends in Cell Biology*, 26(7), 535–546.
- [111] Kory, N., Thiam, A. R., Farese, R. V., & Walther, T. C. (2015). Protein Crowding Is a Determinant of Lipid Droplet Protein Composition. *Developmental Cell*, 34(3), 351–363.
- [112] Kovalčíková, J., Vrbacký, M., Pecina, P., Tauchmannová, K., Nůsková, H., Kaplanová, V., Brázdová, A., Alán, L., Eliáš, J., Čunátová, K., Kořínek, V., Sedlacek, R., Mráček, T., &

- Houšťek, J. (2019). TMEM70 facilitates biogenesis of mammalian ATP synthase by promoting subunit c incorporation into the rotor structure of the enzyme. *FASEB Journal*, 33(12), 14103–14117.
- [113] Krahmer, N., Guo, Y., Wilfling, F., Hilger, M., Lingrell, S., Heger, K., Newman, H. W., Schmidt-Supprian, M., Vance, D. E., Jr, R. V. F., Walther, T. C., Mann, M., Farese, R. V., & Walther, T. C. (2011). Phosphatidylcholine Synthesis for Lipid Droplet Expansion Is Mediated by Localized Activation of CTP:Phosphocholine Cytidylyltransferase. *Cell Metabolism*, 14(4), 504–515.
- [114] Krahmer, N., Hilger, M., Kory, N., Wilfling, F., Stoehr, G., Mann, M., Farese, R. V., & Walther, T. C. (2013). Protein correlation profiles identify lipid droplet proteins with high confidence. *Mol. Cell Proteomics*, 12(5), 1115–1126.
- [115] Krahmer, N., Najafi, B., Schueder, F., Quagliarini, F., Steger, M., Seitz, S., Kasper, R., Salinas, F., Cox, J., Uhlenhaut, N. H., Walther, T. C., Jungmann, R., Zeigerer, A., Borner, G. H. H., & Mann, M. (2018). Organellar Proteomics and Phospho-Proteomics Reveal Subcellular Reorganization in Diet-Induced Hepatic Steatosis. *Developmental Cell*, 47(2), 205–221.
- [116] Kratochvílová, H., Hejzlarová, K., Vrbacký, M., Mráček, T., Karbanová, V., Tesařová, M., Gombitová, A., Cmarko, D., Wittig, I., Zeman, J., & Houšťek, J. (2014). Mitochondrial membrane assembly of TMEM70 protein. *Mitochondrion*, 15(1), 1–9.
- [117] Krogh, A., Larsson, B., von Heijne, G., & Sonnhammer, E. L. (2001). Predicting transmembrane protein topology with a hidden markov model: application to complete genomes. *Journal of Molecular Biology*, 305(3), 567–580.
- [118] Kudo, N., Kumagai, K., Tomishige, N., Yamaji, T., Wakatsuki, S., Nishijima, M., Hanada, K., & Kato, R. (2008). Structural basis for specific lipid recognition by CERT responsible for nonvesicular trafficking of ceramide. *Proceedings of the National Academy of Sciences of the United States of America*, 105(2), 488–493.
- [119] Kumar, N., Leonzino, M., Hancock-Cerutti, W., Horenkamp, F. A., Li, P. Q., Lees, J. A., Wheeler, H., Reinisch, K. M., & De Camilli, P. (2018). VPS13A and VPS13C are lipid transport proteins differentially localized at ER contact sites. *The Journal of cell biology*, 217(10), 3625–3639.
- [120] Kurokawa, K. & Nakano, A. (2019). The ER exit sites are specialized ER zones for the transport of cargo proteins from the ER to the Golgi apparatus. *Journal of Biochemistry*, 165(2), 109–114.
- [121] Lass, A., Zimmermann, R., Oberer, M., & Zechner, R. (2011). Lipolysis – A highly regulated multi-enzyme complex mediates the catabolism of cellular fat stores. *Progress in Lipid Research*, 50(1-4), 14–27.

- [122] Lee, S.-y., Kang, M.-g., Shin, S., Kwak, C., Kwon, T., Seo, J. K., Kim, J.-s., & Rhee, H.-w. (2017). Architecture Mapping of the Inner Mitochondrial Membrane Proteome by Chemical Tools in Live Cells. *Journal of the American Chemical Society*, 139, 3651–3662.
- [123] Lesage, S., Drouet, V., Majounie, E., Deramecourt, V., Jacoupy, M., Nicolas, A., Cormier-Dequaire, F., Hassoun, S. M., Pujol, C., Ciura, S., Erpapazoglou, Z., Usenko, T., Maurage, C. A., Sahbatou, M., Liebau, S., Ding, J., Bilgic, B., Emre, M., Erginel-Unaltuna, N., Guven, G., Tison, F., Tranchant, C., Vidailhet, M., Corvol, J. C., Krack, P., Leutenegger, A. L., Nalls, M. A., Hernandez, D. G., Heutink, P., Gibbs, J. R., Hardy, J., Wood, N. W., Gasser, T., Durr, A., Deleuze, J. F., Tazir, M., Deste??, A., Lohmann, E., Kabashi, E., Singleton, A., Corti, O., & Brice, A. (2016). Loss of VPS13C Function in Autosomal-Recessive Parkinsonism Causes Mitochondrial Dysfunction and Increases PINK1/Parkin-Dependent Mitophagy. *American Journal of Human Genetics*, 98(3), 500–513.
- [124] Lewin, T. M., Granger, D. A., Kim, J. H., & Coleman, R. A. (2001). Regulation of mitochondrial sn-glycerol-3-phosphate acyltransferase activity: Response to feeding status is unique in various rat tissues and is discordant with protein expression. *Archives of Biochemistry and Biophysics*, 396(1), 119–127.
- [125] Li, D., Zhao, Y. G., Li, D., Zhao, H., Huang, J., Miao, G., Feng, D., Liu, P., Li, D., & Zhang, H. (2019). The ER-Localized Protein DFCEP1 Modulates ER-Lipid Droplet Contact Formation. *Cell Reports*, 27(2), 343–358.
- [126] Li, L. O., Mashek, D. G., An, J., Doughman, S. D., Newgard, C. B., & Coleman, R. A. (2006). Overexpression of rat long chain acyl-CoA synthetase 1 alters fatty acid metabolism in rat primary hepatocytes. *Journal of Biological Chemistry*, 281(48), 37246–37255.
- [127] Lin, G. G.-h., Scott, J. G., Bickel, P. E., Tansey, J. T., & Welte, M. A. (2009). PAT proteins, an ancient family of lipid droplet proteins that regulate cellular lipid stores. *Biochimica et biophysica acta*, 1791(6), 419–440.
- [128] Lindén, D., William-Olsson, L., Rhedin, M., Asztély, A.-K., Clapham, J. C., & Schreyer, S. (2004). Overexpression of mitochondrial GPAT in rat hepatocytes leads to decreased fatty acid oxidation and increased glycerolipid biosynthesis. *Journal of Lipid Research*, 45(7), 1279–1288.
- [129] Lizaso, A., Tan, K. T., & Lee, Y. H. (2013). β -adrenergic receptor-stimulated lipolysis requires the RAB7-mediated autolysosomal lipid degradation. *Autophagy*, 9(8), 1228–1243.
- [130] Mallmann, R., Ondacova, K., Moravcikova, L., Jurkovicova-tarabova, B., Pavlovicova, M., Moravcik, R., Lichvarova, L., Kominkova, V., & Klugbauer, N. (2019). Four novel interaction partners demonstrate diverse modulatory effects on voltage-gated $Ca_v2.2$ channels. *European Journal of Physiology*, 471, 861–874.

- [131] Martin, S., Driessen, K., Nixon, S. J., Zerial, M., & Parton, R. G. (2005). Regulated localization of Rab18 to lipid droplets: Effects of lipolytic stimulation and inhibition of lipid droplet catabolism. *Journal of Biological Chemistry*, 280(51), 42325–42335.
- [132] Mashima, T., Seimiya, H., & Tsuruo, T. (2009). De novo fatty-acid synthesis and related pathways as molecular targets for cancer therapy. *British Journal of Cancer*, 100(9), 1369–1372.
- [133] Ménégaut, L., Jalil, A., Thomas, C., & Masson, D. (2019). Macrophage fatty acid metabolism and atherosclerosis: The rise of PUFAs. *Atherosclerosis*, 291(September), 52–61.
- [134] Mesmin, B. (2016). Mitochondrial lipid transport and biosynthesis : A complex balance. *Journal of Cell Biology*, 214(1), 9–11.
- [135] Miyanari, Y., Atsuzawa, K., Usuda, N., Watashi, K., Hishiki, T., Zayas, M., Bartenschlager, R., Wakita, T., Hijikata, M., & Shimotohno, K. (2007). The lipid droplet is an important organelle for hepatitis C virus production. *Nature Cell Biology*, 9(9), 1089–1097.
- [136] Miyata, N., Watanabe, Y., Tamura, Y., Endo, T., & Kuge, O. (2016). Phosphatidylserine transport by Ups2 – Mdm35 in respiration-active mitochondria. *Journal of Cell Biology*, 214(1), 77–88.
- [137] Möller-Hergt, B. V., Carlström, A., Stephan, K., Imhof, A., & Ott, M. (2018). The ribosome receptors Mrx15 and Mba1 jointly organize cotranslational insertion and protein biogenesis in mitochondria. *Molecular Biology of the Cell*, 29(20), 2386–2396.
- [138] MUOIO, D. M., Seefeld, K., Witters, L. A., & COLEMAN, R. A. (1999). AMP-activated kinase reciprocally regulates triacylglycerol synthesis and fatty acid oxidation in liver and muscle: evidence that sn-glycerol-3-phosphate acyltransferase is a novel target. *Biochemical Journal*, 338(3), 783.
- [139] Nagle, C. A., An, J., Shiota, M., Torres, T. P., Cline, G. W., Liu, Z. X., Wang, S., Catlin, R. E. L., Shulman, G. I., Newgard, C. B., & Coleman, R. A. (2007). Hepatic overexpression of glycerol-sn-3-phosphate acyltransferase 1 in rats causes insulin resistance. *Journal of Biological Chemistry*, 282(20), 14807–14815.
- [140] Nassir, F. & Ibdah, J. (2014). Role of mitochondria in nonalcoholic fatty liver disease. *International Journal of Molecular Sciences*, 15(5), 8713–8742.
- [141] Nguyen, D., Stutz, R., Schorr, S., Lang, S., Pfeffer, S., Freeze, H. H., Förster, F., Helms, V., Dudek, J., & Zimmermann, R. (2018). Proteomics reveals signal peptide features determining the client specificity in human TRAP-dependent ER protein import. *Nature Communications*, 9.

- [142] Nordström, E. A., Rydén, M., Backlund, E. C., Dahlman, I., Kaaman, M., Blomqvist, L., Cannon, B., Nedergaard, J., & Arner, P. (2005). A human-specific role of cell death-inducing DFFA (DNA fragmentation factor- α)-like effector A (CIDEA) in adipocyte lipolysis and obesity. *Diabetes*, 54(6), 1726–1734.
- [143] Ogawa, K., Hishiki, T., Shimizu, Y., Funami, K., Sugiyam, K., Miyanari, Y., & Shimotohno, K. (2009). Hepatitis C virus utilizes lipid droplet for production of infectious virus. *Proceedings of the Japan Academy Series B: Physical and Biological Sciences*, 85(7), 217–228.
- [144] Olarte, M. J., Kim, S., Sharp, M. E., Swanson, J. M., Farese, R. V., & Walther, T. C. (2020). Determinants of Endoplasmic Reticulum-to-Lipid Droplet Protein Targeting. *Developmental Cell*, 54(4), 471–487.
- [145] Onal, G., Kutlu, O., Gozuacik, D., & Dokmeci Emre, S. (2017). Lipid Droplets in Health and Disease. *Lipids in Health and Disease*, 16(1), 128.
- [146] Ong, K. T., Mashek, M. T., Davidson, N. O., & Mashek, D. G. (2014). Hepatic ATGL mediates PPAR- α signaling and fatty acid channeling through an L-FABP independent mechanism. *Journal of Lipid Research*, 55(5), 808–815.
- [147] Ozeki, S., Cheng, J., Tauchi-Sato, K., Hatano, N., Taniguchi, H., & Fujimoto, T. (2005). Rab18 localizes to lipid droplets and induces their close apposition to the endoplasmic reticulum-derived membrane. *Journal of Cell Science*, 118(12), 2601–2611.
- [148] Panevska, A., Skočaj, M., Križaj, I., Maček, P., & Sepčić, K. (2019). Ceramide phosphoethanolamine, an enigmatic cellular membrane sphingolipid. *Biochimica et Biophysica Acta - Biomembranes*, 1861(7), 1284–1292.
- [149] Patterson, G. H., Hirschberg, K., Polishchuk, R. S., Gerlich, D., Phair, R. D., & Lippincott-Schwartz, J. (2008). Transport through the Golgi Apparatus by Rapid Partitioning within a Two-Phase Membrane System. *Cell*, 133(6), 1055–1067.
- [150] Pellon-Maison, M., Coleman, R. A., & Gonzalez-Baró, M. R. (2006). The C-terminal region of mitochondrial glycerol-3-phosphate acyltransferase-1 interacts with the active site region and is required for activity. *Archives of Biochemistry and Biophysics*, 450(2), 157–166.
- [151] Pellon-Maison, M., Montanaro, M. A., Coleman, R. A., & Gonzalez-Baró, M. R. (2007). Mitochondrial glycerol-3-P acyltransferase 1 is most active in outer mitochondrial membrane but not in mitochondrial associated vesicles (MAV). *Biochimica et biophysica acta*, 1771(7), 830–838.
- [152] Pfeffer, S. R. (2001). Rab GTPases: Specifying and deciphering organelle identity and function. *Trends in Cell Biology*, 11(12), 487–491.

- [153] Pohl, J., Ring, A., Korkmaz, U., Ehehalt, R., & Stremmel, W. (2005). FAT/CD36-mediated Long-Chain Fatty Acid Uptake in Adipocytes Requires Plasma Membrane Rafts. *Mol Biol Cell*, 16(1), 24–31.
- [154] Pol, A., Gross, S. P., & Parton, R. G. (2014). Biogenesis of the multifunctional lipid droplet: Lipids, proteins, and sites. *Journal of Cell Biology*, 204(5), 635–646.
- [155] Postic, C. & Girard, J. (2008). Contribution of de novo fatty acid synthesis to hepatic steatosis and insulin resistance: lessons from genetically engineered mice. *The Journal of Clinical Investigations*, 118(3), 829–838.
- [156] Prévost, C., Sharp, M. E., Kory, N., Lin, Q., Voth, G. A., Farese, R. V., & Walther, T. C. (2018). Mechanism and Determinants of Amphipathic Helix-Containing Protein Targeting to Lipid Droplets. *Developmental Cell*, 44(1), 73–86.
- [157] Prinz, W. A. (2014). Bridging the gap: Membrane contact sites in signaling, metabolism, and organelle dynamics. *Journal of Cell Biology*, 205(6), 759–769.
- [158] Pulido, M. R., Diaz-Ruiz, A., Jiménez-Gómez, Y., Garcia-Navarro, S., Gracia-Navarro, F., Tinahones, F., López-Miranda, J., Frühbeck, G., Vázquez-Martínez, R., & Malagón, M. M. (2011). Rab18 dynamics in adipocytes in relation to lipogenesis, lipolysis and obesity. *PLoS ONE*, 6(7), e22931.
- [159] Puri, V., Konda, S., Ranjit, S., Aouadi, M., Chawla, A., Chouinard, M., Chakladar, A., & Czech, M. P. (2007). Fat-specific protein 27, a novel lipid droplet protein that enhances triglyceride storage. *Journal of Biological Chemistry*, 282(47), 34213–34218.
- [160] Qi, Y., Sun, L., & Yang, H. (2017). Lipid Droplet Growth and Adipocyte Development: Mechanistically Distinct Processes Connected by Phospholipids. *Biochimica et Biophysica Acta (BBA) - Molecular and Cell Biology of Lipids*.
- [161] Quon, E. & Beh, C. T. (2015). Membrane Contact Sites: Complex Zones for Membrane Association and Lipid Exchange. *Lipid Insights*, 8(Suppl. 1), 55–63.
- [162] Rambold, A. S., Cohen, S., & Lippincott-Schwartz, J. (2015). Fatty acid trafficking in starved cells: Regulation by lipid droplet lipolysis, autophagy, and mitochondrial fusion dynamics. *Developmental Cell*, 32(6), 678–692.
- [163] Rampelt, H., Zerbes, R. M., van der Laan, M., & Pfanner, N. (2017). Role of the mitochondrial contact site and cristae organizing system in membrane architecture and dynamics. *Biochimica et Biophysica Acta - Molecular Cell Research*, 1864(4), 737–746.
- [164] Raturi, A. & Simmen, T. (2013). Where the endoplasmic reticulum and the mitochondrion tie the knot: The mitochondria-associated membrane (MAM). *Biochimica et Biophysica Acta - Molecular Cell Research*, 1833(1), 213–224.

- [165] Rowe, E. R., Mimmack, M. L., Barbosa, A. D., Haider, A., Isaac, I., Ouberai, M. M., Thiam, A. R., Patel, S., Saudek, V., Siniosoglou, S., & Savage, D. B. (2016). Conserved amphipathic helices mediate lipid droplet targeting of perilipins 1-3. *Journal of Biological Chemistry*, 291(13), 6664–6678.
- [166] Roy, R., Ordovas, L., Taourit, S., Zaragoza, P., Eggen, A., & Rodellar, C. (2006). Genomic structure and an alternative transcript of bovine mitochondrial glycerol-3-phosphate acyltransferase gene (GPAM). *Cytogenetic and Genome Research*, 112(1-2), 82–89.
- [167] Rusiñol, A. E., Cui, Z., Chen, M. H., & Vance, J. E. (1994). A unique mitochondria-associated membrane fraction from rat liver has a high capacity for lipid synthesis and contains pre-Golgi secretory proteins including nascent lipoproteins. *Journal of Biological Chemistry*, 269(44), 27494–27502.
- [168] Saito, K., Chen, M., Bard, F., Chen, S., Zhou, H., Woodley, D., Polischuk, R., Schekman, R., & Malhotra, V. (2009). TANGO1 Facilitates Cargo Loading at Endoplasmic Reticulum Exit Sites. *Cell*, 136(5), 891–902.
- [169] Salo, V. T., Belevich, I., Li, S., Karhinen, L., Vihinen, H., Vigouroux, C., Magré, J., Thiele, C., Hölttä-Vuori, M., Jokitalo, E., & Ikonen, E. (2016). Seipin regulates ER–lipid droplet contacts and cargo delivery. *The EMBO Journal*, 35(24), 2699–2716.
- [170] Salo, V. T. & Ikonen, E. (2019). Moving out but keeping in touch: contacts between endoplasmic reticulum and lipid droplets. *Current Opinion in Cell Biology*, 57, 64–70.
- [171] Salo, V. T., Li, S., Vihinen, H., Hölttä-Vuori, M., Szkalicity, A., Horvath, P., Belevich, I., Peränen, J., Thiele, C., Somerharju, P., Zhao, H., Santinho, A., Thiam, A. R., Jokitalo, E., & Ikonen, E. (2019). Seipin Facilitates Triglyceride Flow to Lipid Droplet and Counteracts Droplet Ripening via Endoplasmic Reticulum Contact. *Developmental Cell*, 50(4), 478–493.
- [172] Sánchez-Caballero, L., Elurbe, D. M., Baertling, F., Guerrero-Castillo, S., van den Brand, M., van Strien, J., van Dam, T. J., Rodenburg, R., Brandt, U., Huynen, M. A., & Nitjams, L. G. (2020). TMEM70 functions in the assembly of complexes I and V. *BBA - Biomembranes*, (pp. 183135).
- [173] Santinho, A., Salo, V. T., Chorlay, A., Li, S., Zhou, X., Omrane, M., Ikonen, E., & Thiam, A. R. (2020). Membrane Curvature Catalyzes Lipid Droplet Assembly. *Current Biology*, 30(13), 2481–2494.
- [174] Schindelin, J., Arganda-Carreras, I., Frise, E., Kaynig, V., Longair, M., Pietzsch, T., Preibisch, S., Rueden, C., Saalfeld, S., Schmid, B., Tinevez, J. Y., White, D. J., Hartenstein, V., Eliceiri, K., Tomancak, P., & Cardona, A. (2012). Fiji: An open-source platform for biological-image analysis. *Nature Methods*, 9(7), 676–682.

- [175] Schott, M. B., Weller, S. G., Schulze, R. J., Krueger, E. W., Drizyte-Miller, K., Casey, C. A., & McNiven, M. A. (2019). Lipid droplet size directs lipolysis and lipophagy catabolism in hepatocytes. *Journal of Cell Biology*, 218(10), 3320–3335.
- [176] Schuhmann, K., Almeida, R., Baumert, M., Herzog, R., Bornstein, S. R., & Shevchenko, A. (2012). Shotgun lipidomics on a LTQ Orbitrap mass spectrometer by successive switching between acquisition polarity modes. *Journal of Mass Spectrometry*, 47(1), 96–104.
- [177] Schuldiner, M. & Bohnert, M. (2017). A different kind of love - lipid droplet contact sites. *Biochimica et Biophysica Acta (BBA) - Molecular and Cell Biology of Lipids*, 1862(10), 1118–1196.
- [178] Schulze, R. J., Sathyanarayan, A., & Mashek, D. G. (2017). Breaking fat: The regulation and mechanisms of lipophagy. *Biochimica et Biophysica Acta - Molecular and Cell Biology of Lipids*, 1862(10), 1178–1187.
- [179] Schweiger, M., Schoiswohl, G., Lass, A., Radner, F. P. W., Haemmerle, G., Malli, R., Graier, W., Cornaciu, I., Oberer, M., Salvayre, R., Fischer, J., Zechner, R., & Zimmermann, R. (2008). The C-terminal Region of Human Adipose Triglyceride Lipase Affects Enzyme Activity and Lipid Droplet Binding. *Journal of Biological Chemistry*, 283(25), 17211–17220.
- [180] Sievers, F., Wilm, A., Dineen, D., Gibson, T. J., Karplus, K., Li, W., Lopez, R., McWilliam, H., Remmert, M., Söding, J., Thompson, J. D., & Higgins, D. G. (2011). Fast, scalable generation of high-quality protein multiple sequence alignments using Clustal Omega. *Molecular Systems Biology*, 7(539).
- [181] Sillence, D. J., Puri, V., Marks, D. L., Butters, T. D., Dwek, R. A., Pagano, R. E., & Platt, F. M. (2002). Glucosylceramide modulates membrane traffic along the endocytic pathway. *Journal of Lipid Research*, 43(11), 1837–1845.
- [182] Singh, R., Kaushik, S., Wang, Y., Xiang, Y., Komatsu, M., Tanaka, K., Cuervo, A. M., & Czaja, M. J. (2009). Autophagy regulates lipid metabolism. *Nature*, 458(7242), 1131–1135.
- [183] Slotte, J. P. & Ramstedt, B. (2007). The functional role of sphingomyelin in cell membranes. *European Journal of Lipid Science and Technology*, 109(10), 977–981.
- [184] Smirnova, E., Goldberg, E. B., Makarova, K. S., Lin, L., Brown, W. J., & Jackson, C. L. (2006). ATGL has a key role in lipid droplet/adiposome degradation in mammalian cells. *EMBO Reports*, 7(1), 106–113.
- [185] Soldati, T., Rancano, C., Geissler, H., & Pfeffer, S. R. (1995). Rab7 and Rab9 are recruited onto late endosomes by biochemically distinguishable processes. *Journal of Biological Chemistry*, 270(43), 25541–25548.

- [186] Solinas, G., Borén, J., & Dulloo, A. G. (2015). De novo lipogenesis in metabolic homeostasis: More friend than foe? *Molecular Metabolism*, 4(5), 367–377.
- [187] Soni, K. G., Mardones, G. A., Sougrat, R., Smirnova, E., Jackson, C. L., & Bonifacino, J. S. (2009). Coatomer-dependent protein delivery to lipid droplets. *Journal of Cell Science*, 122(11), 1834–1841.
- [188] Sonnhhammer, E. L. L. & Krogh, A. (2008). A hidden Markov model for predicting transmembrane helices in protein sequence. *Sixth Int. Conf. on Intelligent Systems for Molecular Biology*, (pp.8).
- [189] Steenbergen, R. H., Nanowski, T., Beigneux, A. P., Kulinski, A., Young, S. G., & Vance, J. E. (2005). Disruption of the Phosphatidylserine Decarboxylase Gene in Mice Causes Embryonic Lethality and Mitochondrial Defects. *J Biol Chem*, 280(48), 40032–40040.
- [190] Stenmark, H. (2009). Rab GTPases as coordinators of vesicle traffic. *Nature Reviews Molecular Cell Biology*, 10(8), 513–525.
- [191] Stone, S. J., Levin, M. C., Zhou, P., Han, J., Walther, T. C., & Farese, R. V. (2009). The Endoplasmic Reticulum Enzyme DGAT2 Is Found in Mitochondria-associated Membranes and Has a Mitochondrial Targeting Signal That Promotes Its Association with Mitochondria. *Journal of Biological Chemistry*, 284(8), 5352–5361.
- [192] Stone, S. J. & Vance, J. E. (2000). Phosphatidylserine synthase-1 and -2 are localized to mitochondria-associated membranes. *Journal of Biological Chemistry*, 275(44), 34534–34540.
- [193] Storch, J. & Corsico, B. (2008). The emerging functions and mechanisms of mammalian fatty acid-binding proteins. *Annual review of nutrition*, 28, 73–95.
- [194] Sturmey, R. G., O’Toole, P. J., & Leese, H. J. (2006). Fluorescence resonance energy transfer analysis of mitochondrial: Lipid association in the porcine oocyte. *Reproduction*, 132(6), 829–837.
- [195] Subramanian, V., Rotlienber, A., Gomez, C., Cohen, A. W., Garcia, A., Bhattacharyya, S., Shapiro, L., Dolios, G., Wang, R., Lisanti, M. P., & Brasaemle, D. L. (2004). Perilipin A mediates the reversible binding of CGI-58 to lipid droplets in 3T3-L1 adipocytes. *Journal of Biological Chemistry*, 279(40), 42062–42071.
- [196] Sui, X., Arlt, H., Brook, K. P., Lai, Z. W., DiMaio, F., Marks, D. S., Liao, M., Farese, R. V., & Walther, T. C. (2018). Cryo-electron microscopy structure of the lipid droplet-formation protein seipin. *bioRxiv*, 217(12).
- [197] Suzuki, M., Shinohara, Y., Ohsaki, Y., & Fujimoto, T. (2011). Lipid droplets: Size matters. *Journal of Electron Microscopy*, 60(SUPPL. 1).

- [198] Syamsunarno, M. R. A. A., Iso, T., Hanaoka, H., Yamaguchi, A., Obokata, M., Koitabashi, N., Goto, K., Hishiki, T., Nagahata, Y., Matsui, H., Sano, M., Kobayashi, M., Kikuchi, O., Sasaki, T., Maeda, K., Murakami, M., Kitamura, T., Suematsu, M., Tsushima, Y., Endo, K., Hotamisligil, G. S., & Kurabayashi, M. (2013). A critical role of fatty acid binding protein 4 and 5 (FABP4/5) in the systemic response to fasting. *PLoS ONE*, 8(11).
- [199] Sztalryd, C. & Brasaemle, D. L. (2017). The perilipin family of lipid droplet proteins: Gatekeepers of intracellular lipolysis. *Biochimica et biophysica acta*, 1862(10), 1221–1232.
- [200] Sztalryd, C. & Kimmel, A. R. (2014). Perilipins: Lipid droplet coat proteins adapted for tissue-specific energy storage and utilization, and lipid cytoprotection. *Biochimie*, 96(1), 96–101.
- [201] Tagaya, M., Arasaki, K., Inoue, H., & Kimura, H. (2014). Moonlighting functions of the NRZ (mammalian Dsl1) complex. *Frontiers in cell and developmental biology*, 2(June), 25.
- [202] Takeuchi, K. & Reue, K. (2009). Biochemistry, physiology, and genetics of GPAT, AGPAT, and lipin enzymes in triglyceride synthesis. *AJP: Endocrinology and Metabolism*, 296(6), E1195–E1209.
- [203] Tasseva, G., Bai, H. D., Davidescu, M., Haromy, A., Michelakis, E., & Vance, J. E. (2013). Phosphatidylethanolamine deficiency in mammalian mitochondria impairs oxidative phosphorylation and alters mitochondrial morphology. *Journal of Biological Chemistry*, 288(6), 4158–4173.
- [204] Tauchi-Sato, K., Ozeki, S., Houjou, T., Taguchi, R., & Fujimoto, T. (2002). The surface of lipid droplets is a phospholipid monolayer with a unique fatty acid composition. *Journal of Biological Chemistry*, 277(46), 44507–44512.
- [205] Te Vruchte, D., Lloyd-Evans, E., Veldman, R. J., Neville, D. C., Dwek, R. A., Platt, F. M., Van Blitterswijk, W. J., & Sillences, D. J. (2004). Accumulation of glycosphingolipids in Niemann-Pick C disease disrupts endosomal transport. *Journal of Biological Chemistry*, 279(25), 26167–26175.
- [206] Thiam, A. R., Antonny, B., Wang, J., Delacotte, J., Wilfling, F., Walther, T. C., Beck, R., Rothman, J. E., & Pincet, F. (2013a). COPI buds 60-nm lipid droplets from reconstituted water-phospholipid-triacylglyceride interfaces, suggesting a tension clamp function. *Proceedings of the National Academy of Sciences*, 110(33), 13244–13249.
- [207] Thiam, A. R. & Beller, M. (2017). The why, when and how of lipid droplet diversity. *Journal of Cell Science*, 130(2), 315–324.
- [208] Thiam, A. R. & Dugail, I. (2019). Lipid droplet-membrane contact sites - From protein binding to function. *Journal of Cell Science*, 132(12).

- [209] Thiam, A. R., Farese Jr, R. V., & Walther, T. C. (2013b). The biophysics and cell biology of lipid droplets. *Nat Rev Mol Cell Biol*, 14(12), 775–786.
- [210] Thiam, A. R. & Forêt, L. (2016). The physics of lipid droplet nucleation, growth and budding. *Biochimica et Biophysica Acta - Molecular and Cell Biology of Lipids*, 1861(8), 715–722.
- [211] Thomas, L. L., Joiner, A. M., & Fromme, J. C. (2018). The TRAPPI II complex activates the GTPase Ypt1 (Rab1) in the secretory pathway. *Journal of Cell Biology*, 217(1), 283–298.
- [212] Thul, P. J., Tschapalda, K., Kolkhof, P., Thiam, A. R., Oberer, M., & Beller, M. (2017). Targeting of the Drosophila protein CG2254/Ldsdh1 to a subset of lipid droplets. *Journal of Cell Science*, 130(18), 3141–3157.
- [213] Tidhar, R. & Futerman, A. H. (2013). The complexity of sphingolipid biosynthesis in the endoplasmic reticulum. *Biochimica et Biophysica Acta - Molecular Cell Research*, 1833(11), 2511–2518.
- [214] Tsai, P. I., Papakyrikos, A. M., Hsieh, C. H., & Wang, X. (2017). Drosophila MIC60/mitoflin conducts dual roles in mitochondrial motility and crista structure. *Molecular Biology of the Cell*, 28(24), 3471–3479.
- [215] Tuschl, T. (2006). Annealing siRNAs to Produce siRNA Duplexes. *Cold Spring Harbor Protocols*, 2006(1), pdb.prot4340.
- [216] Vacaru, A. M., Tafesse, F. G., Ternes, P., Kondylis, V., Hermansson, M., Brouwers, J. F., Somerharju, P., Rabouille, C., & Holthuis, J. C. (2009). Sphingomyelin synthase-related protein SMSr controls ceramide homeostasis in the ER. *Journal of Cell Biology*, 185(6), 1013–1027.
- [217] Vacaru, A. M., Van Den Dikkenberg, J., Ternes, P., & Holthuis, J. C. (2013). Ceramide phosphoethanolamine biosynthesis in Drosophila is mediated by a unique ethanolamine phosphotransferase in the golgi lumen. *Journal of Biological Chemistry*, 288(16), 11520–11530.
- [218] Vance, J. E. (2014). MAM (mitochondria-associated membranes) in mammalian cells : Lipids and beyond. *BBA - Molecular and Cell Biology of Lipids*, 1841(4), 595–609.
- [219] Vance, J. E. (2015). Phospholipid Synthesis and Transport in Mammalian Cells. *Traffic*, 16(1), 1–18.
- [220] Vance, J. E. & Tasseva, G. (2013). Formation and function of phosphatidylserine and phosphatidylethanolamine in mammalian cells. *Biochimica et Biophysica Acta - Molecular and Cell Biology of Lipids*, 1831(3), 543–554.

- [221] Veen, J. N. V. D., Kennelly, J. P., Wan, S., Vance, J. E., Vance, D. E., & Jacobs, R. L. (2017). The critical role of phosphatidylcholine and phosphatidylethanolamine metabolism in health and disease □. *BBA - Biomembranes*, 1859(9), 1558–1572.
- [222] Vizcaíno, J. A., Csordas, A., Del-Toro, N., Dianes, J. A., Griss, J., Lavidas, I., Mayer, G., Perez-Riverol, Y., Reisinger, F., Ternent, T., Xu, Q. W., Wang, R., & Hermjakob, H. (2016). 2016 update of the PRIDE database and its related tools. *Nucleic Acids Research*, 44(D1), D447–D456.
- [223] Vrbacký, M., Kovalčíková, J., Chawengsaksophak, K., Beck, I. M., Mráček, T., Nůsková, H., Sedmera, D., Papoušek, F., Kolář, F., Sobol, M., Hozák, P., Sedlacek, R., & Houštěk, J. (2016). Knockout of Tmem70 alters biogenesis of ATP synthase and leads to embryonal lethality in mice. *Human Molecular Genetics*, 25(21), 4674–4685.
- [224] Walther, T. C., Chung, J., & Farese Jr, R. V. (2017). Lipid Droplet Biogenesis. *Annual review of cell and developmental biology*, 33(14), 395–401.
- [225] Walther, T. C. & Farese Jr, R. V. (2012). Lipid Droplets And Cellular Lipid Metabolism. *Annual review of biochemistry*, 81, 687–714.
- [226] Wanders, R. J. & Brites, P. (2010). Biosynthesis of ether-phospholipids including plasmalogens, peroxisomes and human disease: New insights into an old problem. *Clinical Lipidology*, 5(3), 379–386.
- [227] Wang, H., Becuwe, M., Housden, B. E., Chitraju, C., Porras, A. J., Graham, M. M., Liu, X. N., Thiam, A. R., Savage, D. B., Agarwal, A. K., Garg, A., Olarte, M.-J., Lin, Q., Fröhlich, F., Hannibal-Bach, H. K., Upadhyayula, S., Perrimon, N., Kirchhausen, T., Ejsing, C. S., Walther, T. C., & Farese, R. V. (2016). Seipin is required for converting nascent to mature lipid droplets. *eLife*, 5(2), 133–150.
- [228] Wang, L. J., Hsu, T., Lin, H. L., & Fu, C. Y. (2020). Drosophila MICOS knockdown impairs mitochondrial structure and function and promotes mitophagy in muscle tissue. *Biology Open*, 9(12).
- [229] Wang, S., Idrissi, F. Z., Hermansson, M., Grippa, A., Ejsing, C. S., & Carvalho, P. (2018). Seipin and the membrane-shaping protein Pex30 cooperate in organelle budding from the endoplasmic reticulum. *Nature Communications*, 9(1), 1–12.
- [230] Wendel, A. A., Cooper, D. E., Ilkayeva, O. R., Muoio, D. M., & Coleman, R. A. (2013). Glycerol-3-phosphate acyltransferase (GPAT)-1, but not GPAT4, incorporates newly synthesized fatty acids into triacylglycerol and diminishes fatty acid oxidation. *Journal of Biological Chemistry*, 288(38), 27299–27306.
- [231] Wendel, A. A., Lewin, T. M., & Coleman, R. A. (2009). GPATs: rate limiting enzymes of TAG biosynthesis. *Biochimica et biophysica acta*, 1791(6), 501–506.

- [232] Wilfling, F., Haas, J. T., Walther, T. C., & Jr, R. V. F. (2014a). Lipid droplet biogenesis. *Current Opinion in Cell Biology*, 29(1), 39–45.
- [233] Wilfling, F., Thiam, A. R., Olarte, M. J., Wang, J., Beck, R., Gould, T. J., Allgeyer, E. S., Pincet, F., Bewersdorf, J., Farese, R. V., & Walther, T. C. (2014b). Arf1/COPI machinery acts directly on lipid droplets and enables their connection to the ER for protein targeting. *eLife*, 2014(3), 1–20.
- [234] Wilfling, F., Wang, H., Haas, J. T., Kraemer, N., Gould, T. J., Cheng, J.-x. X., Graham, M., Christiano, R., Fröhlich, F., Buhman, K. K., Coleman, R. A., Bewersdorf, J., Farese, R. V., Walther, T. C., Uchida, A., Cheng, J.-x. X., Graham, M., Christiano, R., Fröhlich, F., Liu, X., Buhman, K. K., Coleman, R. A., Bewersdorf, J., Farese, R. V., & Walther, T. C. (2013). Triacylglycerol synthesis enzymes mediate lipid droplet growth by relocating from the ER to lipid droplets. *Developmental Cell*, 24(4), 384–399.
- [235] Wollweber, F., von der Malsburg, K., & van der Laan, M. (2017). Mitochondrial contact site and cristae organizing system: A central player in membrane shaping and crosstalk. *Biochimica et Biophysica Acta - Molecular Cell Research*, 1864(9), 1481–1489.
- [236] Wu, L., Li, D., Li, J.-l., Cao, J., Tobin, J. F., Gimeno, R. E., Hurov, J., & Shan, D. (2010). GPAT₃ and GPAT₄ are regulated by insulin-stimulated phosphorylation and play distinct roles in adipogenesis. *Journal of Lipid Research*, 51(7), 1971–1981.
- [237] Xu, D., Li, Y. Y., Wu, L., Li, Y. Y., Zhao, D., Yu, J., Huang, T., Ferguson, C., Parton, R. G., Yang, H., & Li, P. (2018a). Rab18 promotes lipid droplet (LD) growth by tethering the ER to LDs through SNARE and NRZ interactions. *Journal of Cell Biology*, 217(3), 975–995.
- [238] Xu, N., Zhang, S. O., Cole, R. a., McKinney, S. a., Guo, F., Haas, J. T., Bobba, S., Farese, R. V., & Mak, H. Y. (2012). The FATP₁-DGAT₂ complex facilitates lipid droplet expansion at the ER-lipid droplet interface. *The Journal of cell biology*, 198(5), 895–911.
- [239] Xu, S., Zhang, X., & Liu, P. (2018b). Lipid droplet proteins and metabolic diseases. *Biochimica et Biophysica Acta - Molecular Basis of Disease*, 1864(5), 1968–1983.
- [240] Xu, Y., Zhang, F., Su, Z., McNew, J. A., & Shin, Y. K. (2005). Hemifusion in SNARE-mediated membrane fusion. *Nature Structural and Molecular Biology*, 12(5), 417–422.
- [241] Yamasaki, A., Menon, S., Yu, S., Barrowman, J., Meerloo, T., Oorschot, V., Klumperman, J., Satoh, A., & Ferro-Novick, S. (2009). mTrs130 Is a Component of a Mammalian TRAPP_{II} Complex, a Rab1 GEF That Binds to COPI-coated Vesicles. *Molecular biology of the cell*, 20, 4205–4215.
- [242] Yamashita, A., Hayashi, Y., Matsumoto, N., Nemoto-Sasaki, Y., Oka, S., Tanikawa, T., & Sugiura, T. (2014). Glycerophosphate/Acylglycerophosphate Acyltransferases. *Biology*, 3(4), 801–830.

- [243] Yang, L., Yang, J. B., Chen, J., Yu, G. Y., Zhou, P., Lei, L., Wang, Z. Z., Chang, C. C., Yang, X. Y., Chang, T. Y., & Li, B. L. (2004). Enhancement of human ACAT1 gene expression to promote the macrophage-derived foam cell formation by dexamethasone. *Cell Research*, 14(4), 315–323.
- [244] Yao, C. H., Fowle-Grider, R., Mahieu, N. G., Liu, G. Y., Chen, Y. J., Wang, R., Singh, M., Potter, G. S., Gross, R. W., Schaefer, J., Johnson, S. L., & Patti, G. J. (2016). Exogenous Fatty Acids are the Preferred Source of Membrane Lipids in Proliferating Fibroblasts. *Cell Chem Biol*, 23(4), 483–493.
- [245] Yip, C. K., Berscheminski, J., & Walz, T. (2010). Molecular architecture of the TRAPP1 complex and implications for vesicle tethering. *Nature Structural & Molecular Biology*, 17(11), 1298–1304.
- [246] Yu, J., Zhang, S., Cui, L., Wang, W., Na, H., Zhu, X., Li, L., Xu, G., Yang, F., Christian, M., & Liu, P. (2015). Lipid droplet remodeling and interaction with mitochondria in mouse brown adipose tissue during cold treatment. *Biochimica et Biophysica Acta - Molecular Cell Research*, 1853(5), 918–928.
- [247] Yu, X., Breitman, M., & Goldberg, J. (2012). A Structure-based mechanism for Arf1-dependent recruitment of coatamer to membranes. *Cell*, 148(3), 530–542.
- [248] Yuan, Y., Li, P., & Ye, J. (2012). Lipid homeostasis and the formation of macrophage-derived foam cells in atherosclerosis. *Protein and Cell*, 3(3), 173–181.
- [249] Zechner, R., Kienesberger, P. C., Haemmerle, G., Zimmermann, R., & Lass, A. (2009a). Adipose triglyceride lipase and the lipolytic catabolism of cellular fat stores. *Journal of Lipid Research*, 50(1), 3–21.
- [250] Zechner, R., Madeo, F., & Kratky, D. (2009b). Cytosolic lipolysis and lipophagy: two sides of the same coin. *Nature Publishing Group*, 2009.
- [251] Zechner, R., Zimmermann, R., Eichmann, T. O., Kohlwein, S. D., Haemmerle, G., Lass, A., & Madeo, F. (2012). FAT SIGNALS - Lipases and lipolysis in lipid metabolism and signaling. *Cell Metabolism*, 15(3), 279–291.
- [252] Zhang, H., Wang, Y., Li, J., Yu, J., Pu, J., Li, L., Zhang, H., Zhang, S., Peng, G., Yang, F., & Liu, P. (2011). Proteome of skeletal muscle lipid droplet reveals association with mitochondria and apolipoprotein A-I. *Journal of Proteome Research*, 10(10), 4757–4768.
- [253] Zimmermann, L., Stephens, A., Nam, S. Z., Rau, D., Kübler, J., Lozajic, M., Gabler, F., Söding, J., Lupas, A. N., & Alva, V. (2018). A Completely Reimplemented MPI Bioinformatics Toolkit with a New HHpred Server at its Core. *Journal of Molecular Biology*, 430(15), 2237–2243.

- [254] Zimmermann, R. (2004). Fat Mobilization in Adipose Tissue Is Promoted by Adipose Triglyceride Lipase. *Science*, 306(5700), 1383–1386.
- [255] Zlobine, I., Gopal, K., & Ussher, J. R. (2016). Lipotoxicity in obesity and diabetes-related cardiac dysfunction. *Biochimica et Biophysica Acta - Molecular and Cell Biology of Lipids*, 1861(10), 1555–1568.
- [256] Zoni, V., Khaddaj, R., Campomanes, P., Thiam, A. R., Schneider, R., & Vanni, S. (2019). Lipid droplet biogenesis is driven by liquid-liquid phase separation. *bioRxiv*, (pp. 1–30).



THIS THESIS WAS TYPESET using \LaTeX , originally developed by Leslie Lamport and based on Donald Knuth's \TeX . The body text is set in 11 point Egenolff-Berner Garamond, a revival of Claude Garamont's humanist typeface. The above illustration, "Science Experiment 02", was created by Ben Schlitter and released under [CC BY-NC-ND 3.0](#). A template that can be used to format a PhD thesis with this look and feel has been released under the permissive MIT (X11) license, and can be found online at github.com/suchow/Dissertate or from its author, Jordan Suchow, at suchow@post.harvard.edu.